POLITECNICO DI MILANO
Scuola di Ingegneria Industriale e dell'Informazione
Corso di Laurea Magistrale in Ingegneria Elettrica

Synthetic inertia in wind power systems with DFIGs and HVDC connections

Analysis and simulations of some control systems

Relatore: Prof. Roberto Perini

Tesi di Laurea Magistrale di:
Mattia Cabiati, matricola 813725

Anno Accademico 2014-2015

Contents

List of Figures

List of Tables

Abstract

Inertia is the intrinsic property of any system with energy storage that represents the system resistance to any change of its energy state. State variables are quantities that represent the energetic state of the system and cannot vary instantaneously. In a power system the rotating masses of generators are the energy storage and angular speed is the state variable. Electrical frequency and mechanical rotational frequency are strongly linked by the electromagnetic field inside the generators and a change of rotating speed results in electrical frequency variation and vice-versa.

In the steady state operation of power systems, there is a dynamical equilibrium, power generation and consumption are equal and so the frequency is constant, but if generation or load change, the first thing that begins to vary, instantaneously but in a continuous way, is the energy stored in the rotating masses which absorb the power imbalance. This results in a variation of the rotating speed of the generator shafts and so a variation of the grid frequency. How fast the frequency will vary depends on how much inertia the power system has at that moment. Soon after the frequency deviation takes place, primary frequency control will act in order to recover the perfect power balance. This is what happens in case generators are rotating electrical machines directly connected to the grid. But nowadays power plants with power electronic interfaces with the grid are becoming more and more popular. This is typical for distributed energy sources. In these cases the kinetic energy storage, even if it is present, is not linked directly with grid frequency and so they don't take part in the overall system inertia. This is not a problem if they are a negligible amount with respect to the total power generation, but nowadays they are becoming a considerable amount and there is concern about the overall inertia, essential for frequency stability.

To overcome this issue we need to implement a control system able to deliver or absorb power in a fast way, taking or delivering it from the energy storage at disposal. In this way an inertial response can be simulated, we can say we have created some "synthetic inertia".

In chapter one there is a brief description of the power system new trends and a panoramic view of some new technologies that are being developed to deal with the decreasing inertia issue. In chapter two we will analyse various methods to implement synthetic inertia dealing with HVDC connections and wind power

plants. Then we will study a HVDC connection (chapters three and four), stability analysis and simulations with the control systems described in chapter two will be done. Eventually in chapter five we will study a wind turbine equipped with a doubly fed induction generator (DFIG) and the ways we can supply synthetic inertia and primary reserve to the grid, we will do stability analysis and simulations with the proposed control systems.

Sommario

L'inerzia è la proprietà intrinseca di qualsiasi sistema con accumulo di energia che rappresenta la resistenza del sistema a un cambiamento del suo stato energetico. Le variabili di stato sono le quantità che rappresentano lo stato energetico del sistema e non possono variare istantaneamente. In un sistema elettrico di potenza le masse rotanti dei generatori sono l'accumulo di energia e la velocità angolare è la variabile di stato. Frequenza elettrica e frequenza di rotazione meccanica sono strettamente legati dal campo elettromagnetico all'interno dei generatori e un cambio di velocità in rotazione risultata in una variazione della frequenza elettrica e viceversa.

Nel sistema, a regime, vi è un equilibrio dinamico, generazione e consumo energetico sono uguali e quindi la frequenza è costante, ma se la generazione o il carico variassero, la prima cosa che comincerebbe a variare, istantaneamente ma in modo continuo, è l'energia immagazzinata nelle masse rotanti che assorbono lo squilibrio di potenza. Ciò si traduce in una variazione della velocità di rotazione degli alberi generatori e quindi in una variazione della frequenza di rete. Quanto è veloce la variazione di frequenza dipende da quanto vale l'inerzia del sistema elettrico di potenza in quel momento. Subito dopo la deviazione di frequenza ha luogo il controllo primario della frequenza che agisce al fine di recuperare l'equilibrio tra potenza generata e consumata. Questo è ciò che accade nel caso in cui generatori sono macchine elettriche rotanti direttamente collegati alla rete. Ma al giorno d'oggi le centrali elettriche interfacciate alla rete con convertitori elettronici di potenza stanno diventando sempre più comuni. Questo è tipico per le fonti di energia distribuite. In questi casi l'accumulo di energia cinetica, anche se fosse presente, non è legato direttamente alla frequenza di rete e quindi non prendono parte alla formazione dell'inerzia complessiva del sistema. Questo non è un problema se sono una quantità trascurabile rispetto al totale della generazione, ma oggi stanno diventando una notevole quantità e vi è preoccupazione per l'inerzia complessiva del sistema elettrico, essenziale per la stabilità di frequenza.

Per ovviare a questo problema abbiamo bisogno di implementare un sistema di controllo in grado di fornire o assorbire energia in modo veloce, prendendola dall'accumulo di energia a disposizione. In questo modo una risposta inerziale può essere simulata, cioè possiamo dire di aver creato un'"inerzia sintetica".

Nel primo capitolo vi è una breve descrizione delle nuove tendenze riguardanti il sistema elettrico di potenza e una vista panoramica di alcune nuove tecnologie che si stanno sviluppando per affrontare il problema della diminuzione dell'inerzia. Nel secondo capitolo analizzeremo vari metodi per implementare l'inerzia sintetica con collegamenti HVDC e impianti eolici. Poi studieremo un collegamento HVDC (capitoli tre e quattro), analisi di stabilità e simulazioni con i sistemi di controllo descritti nel capitolo due saranno eseguiti. Alla fine, nel quinto capitolo studieremo una turbina eolica dotata di un generatore a doppia alimentazione (DFIG) e il modo in cui possiamo fornire inerzia sintetica e riserva primaria alla rete, faremo l'analisi di stabilità e simulazioni con i sistemi di controllo proposti.

Chapter 1

Changes in power system

1.1 Introduction

Nowadays power system is changing toward the integration of a steadily larger number of renewable energy sources. This direction is encouraged by governments and European Union in order to reduce carbon emissions, ensure security of power supply and improving European Union competitiveness, as said in the official document that sets the targets in energy field until the year 2050 [1]. The ultimate goal is to achieve 80% to 95% reduction of all carbon emission, and for electric sector is to generate 34% of total power from renewable resources by 2020 and 100% by 2050.

This involves modifications in power system due to the nature or renewable sources. The model of a power system based on big power plants is to be reconsidered in favour of a model capable of incorporating an increasingly amount of distributed energy generation.

In the next graphs (figures 1.1 and 1.2), it is shown how energy production is shared between sources in Italy from 2007 to 2013 (last available data from Terna, the Italian TSO)[2]. Graphs are in percentage value (year by year), to retrieve an approximated value in GWh we can take into account that for the year 2013 the value 100% corresponds to 300 043 GWh.

Apart from hydro power plants, a technology already well exploited, and whose production variation is due, for the most part, to the variability of water at disposal due to weather reasons, we can see a big increment of production of other renewable sources. Photovoltaic production grew from 0.6% of 2010 to 6,5% in 2013. Wind energy has seen a more gradual increment, but in 2013 covered 4.5% of consumption. Also energy production from biomasses is increased, but in this case are thermal power plant, maybe small in size, but similar to the traditional ones.
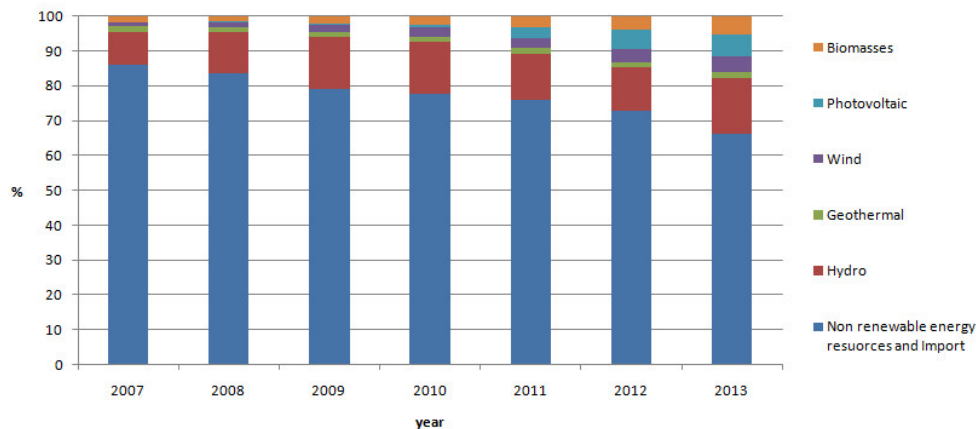
Figure 1.1: Share out of the energy production in Italy for different energy sources (source: Terna)
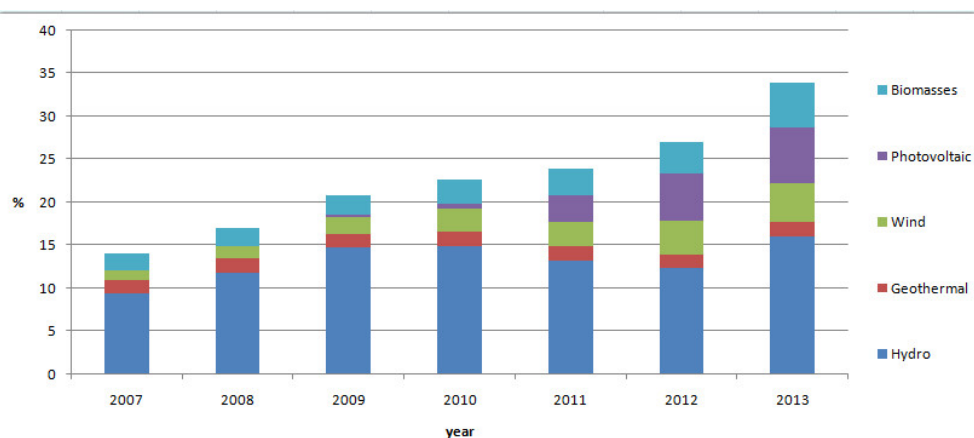
Figure 1.2: Share out of the energy production in Italy between renewable energy sources (source: Terna)

Also among non renewable energy sources the trend is to build smaller power plants, especially after the liberalization of the electricity market, such as combined heat power plants (CHP). So we are going towards a system with a power production more distributed on the territory, smaller power plants and in some cases with characteristic of control totally different from the traditional power plants. This brings new problems and new challenges, and especially the integration of renewable sources interfaced to the grid with power electronic brings the new issues. Among them, as explained in the abstract, there is the decreasing value of the overall inertia.

1.2   Strategy to deal with the decreasing inertia issue, a survey

Small level of inertia is a problem already present in small isolated grids such as small islands or grids not connected to the main system. The problem can be solved introducing more rotating masses, or introducing an energy storage interfaced to the power system with a power electronic converter controlled in order to sustain frequency during transients. Energy storage available for this purpose are of various types, each one with his limitation and advantages. Main limitations are power deliverable and energy accumulated. In figure 1.3 we can see performances of various electrical energy storage technologies [3]. To sustain frequency due to fast power variation (in generation or consumption) some systems have been studied and built, as in La Palma island (Spain) [4] or in Guadalupe island (France) [5], where a supercapacitor is used as an energy storage to absorb frequency variations. In La Palma island where the installed power capacity is $103.1MW$, a supercapacitor able to deliver $4MW$ for $5s$ is used. They control the ultracapacitor power support according to grid frequency deviation and the grid frequency time derivative. They made simulation and field tests of the system stressed with a sudden load imbalance of $2.5MW$. Instead in Guadalupe island a system equipped with a supercapacitor of $500kW$ is used with the objective to deal with noninertia types of generators, in that case wind and solar power plants. In general we can say that supercapacitors are suitable for this purpose because they have high power density. Instead if we want a system able to absorb power excursion for a long time we need other devices more energy-oriented.

Other studies, especially in the direction of developing microgrid as a part of the future power system, have been done to create a device able to simulate a synchronous machine, named virtual synchronous generator (VSG) or virtual synchronous machine (VSMA). These devices are made through an energy storage, a power electronic converter and a control system. They mimic the dynamic behaviour of a synchronous machine in order to deal with grid frequency disturbances. Various papers present the dynamical benefits that such device brings to the grid, but, like supercapacitors, it is a new component to introduce into the grid. In [6] we can find a survey of these devices.

Following the thread of small size distributed generators we encounter other problems related to the low voltage systems (where small energy sources are typically connected), such as the different nature of the grid: if in high and medium voltage the grid can be assumed inductive, for lower voltages the resistive nature of the grid has to be taken into account. This causes problems in the control system due to the fact that we cannot easily decouple the power control in two separate controls, one for active and one reactive power as we can do if the grid is inductive or resistive. To overcome this issue we can introduce a
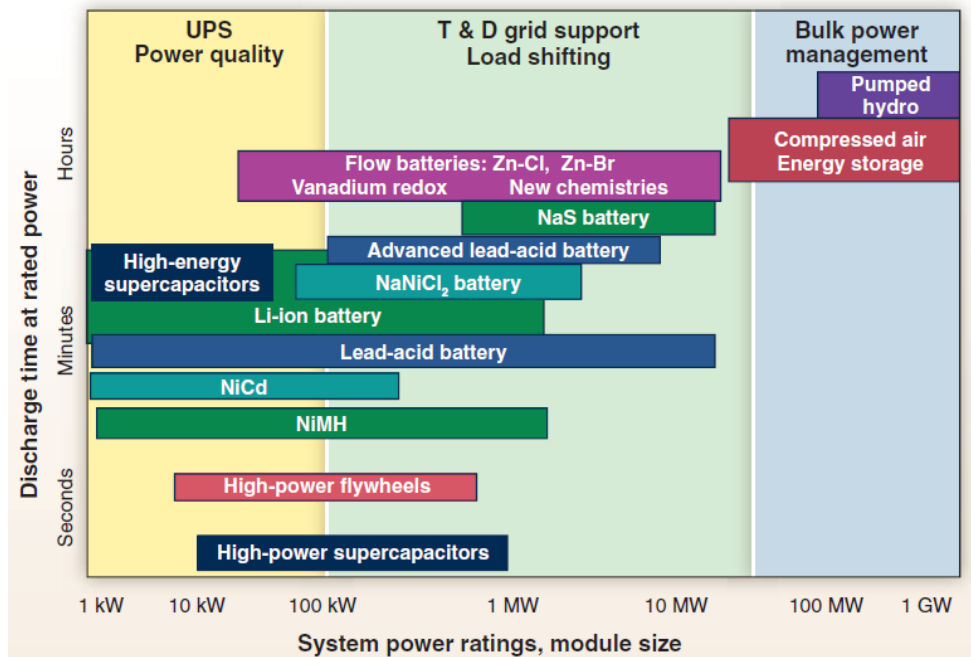
Figure 1.3: Comparison of discharge time and power rating for various electrical energy storage technologies

virtual impedance or a rotational matrix. These points are studied in [7] and in [8] respectively.

All these solutions to the decreasing inertia issue introduce news devices, and in a large power system this can be costly. There are some other proposed ideas that use energy storage already present in the grid, but not coupled with frequency. That is the case of wind farms with their rotating wind turbines, or HVDC connection where electrostatic energy is present. We will now analyse these solutions.

Chapter 2

Wind power plants frequency support

2.1 Introduction

Active power reserves are needed for the power system operation. These reserves, essential to deal with load changing, are usually provided by traditional power plants, such as hydro or thermal power plants. Nowadays with the progressive penetration of non-synchronized energy source into power system such as wind or photovoltaic power plants, the level of active power reserves is decreasing. In this chapter nomenclature of power reserve and participation method for wind power plants will be analysed.

2.2 Power reserves

We can distinguish four types of power reserves [9]:

- instantaneous power reserve

- primary power reserve

- secondary power reserve

- tertiary power reserve

The *instantaneous power reserve* is the inertia of synchronous generators that gives a stabilizing effect. After a load change, the rate of change of frequency (ROCOF) depends on this power reserve in a way that we will describe later in section 2.4. Wind power plants have not this kind of power reserve, neither if the turbines are interfaced with the grid by a full scale converter, or if they are DFIGs.

The *primary power reserve* is the additional power that can be delivered locally and automatically by power plants to balance a power consumption change and stop frequency deviation. This reserve is generally controlled by a droop control where the frequency deviation implies a new power set point. It has to be activated within few seconds after the disturbance took place and has to last until the secondary reserve has restored the frequency near to the nominal value. The amount of the primary reserve is defined through the so called reference incident, such as the trip of the biggest power plant in the synchronous power system. In continental Europe the overall amount of the primary reserves is 3000 MW.

The *secondary power reserve* is activated to restore the rated frequency of the system, releasing primary reserves and to restore active power interchanges between power system areas to their set point values. This reserve is activated by TSOs changing generators power set points.

The *tertiary power reserve* is intended to replace the secondary power reserve, restore the nominal frequency value if the secondary reserve were not enough and for economical power dispatch.

2.2.1   New trends in requirements to renewable energy sources

In the past non conventional energy sources did not provide any power reserve. But nowadays the situation is changing, especially in Ireland and Great Britain where the reserve issue is more severe due to small size of power system synchronous area (Ireland and Great Britain form two synchronous areas [10]) and high presence of wind power plants [9]; the local TSOs are already requiring primary frequency support to renewable energy sources. In continental Europe the situation varies from country to country, but in general it is not required a power reserve, but only to disconnect the plant above a certain frequency and to introduce the power production in a soft manner such as ramping the power delivered to the power system.

This for primary reserve, but ENTSO-e introduced also the concept of *synthetic inertia*, defined as the facility "to replicate the effect of Inertia of a Synchronous Power Generating Module " [10] for a non-synchronized generating unit. In the next part of the thesis we will analyse this concept and the proposed application solutions.

2.3   Wind power plant inertia support

Power electronics converters are a typical way to connect wind power plants to the main grid. This has many advantages, but, as said before, it also decouples the rotating masses from the grid frequency, avoiding that their inertia is added to the overall one. Nowadays wind power plants are becoming a non negligible

amount of the total power production and it can be useful if they can support grid also with some inertia.

To do this we can rely on the kinetic energy storage of the turbines and on fast power electronic converters.

In the figure 2.1 we represent a wind farm equipped with doubly fed induction generators (DFIG) because they have some advantages and are widely used, but general concepts are applicable also to other wind power plant solutions.
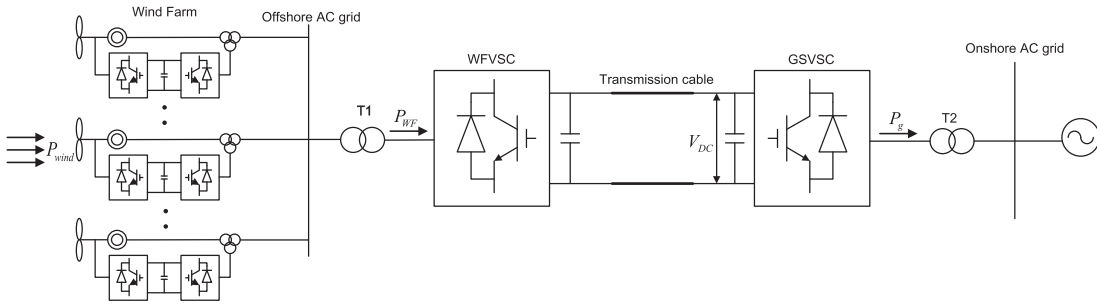
Figure 2.1: Example of wind power plant equipped with DFIG

If the wind power plant is off-shore, like the one in figure 2.1, probably it is connected to the grid through a high voltage DC connection (HVDC). Here we can find an other energy storage. HVDC in fact acts as a capacitor and if we can modify the voltage of the link this can act as an energy storage and can be used to provide inertia. Moreover we can exploit the DC link to overcome the problem of sending information about the grid frequency to the off-shore turbines. In fact if we use the DC link to provide inertia the DC voltage will vary during transients, so we can simply measure the voltage at the off-shore side to understand what is happening in the main on-shore grid and act consequently.

2.4 Inertia response of a non controlled machine

Let's now analyse the inertia response of a non controlled machine, that is synchronous generator if its control system is neglected (we can say that in the first instants after a transient the control system do not react promptly). As said before, in a power system during steady state operation there is a perfect match between power generation and consumption. All generators are rotating with a synchronous electrical speed. If the perfect balance is lost, due to a load change or other causes, the power generated will be higher or lower than power consumption. This difference will vary the kinetic energy stored in the rotating masses connected directly to the system. In the case that the generation is higher than consumption the synchronous generators will accelerate, in the other case they

will slow down. We can describe this phenomenon mathematically, for simplicity we consider only one synchronous generator.

A sudden load change is an imbalance between the mechanical moving torque (T_m) and the electrical resisting torque (T_e). The speed will vary according to the following equation

$$T_m - T_e = J\frac{d\Omega}{dt} \tag{2.1}$$

we name $T_m - T_e = \Delta T$ accelerating torque

$$\Delta T = J\frac{d\Omega}{dt} \tag{2.2}$$

we divide by T_0 to bring the equation in p.u. (small case letter or a dot over the letter indicates a p.u. variable)

$$\Delta\dot{T} = \frac{J\Omega_0}{T_0}\frac{d\omega}{dt} \tag{2.3}$$

If during the transient the speed variation is small we can multiply by the nominal speed in p.u. and put in evidence a power imbalance instead of a torque imbalance

$$\Delta\dot{T}\omega_0 = \frac{J\Omega_0\omega_0}{T_0}\frac{d\omega}{dt} \tag{2.4}$$

and recognising that $\omega_0 = 1$ p.u.

$$\Delta\dot{p} = \frac{J\Omega_0}{T_0}\frac{d\omega}{dt} \tag{2.5}$$

We now recognise that

$$\frac{J\Omega_0}{T_0} = 2\frac{\frac{1}{2}J\Omega_0^2}{T_0\Omega_0} = T_a \tag{2.6}$$

is the starting time, that is the time necessary to the machine to reach the rated speed starting from standstill, without load and with a constant accelerating torque equal to the nominal one. T_a is also the double of the inertia constant (H) that is the time necessary to a machine to reach the nominal speed starting from standstill, without load and with a constant accelerating power. So we can write

$$\Delta\dot{p} = T_a\frac{d\omega}{dt} \tag{2.7}$$

$$\Delta\dot{p} = 2H\frac{d\omega}{dt} \tag{2.8}$$

H, or T_a, is an important parameter for a generating group, because it synthesizes how the angular speed will vary after a power disturbance. A typical value for H for synchronous generator is in the range of 4 to 8 seconds, depending on the type of the machine (salient poles or not), but varying very little with the rated power of the machine.

2.5 Wind farm inertia emulation

As said before, to emulate inertia we can act on DC link voltage and turbine speed. Firstly two control methods ([12], [11]) to use the electrical energy of the DC link are shown, then a method to draw energy from the rotors ([12]).

2.5.1 DC capacitor inertia support, DC voltage droop

We can deliver more ore less energy to the grid modifying the DC link voltage as a synchronous generator naturally modifies his rotational speed losing or taking energy with respect to the grid. We can do this through the power electronic converter and to emulate inertia we have to act like a synchronous generator, which means following a law like the one expressed in equation (2.8), law which now we rewrite with reference to our new system

$$p_{wf} - p_g = 2H_{dc}\frac{df}{dt} \tag{2.9}$$

With reference to the figure 2.1, f is the on shore grid frequency (in p.u.), P_{WF} is the power from the wind farm and P_G is the power delivered to the main grid. We have now to find H_{dc}(inertia constant of our system) that is the key parameter of our action and that can be compared to the one of a traditional synchronous machine even if it has a different origin. H_{dc} has his origin in a control technique, H is a property of the electrical generator.

Modelling DC link as a capacitor we can write the following balance: the time derivative of the electrostatic energy equals the difference between the input and output power of the DC link

$$CV_{DC}\frac{dV_{DC}}{dt} = P_{WF} - P_G \tag{2.10}$$

dividing by P_b, base power, naming $\frac{CV_{DCn}^2}{P_b} = T_c$, we can now rewrite the expression using per unit values. Small case letter indicates p.u. values

$$T_c v_{dc}\frac{dv_{dc}}{dt} = p_{wf} - p_g \tag{2.11}$$

We can now make a parallelism between the former equation and (2.8) which was stated for a synchronous machine, $p_{wf} - p_g$ can be seen as Δp of (2.8), so p_m corresponds to p_{wf} and here it is considered constant, p_e corresponds to p_g. But there are some considerations to take into account

- p_e varies according to the grid requirement, and so causes a ω variation, here p_g is controlled by the electronic converter and so v_{dc} is under control.

- p_g can be controlled very quickly through power electronic converter;

- a ω variation for a synchronous machine is to avoid, here a change in DC link voltage is not to avoid, but the mean to support the grid.

Taking in mind these considerations we can combine equation (2.9) with (2.11) writing

$$T_c v_{dc}\frac{dv_{dc}}{dt} = 2H_{dc}\frac{df}{dt} \tag{2.12}$$

we now integrate two sides over time

$$\int_{v_{dc0}}^{v_{dc}} T_c v_{dc}\frac{dv_{dc}}{dt}\,dt = \int_{f_0}^{f} 2H_{dc}\frac{df}{dt}\,dt \tag{2.13}$$

$$\frac{T_c(v_{dc}^2 - v_{dc0}^2)}{2} = 2H_{dc}(f - f_0) \tag{2.14}$$

where v_{dc0} and f_0 are the equilibrium point, typically the nominal value of the DC link voltage and the grid frequency. Considering that DC link voltage can vary only within a small range we can linearise the equation around the equilibrium point

$$T_c v_{dc0}\Delta v_{dc} = 2H_{dc}\Delta f \tag{2.15}$$

considering that $\Delta v_{dc} = v_{dc} - v_{dc0}$ we say

$$v_{dc} = \frac{2H_{dc}\Delta f}{T_c v_{dc0}} + v_{dc0} \qquad (2.16)$$

If we vary v_{dc}, whose variation will result in an output power variation, according to this equation the DC link will have an inertia response with inertia constant H_{dc}. Looking at the expression we can recognise that is a droop control of parameter $K_{dc} = \frac{2H_{dc}}{T_c v_{dc0}}$ and write the following law to control v_{dc}

$$v_{dc} = K_{dc}\Delta f + v_{dc0} \qquad (2.17)$$

We can control the value of K_{dc} in order to obtain various values of H_{dc}

$$H_{dc} = \frac{K_{dc}T_c v_{dc0}}{2} \qquad (2.18)$$

In figure 2.2 we can see the graph representation of (2.17).
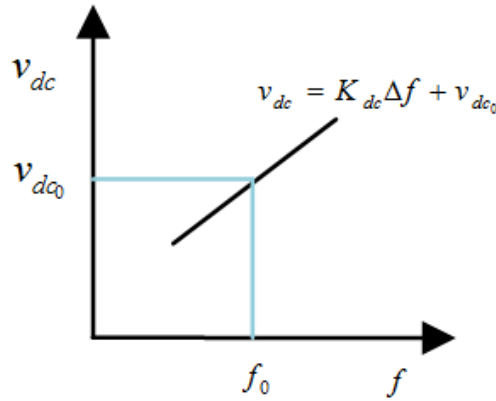
Figure 2.2: Representation of (2.17)

We name this kind of equation, where a positive deviation of the frequency generates a positive variation of the control variable, "droop" since this is the term used in literature. But for traditional power plant, where the control variable is the output power, the name "droop" is referred to a negative slope, id est a frequency negative deviation causes an increment of the power set point, as we can see from figure 2.3. The control variable is in the x-axis because traditionally

is represented in that way. Instead a positive slope curve, as the one in figure 2.2 would be traditionally named "compound". But here we use the term now common in literature.
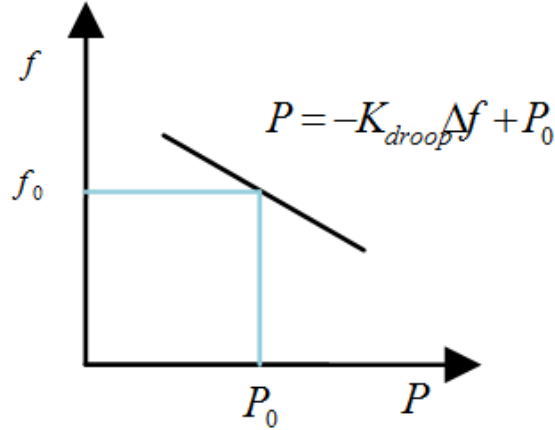
Figure 2.3: Traditional power plants droop control

2.5.2   DC capacitor inertia support, method two

Another control method to emulate inertia can be found [11]. We start from (2.14) which we found before. Let's recall it

$$\frac{T_c(v_{dc}^2 - v_{dc0}^2)}{2} = 2H_{dc}(f - f_0) \tag{2.19}$$

Now we don't linearise the equation around the equilibrium point as previously done, we just reorganise it

$$\frac{T_c v_{dc}^2}{2} = 2H_{dc}f + \frac{T_c v_{dc0}^2}{2} - 2H_{dc}f_0 \tag{2.20}$$

from this equation we can find v_{dc}

$$v_{dc} = \sqrt{\frac{4H_{dc}f}{T_c} - K_2} \tag{2.21}$$

with $K_2 = \frac{4H_{dc}f_0}{T_c} - v_{dc0}^2$. So, we have found the rule to regulate the voltage of the DC link in order to obtain an inertia response. Now we have to find the

expression of H_{dc}. We start again from the (2.14) and we manipulate the first term in order to put in evidence Δv_{dc}. Let's write all the passages. We start multiplying and dividing the left side of (2.14) by v_{dc0}^2

$$v_{dc0}^2 \frac{T_c(v_{dc}^2 - v_{dc0}^2)}{2v_{dc0}^2} = 2H_{dc}(f - f_0) \tag{2.22}$$

than we add and subtract v_{dc0}^2 and $2v_{dc}v_{dc0}$ in the expression between brackets

$$\frac{v_{dc0}^2 T_c}{2} \frac{(v_{dc}^2 - 2v_{dc}v_{dc0} + v_{dc0}^2 + 2v_{dc}v_{dc0} - 2v_{dc0}^2)}{v_{dc0}^2} = 2H_{dc}(f - f_0) \tag{2.23}$$

we recognise that

$$\frac{v_{dc0}^2 T_c}{2} \left[\frac{(v_{dc} - v_{dc0})^2}{v_{dc0}^2} + \frac{2(v_{dc} - v_{dc0})}{v_{dc0}} \right] = 2H_{dc}(f - f_0) \tag{2.24}$$

and then

$$\frac{v_{dc0}^2 T_c}{2} \left[\left(\frac{(v_{dc} - v_{dc0})}{v_{dc0}} + 1 \right)^2 - 1 \right] = 2H_{dc}(f - f_0) \tag{2.25}$$

and so naming $v_{dc} - v_{dc0} = \Delta v_{dc}$ and $f - f_0 = \Delta f$

$$\frac{T_c v_{dc0}^2}{2} \left[\left(\frac{\Delta v_{dc}}{v_{dc0}} + 1 \right)^2 - 1 \right] = 2H_{dc}(\Delta f) \tag{2.26}$$

finally we find H_{dc}

$$H_{dc} = \frac{\frac{T_c v_{dc0}^2}{2} \left[\left(\frac{\Delta v_{dc}}{v_{dc0}} + 1 \right)^2 - 1 \right]}{2(\Delta f)} \tag{2.27}$$

It results that H_{dc} depends on Δv_{dc} and not only on v_{dc0} as found with the previous method (2.18). This is due to the fact that we choose not to linearise the (2.14). In such a way we take into account that the energy storable with some increase of v_{dc} does not depend linearly on the final value of v_{dc}.
From (2.27) it turns out that we can also choose the value of the inertia constant with this method. This is true, but we need also to remember the limits of the control system. In fact as we can see from (2.27) the value of H_{dc} depends on the grid voltage deviation. It is said that $\mp 5\ \%$ is an acceptable range of DC voltage variation [11]. Moreover we had to take also into account that higher values of the inertia constant imply high active power output, so we need also to take into account that we need to respect the converter limits.
Let's now compute a reasonable value for H_{dc}. To do this we need the actual

capacitance of the DC link. We choose $C = 15 \ mF$. This capacitance takes into account the capacitance of the DC link cables which varies with the extension of the plant and the added capacitance by added capacitor near the VSC stations. This value is chosen considering that it permits [11] a small voltage variation during the inertia supplying process. Considering a system with nominal DC voltage $V_{dcn} = 367 \ kV$ and nominal power $P_b = 300 \ MW$ (this values will be also used in section 4), this capacitance supplies a "natural" inertia constant equal to

$$\frac{T_c}{2} = \frac{1}{2}\frac{CV_{DCn}^2}{P_b} = 3.375 \ s \tag{2.28}$$

At this point we can consider a frequency variation of 2 % (a value acceptable during transients), and a maximum DC voltage variation of 5 %. We can now compute the value of H_{dc} with this assumptions by (2.27), which results

$$H_{dc} \approx 12 \ s \tag{2.29}$$

2.5.3   Inertia support from kinetic rotor energy

In a DFIG the power output is controlled by the electronic converter, we can draw more electric power than the one that is coming from the wind slowing down the rotating masses or we can deliver to the grid less power than the one coming from the wind accelerating the rotors. Angular speed ω_d will vary according to the law derived in section 2.4 (the power imbalance equals the time derivative of the kinetic energy, the equation is in p.u.)

$$2H_t\omega_d\frac{d\omega_d}{dt} = p_{wind} - p_{wf} \tag{2.30}$$

H_t is the inertia constant of the machine calculated in the usual way (rated kinetic energy divided by rated power). If we have more than one machine, like in the system in figure 2.1, H_t would be the equivalent inertia constant for all the machines. It is reported that wind turbine inertia constants are in the range of 4-6 seconds [9]. These values are comparable with the ones of classical synchronous generators that present inertia constants in the range 3-8 seconds, depending on the type of generator. Moreover, with wind turbine, since we can control power output we can decide how much energy deliver to the grid. This is important since with variable speed wind turbines we can vary the velocity in the range between 0.7 and 1.3 p.u., instead synchronous generator are limited in the range of $47.5 - 52.5Hz$ id est $0.95 - 1.05$ p.u. This means that with wind turbines we can deliver much more kinetic energy to the grid. Nevertheless we have to

underline that doing this the machine will slow down to a velocity where is much less efficient (see chapter 5) so after the transient we need a procedure to recover the correct angular speed.

Coming back to equations, if we approximate the rotor speed as a constant equal to the nominal one ($\omega_d = 1 \ p.u.$) we found the equation (2.8).

The situation is similar to the one we dealt with before, described in section 2.5.1. In fact (2.30) is similar to (2.9), so as done before, since we can modify the wind farm power output in a very fast way and considering p_{wind} constant, we can introduce another inertia constant H_w and we write the following equation where f is the grid frequency.

$$2H_t \omega_d \frac{d\omega}{dt} = 2H_w \frac{df}{dt} \tag{2.31}$$

we now integrate two sides over time and we linearise around the equilibrium point obtaining

$$H_t \omega_{d0} \Delta \omega_d = H_w \Delta_f \tag{2.32}$$

From this equation we can see that the amount of inertia H_w given to the grid depends on ω_{d0} and the value of the rotor speed variation. So ω_d is the variable that influences the inertia we are able to supply, as it was the DC link voltage for the VSC. The difference here is that we do not directly control ω_d, but the power output of the wind farm as explained later in the chapter dedicated to DFIG. This does not permit to elaborate (2.32) to arrive at a formula similar to (2.16).

2.6 Inertia support with time derivative of frequency

Here we explain another method to supply inertia. Probably this is the most "natural" to think and it is proposed by some articles (as [9]), but has the inconvenience of the measurements of the time derivative of the grid frequency. This can be troublesome because can cause noise amplification.

As explained in sections 2.2 and 2.4 for traditional synchronous generators inertia is an "embedded" property. They sense a power imbalance and they react with a change in rotating speed. Instead if the system is interfaced with power electronics, the behaviour depends on the control system. We can imagine to vary the output power according to the time derivative of the grid frequency; if we act in this way we will emulate an inertia behaviour but it is not strictly the same as classical inertia because we start from a frequency time derivative to produce a change in the output power, instead of naturally mutating the rotational speed after a power imbalance. Let's now look at figure 2.4.

$$P_{wf} = P_{wf_0} + \Delta P_{wf}$$

$$P_{sg} = P_{sg_0} + \Delta P_{sg}$$

Power system

$$P_{load} = P_{load_0} + \Delta P_{load}$$
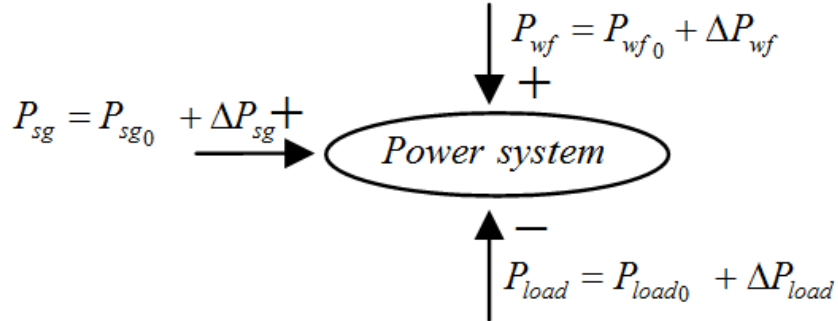
Figure 2.4: Schematic representation of the power system under study

P_{sg} is the traditional power plant power production, P_{wf} is the wind farm power production and P_{load} is the power drawn by loads. Droop regulators and other regulator systems of traditional power plants are not taken into account, so in the following $\Delta P_{sg} = 0$. The quantities with subscript 0 are the equilibrium point quantities, so we can say that

$$P_{sg_0} + P_{wf_0} - P_{load_0} = 0 \tag{2.33}$$

considering this we can draw the scheme in figure 2.5

$$\Delta P_{wf}$$

$$\Delta P_{sg}$$

Power system

$$\Delta P_{load}$$
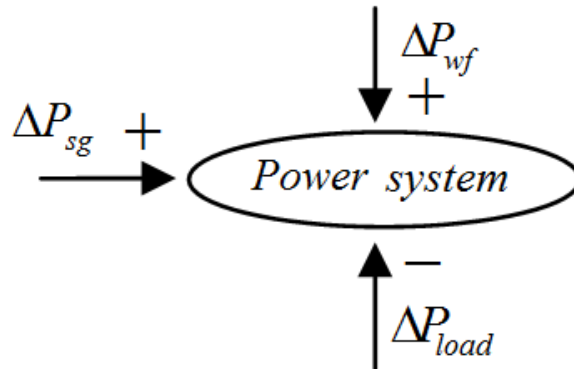
Figure 2.5: Schematic representation of the power system under study taking into account only power variations

Now, if we vary the power output of our wind farm (P_{wf}) according to

$$\Delta P_{wf} = -K_d \frac{d\Delta f}{dt} \tag{2.34}$$

where K_d is a gain to be selected according to the plant properties, we can emulate inertia. To demonstrate this let's consider the scheme in figure 2.6.
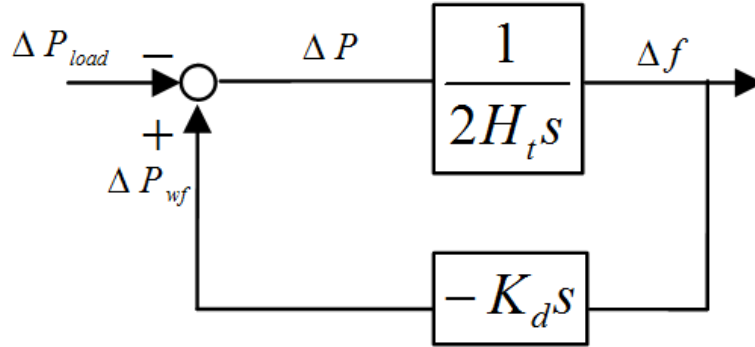
Figure 2.6: Inertia emulation scheme

The traditional power plants are represented by an inertia constant H_t and their power output control is neglected. It is also represented (2.34). Now we computed the transfer function between the load power variation and the frequency variation and we obtain

$$\frac{\Delta f}{\Delta P_{load}} = \frac{-1}{(K_d + 2H_t)s} \tag{2.35}$$

We can note from the above equation that the term K_d is summed with the grid inertia constant. So we can say that we made some synthetic inertia through controlling power output according to the time derivative of the frequency.

Chapter 3

VSC-HVDC connection lcl

3.1   Introduction

Voltage source converter (VSC) HVDC is a solution to connect large wind farms, especially off-shore, to the main grid. We can see in figure 3.1 a typical scheme of these power plants. VSC-HVDC resolves some issues of long AC cables such as high reactive power consumption and high losses. But this connection decouples the frequency of the off-shore wind farm from the grid frequency. Converters are typically made with IGBTs modulated with PWM method. In the figure 3.1 we can see a scheme of the system. Reactors and shunt capacitors work as filters for high order harmonics produced by the PWM converter.
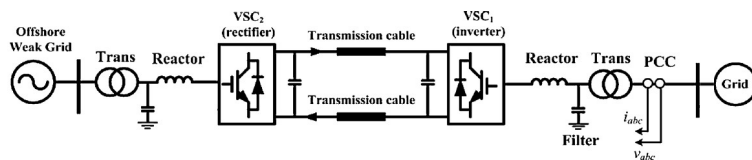
Figure 3.1: Single line diagram of the grid side VSC and DC link

We will now describe the system in detail, we will develop a model and we will try to develop a control system. This attempt is not well concluded since the control system we choose, adapting it from the one proposed by many articles (such as [11] and [12]) is not suitable for a system considering also reactor and filter capacitor and not measuring grid voltages. The articles that deal with synthetic inertia present a simpler model of the system, neglecting the filter capacitor and considering the VSC connected to the grid through an inductor (a transformer) and moreover measuring grid voltages. In the next chapter (4) we will develop in detail such a model. Here we report the attempt to consider the complete system.

3.2   System model

Since we want to investigate the inertia support given by the HVDC link by means of electrostatic energy accumulated in the equivalent capacitance of the HVDC link, we simplify the system modelling the off-shore VSC as a constant power source ($P_{wf} = const$). In the following the off-shore grid and VSC are modelled as a controlled current source with equation $i_{wf} = P_{wf}/v_{dc}$, that is a constant DC power source. In figure 3.2 we can see the single line diagram of the system under study.
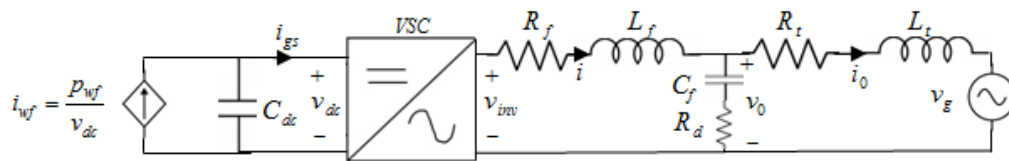
Figure 3.2: Single line diagram of the grid side VSC and DC link

3.2.1   AC side

The two sides of the HVDC link present the same AC circuit made up of a phase reactor (L_f), a shunt capacitor (C_f) and a transformer (L_t). In figure 3.3 we can see the circuital representation of this system, where are also represented the resistors which model the losses in the transformer (R_t) and in the phase reactor (R_f). The capacitor is assumed as ideal, the series resistance R_d is there to avoid resonance phenomena as explained later. The grid is modelled as a constant voltage source v_g.
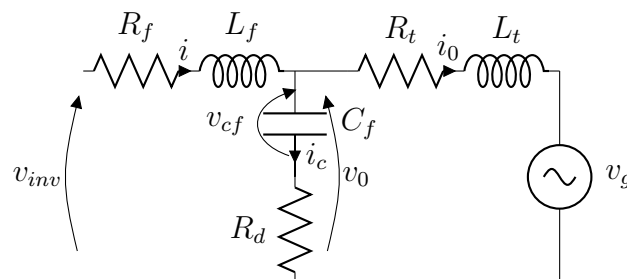
Figure 3.3: Circuital phase representation of the connection of the VSC with the grid

The differential equations for the circuit in figure 3.3 are

$$\frac{di_0}{dt} = (v_{cf} + R_d(i - i_0) - v_{grid} - R_t i_0)/L_t \tag{3.1a}$$

$$\frac{di}{dt} = (v_{inv} - v_{cf} - R_d(i - i_0) - R_f i)/L_f \tag{3.1b}$$

$$\frac{dv_{cf}}{dt} = (i - i_0)/C_f \tag{3.1c}$$

where L_f and L_t are the service inductances, they already take into account mutual coupling between phases.

3.2.2 DC link

The DC link is modelled as a capacitance (C_{dc}) which includes the cable capacitance and the capacitance added with DC capacitors in order to increase the overall one and so to be able to supply synthetic inertia to the grid. With reference to figure 3.2 we can write the following equation

$$\frac{dv_{dc}}{dt} = \frac{(i_{wf} - i_{gs})}{C_{dc}} \tag{3.2}$$

3.2.3 Link between AC and DC side

We choose to measure the voltage v_0, the current i_0 and i. Grid voltage is not measured. To compute delivered power (p_{ac}) we use v_0 and i_0, so $p_{ac} = v_0 i_0$. It could also be used i, but this doesn't change so much the things. i_0 and i differs only for the current that flows through the capacitor filter which is up to the 5% of the nominal value. The power electronic converter is assumed lossless and the losses on R_f, R_t and R_d are neglected. So the link between DC and AC side can be made by a power balance. This achievement will be used in the control system.

$$p_{ac} = p_{dc} \tag{3.3}$$

Since $p_{dc} = v_{dc} i_{gs}$ we can link AC power output with DC grid side current (i_{gs}) .

$$i_{gs} = \frac{p_{ac}}{v_{dc}} \tag{3.4}$$

3.3   Values and per unit transformation

We decide to study a system of nominal power of $300MVA$ and AC line to line
voltage of $\sqrt{3}\,150 \approx 260kV$ id est a phase voltage of $150\,kV$. Nominal DC voltage
is chosen equal to $\sqrt{2}\sqrt{3}\,150\,kV$ and the DC total capacitance (the one given
by cables and the added one) is equal to $15mF$ (see the last part of section 2.5.2
for more details on this value). The value of L_t and R_t are typical value for a
transformer of $300MVA$ rated power, C_f, R_d, L_f and R_f are chosen as described
section 3.3.1.

The system will be studied in p.u. quantities. Chosen reference values are listed

Table 3.1: Reference values

Parameter	Value
A_b	$300\ MVA$
V_b	$\sqrt{3}\ 150\ kV$
w_b	$2\pi50\ rad/s$
$I_b = \dfrac{A_b}{V_b}$	$1.1547\ kA$
$Z_b = \dfrac{V_b}{I_b}$	$225\ \Omega$
$L_b = \dfrac{Z_b}{w_b}$	$716.2\ mH$
$C_b = \dfrac{1}{Z_b w_b}$	$14.15\ \mu F$

Table 3.2: Physical system parameters. L_f: filter inductance, R_f: resistance of
the filter inductance, C_f: filter capacitance, R_d: resistance series connected to the
filter capacitance to avoid resonant problems, L_t, R_t: inductance and resistance
of the transformer

Parameter	Value (p.u.)
L_f	0.04
R_f	0.002
L_t	0.1198
R_t	0.005
C_f	0.07
R_d	0.119
C_d	1060

in table 3.1. In table 3.2 we list the values of all the elements of the system. The
choice of R_d and C_f are explained in the section 3.3.1.

3.3.1   AC side resonance problem

This scheme of VSC is typical for power electronics devices of any power level. Generally the inductances are chosen in order to give a total voltage drop of less than 10% [13]. In our case, since the rated power of the plant is huge (300 MVA), the transformer itself will have a voltage drop of 12% at rated current. For this reason the phase reactor inductance is chosen not much high. The filter capacitor is designed in order to absorb reactive power equal to 5% of the nominal power. The value of the phase reactor losses is derived taking into account that such devices have a quality factor ($\frac{wL}{R}$) of a value around 20. Values are listed in table 3.2.

At this point we have to find the frequency response of the system in order to understand if some resonant phenomena can take place. We compute the transfer function (firstly neglecting resistances) between the input voltage (v_{inv}) and the output current (i_0). Once we've made the circuit passive we can write the transfer function. The equation is written in $p.u.$.

$$\frac{i_{0(s)}}{v_{inv(s)}} = \frac{w_b}{s(s^2 L_f L_t C_d / w_b^2 + (L_t + L_f))} \tag{3.5}$$

We can see from the equation that without considering the resistances there is a resonant pick at a frequency equal to $\sqrt{\frac{L_t + L_f}{L_t L_f C_d}}$ which in our case means 1.19 kHz. The resonant pick, according to [13], has to be placed at least the half of the switching frequency and at least ten times bigger than the fundamental frequency. If figure 3.4 we can see the plot of the transfer function in 3.5 and below (figure 3.5) the plot of the module of the transfer function between the input voltage (v_{inv}) and the output current (i_0) considering also R_t and R_f (the expression is written in (3.6)). We can note the two plot are similar. One difference is that the second doesn't go to infinite at resonant frequency, but this cannot be noted from the graphs for numerical reasons.

$$\frac{i_{0(s)}}{v_{inv(s)}} = \frac{1}{(a_3 s^3 + a_2 s^2 + s + a_0)} \tag{3.6}$$

with

$$a_3 = \frac{C_f L_f L_t}{w_b^3} \tag{3.7}$$

$$a_2 = \frac{C_f L_f R_t + C_f L_t R_f}{w_b^2} \tag{3.8}$$

$$a_1 = \frac{C_f R_f R_t + L_f + L_t}{w_b} \tag{3.9}$$

$$a_0 = R_f + R_t \tag{3.10}$$
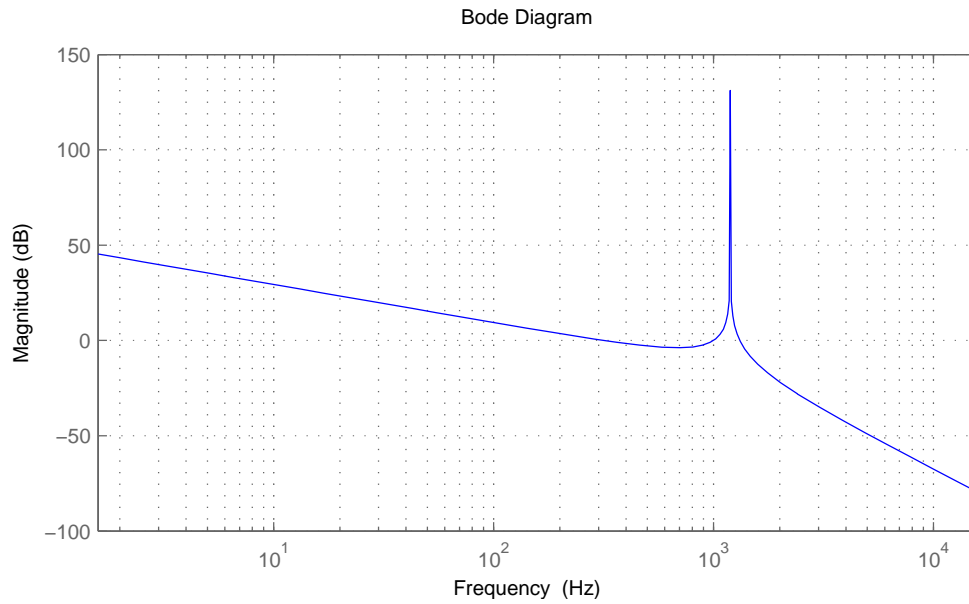
Figure 3.4: Bode plot of the magnitude of the transfer function between the input voltage (v_{inv}) and the output current (i_0) neglecting R_f and R_t (3.5)
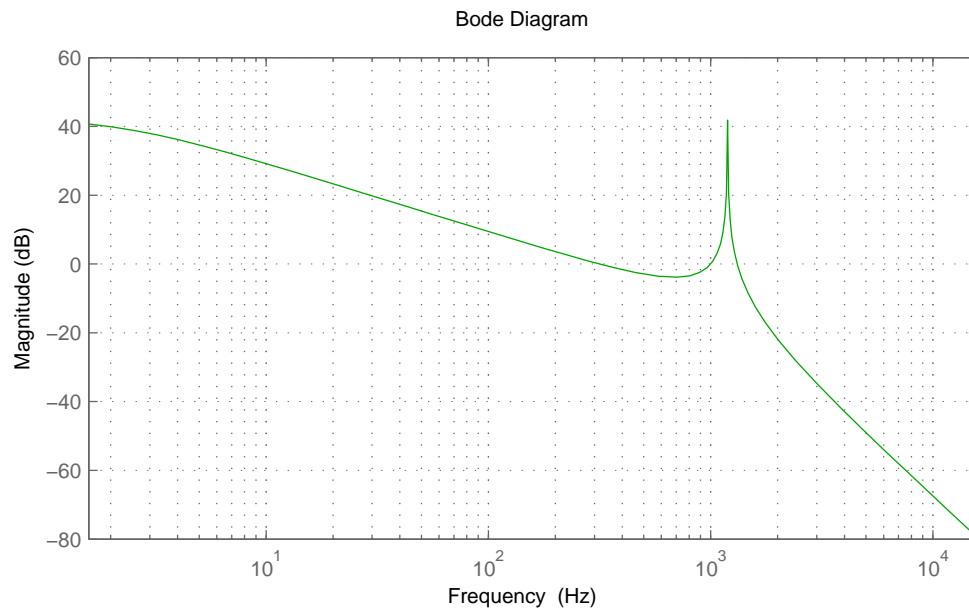
Figure 3.5: Bode plot of the magnitude of the transfer function between the input voltage (v_{inv}) and the output current (i_0) considering R_f and R_t

The resonant frequency is at $1.19kHz$ and the constrains are almost reached, but we cannot accept a circuit like this since the resonant peak is much to high. To deal with this issue we have to add a resistance R_d in series to the filter capacitor. We choose R_d equal to one third of the capacitive impedance of the capacitor filter C_f at the switching frequency, that is

$$R_d = \frac{1}{3C_d 2\pi f_{sw}} \tag{3.11}$$

where $f_{sw} = 2\ kHz$ is the switching frequency. Adding this resistance the module of the transfer function between the input voltage (v_{inv}) and the output current (i_0) becomes the one in figure 3.6. In this way we avoid to have a dangerous resonance peak.
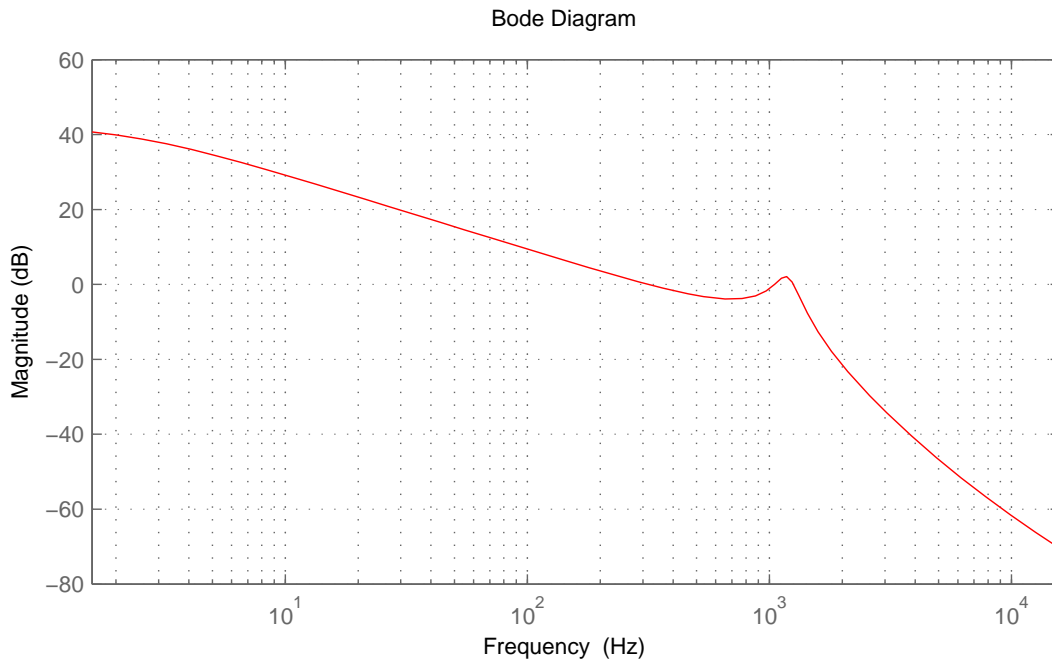
Figure 3.6: Bode plot of the magnitude of the transfer function between the input voltage (v_{inv}) and the output current (i_0) considering R_f, R_t and R_d
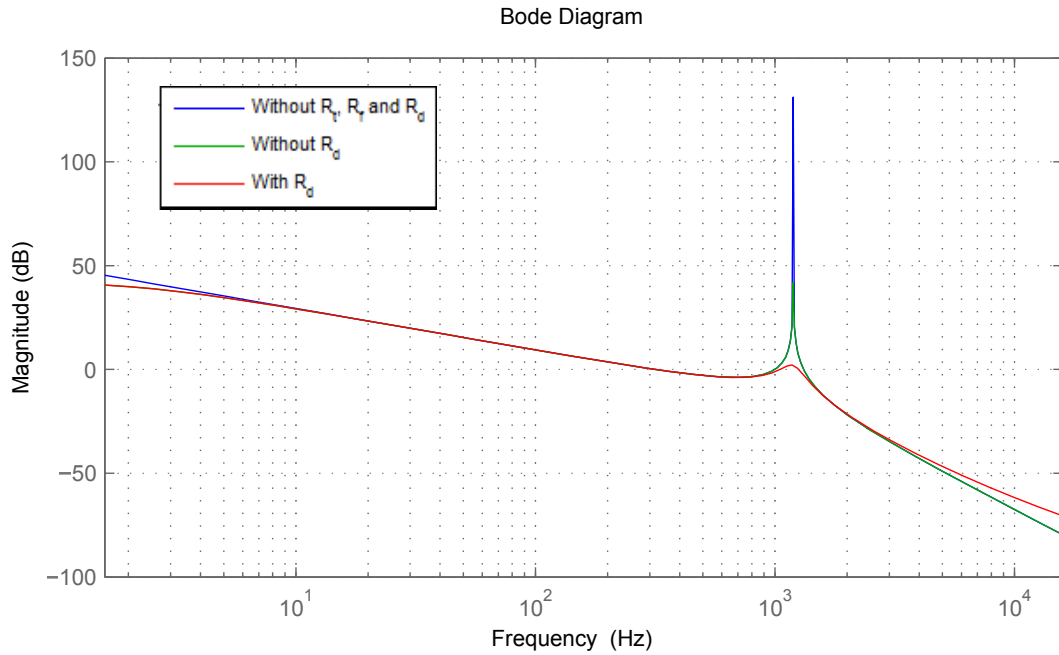
Figure 3.7: Bode plots of the magnitude of the transfer function between the input voltage (v_{inv}) and the output current (i_0) for the the three different cases

In figure 3.7 we sum up the Bode plots of figures 3.4, 3.5 and 3.6. We can note that with the introduction of R_d the resonant peak is very low.

3.4   Vector control attempt

In this chapter we try to investigate if the control system based on two nested loops in dq reference frame with proportional integral regulators can be applied to a complete lcl system without measuring the grid voltage. This will result in a failure, to run the system without the grid voltage measurement is necessary to change the control system. We found some suitable control systems such as the one proposed in [14] but the analysis of such a system may be object of a future work.

The angle for the dq transformation in the real system will be retrieved from the measured voltage (in this case $\bar{v}_0$) by a phase locked loop (PLL) as explained in section 4.5. Here this system is not taken into account and we assume to measure this angle from the system in an ideal way. So, we can transform the equations in 3.1 in dq axes reference frame. Moreover we transform the equations in 3.1 in p.u. This leads to the following equations

$$\frac{di_d}{dt} = (v_{inv_d} - v_{0d} - R_f i_d + wL_f i_q)\frac{wb}{L_f} \tag{3.12a}$$

$$\frac{di_q}{dt} = (v_{inv_q} - v_{0q} - R_f i_q - wL_f i_d)\frac{wb}{L_f} \tag{3.12b}$$

$$\frac{dv_{cf_d}}{dt} = (i_d - i_{0_d} + wC_f v_{cf_q})\frac{wb}{C_f} \tag{3.12c}$$

$$\frac{dv_{cf_q}}{dt} = (i_q - i_{0_q} - wC_f v_{cf_d})\frac{wb}{C_f} \tag{3.12d}$$

$$\frac{di_{0_d}}{dt} = (v_{cf_d} + R_d(i_d - i_{0_d}) - v_{g_d} - R_t i_{0_d} + wL_t i_{0_q})\frac{wb}{L_t} \tag{3.12e}$$

$$\frac{di_{0_q}}{dt} = (v_{cf_q} + R_d(i_q - i_{0_q}) - v_{g_q} - R_t i_{0_q} - wL_t i_{0_d})\frac{wb}{L_t} \tag{3.12f}$$

$$\frac{dvdc}{dt} = (-i_{gs} + i_{wf})\frac{wb}{C_{dc}} \tag{3.12g}$$

Power can be expressed in this way

$$p = v_{0_d} i_{0_d} + v_{0_q} i_{0_q} \tag{3.13a}$$

$$q = v_{0_q} i_{0_d} - v_{0_d} i_{0_q} \tag{3.13b}$$

since in our control system v_{0_q} is zero (we suppose to be always aligned with our control system to the voltage v_0), we can say that d current is devoted to the real power control and q current to the reactive power control.

We can see in figure 3.8 and 3.9 the block schemes of the system on d and q axes. Let's now analyse the current loops: they are the same on both axes and they are coupled each others. In the figures (3.8 and 3.9) we can also see feedback decoupling terms. We compute the value of the inner PI controller (listed in table 3.3), that are the same on d and q axes since the inner loop is equal. We use the method explained in appendix A. We choose a passing band equal to $100\ Hz$ since the system has to be much slower than the sampling frequency.
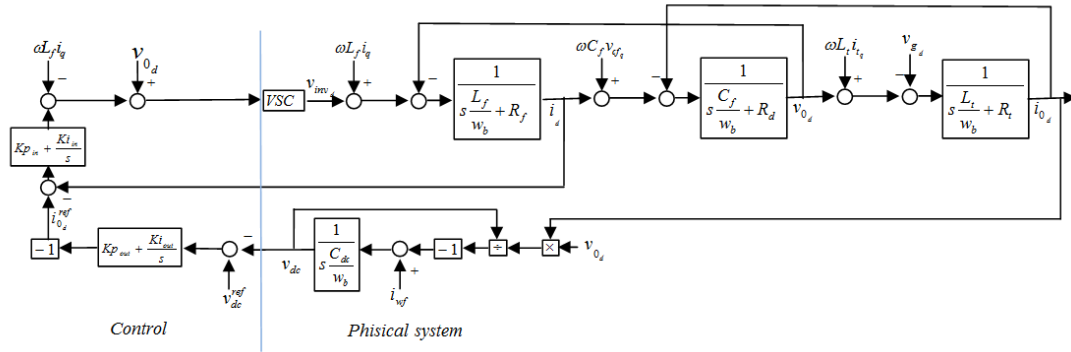
Figure 3.8: System block diagram on d axis
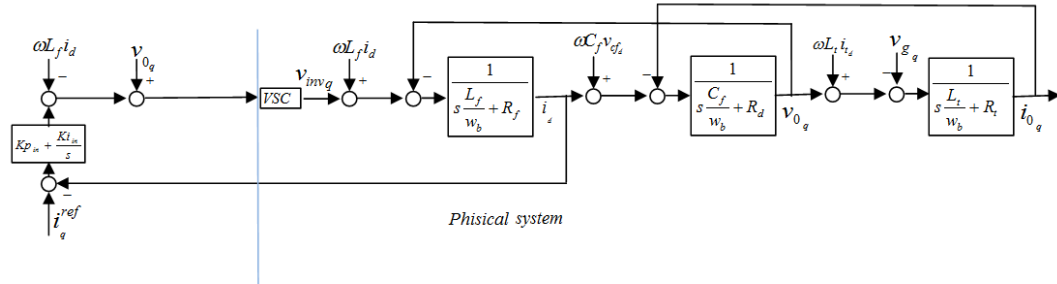
Figure 3.9: System block diagram on d axis
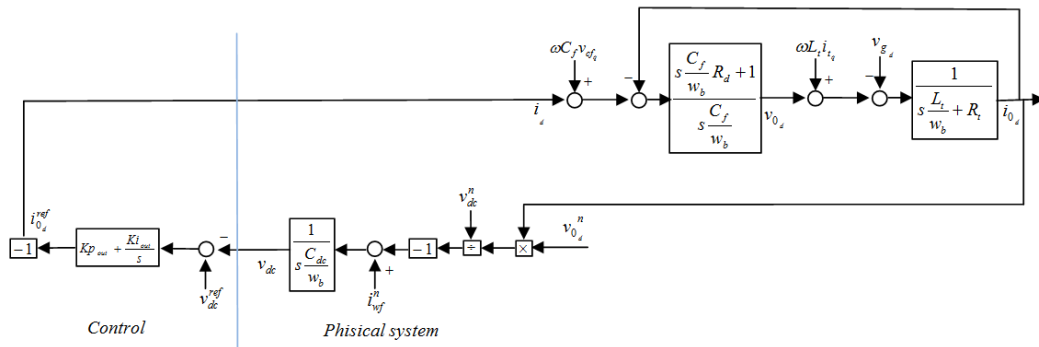
Figure 3.10: Linearised system block diagram of the outer loop on d axis

Now we have to compute the parameters for the controller for the outer loop on d axis. The outer loop on q axis does not exist since we set $i_q^{ref} = 0$. From (3.13)b and remembering that $v_{0_q} = 0$, we can see that to avoid exchanging reactive power i_{0_q} has to be zero. But in our control system we don't control the current $\bar{i}_0$, but we control the current i. So we set as a reference $i_q^{ref} = 0$ even

if we know that this will cause a reactive power flow from the grid to the filter capacitor, but at this stage of the work this is not considered a problem since the reactive power consumption is low and we are mainly interested in active power flow.

Now we have to find the value of the parameters of the outer controller on d axis. Looking at figure 3.8 we can note that the loop isn't linear. So we had to linearise it. We assume as constant and equal to the nominal value the DC link voltage in the division to compute i_{gs} and also constant and equal to the nominal value the voltage v_0. Also the current i_{wf} is assumed equal to the nominal value. We can see such assumptions in figure 3.10. In this scheme we can also note the inner loop assumed as a unit gain. This assumption is possible since the two loops has to have very different passing bands: the inner one has to be much faster than the outer one. Looking at figure 3.10 it is clear the outer loop. We apply again the method in appendix A to find the controller parameters. In table 3.3 the values of the parameter of the controllers. With reference to the method in A we choose a passing band of 1 Hz for the outer loop on d axis.

Table 3.3: PI controller parameters

Parameter	Value
Kp_{in}	0.0784 p.u.
Ki_{in}	9.96 p.u./s
Kp_{out}	0.0143 p.u.
Ki_{out}	2.7910^{-3} p.u./s

At this point we find the equilibrium point with the Newton-Raphson method and than we made find the eigenvalues. The eigenvalues for this attempt are listed in table 3.4. As we can see there are two eigenvalues positive, so the system is not stable. We made some other attempts changing the controller parameters, but we weren't able to find all eigenvalues negative, here we don't report all the values.

Table 3.4: Eigenvalues of the linearised system around the equilibrium point. Two of them are positive, the system isn't stable

Parameter	Value (rad/s)
λ_1	$-162.5189 + 3.7396i \ 10^3$
λ_2	$-162.5189 - 3.7396i \ 10^3$
λ_3	$-162.5189 + 3.1112i \ 10^3$
λ_4	$-162.5189 + 3.1112i \ 10^3$
λ_5	-462.5180
λ_6	$140.8500 \ 10^{-3}$
λ_7	$4.2387 \ 10^{-3}$
λ_8	-462.5219
λ_9	-169.2329
$\lambda_1 0$	-169.2314

Chapter 4

VSC-HVDC connection

4.1 Introduction

In this chapter we want to investigate the inertia support given by the HVDC link by means only of electrostatic energy accumulated in the equivalent capacitance of the HVDC link. So we simplify the system modelling the off-shore VSC as a constant power source ($P_{wf} = const$). In the following the off-shore grid and VSC are modelled as a controlled current source with equation $i_{wf} = Pwf/v_{dc}$, that is a constant DC power source. Moreover we neglect the reactor and the shunt capacitor since they are not important for inertia emulation concept.

4.2 System modelling

In figure 4.1 we can see the single line diagram of the system under study. Let's now write the equations.
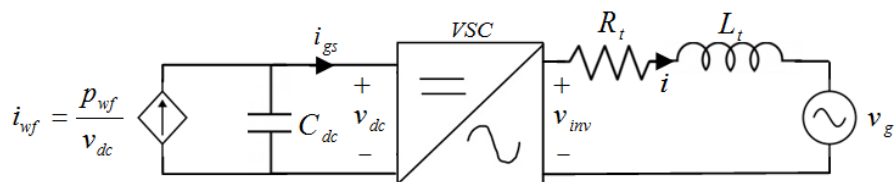
Figure 4.1: Single line diagram of the grid side VSC and DC link

4.2.1   AC side

L_t and R_t are the transformer inductance and resistance, v_g is the grid voltage assumed stiff and v_{inv} is the first harmonic of the voltage at the output of the converter.We write the equations for the three phase system where L is the service inductance that already takes into account the mutual coupling between phases.

$$v_{inv_a} = v_{g_a} + L\frac{di_a}{dt} + Ri_a \tag{4.1a}$$

$$v_{inv_b} = v_{g_b} + L\frac{di_b}{dt} + Ri_b \tag{4.1b}$$

$$v_{inv_c} = v_{g_c} + L\frac{di_c}{dt} + Ri_c \tag{4.1c}$$

We now transform these equations by Park Transformation on rotating d and q axis (in appendix A the transformation matrix used). d axis is aligned with the grid voltage through a phase locked loop (PLL). This device will be described in section 4.5.

$$v_{inv_d} = v_{g_d} + L\frac{di_d}{dt} + Ri_d - \omega Li_q \tag{4.2a}$$

$$v_{inv_q} = v_{g_q} + L\frac{di_q}{dt} + Ri_q + \omega Li_d \tag{4.2b}$$

The system is assumed symmetrical and balanced and so no zero component shows up.

4.2.2   DC link

The DC link is modelled as a capacitance (C_{dc}) which includes the cable capacitance and the capacitance added with DC capacitors in order to increase the overall one and so to be able to supply synthetic inertia to the grid. With reference to figure 4.1 we can write the following equation

$$\frac{dv_{dc}}{dt} = \frac{(i_{wf} - i_{gs})}{C_{dc}} \tag{4.3}$$

4.2.3   Link between AC and DC side

The converter is assumed as lossless and the resistance R_t is neglected.The link between DC and AC side is made by a power balance. This achievement will be

used in the control system.

$$p_{ac} = p_{dc} \tag{4.4}$$

Since $p_{dc} = v_{dc}i_{gs}$ we can link AC power output with DC grid side current.

$$i_{gs} = \frac{p_{ac}}{v_{dc}} \tag{4.5}$$

4.3 Values and per unit transformation

We decide to study a system of nominal power of $300MVA$ and AC phase voltage of $150kV$. Nominal DC voltage is chosen equal to $\sqrt{2}\sqrt{3}\ 150kV$ and the DC total capacitance (the one given by cables and the added one) equal to $15mF$. The capacitance is chosen high in order to be able to supply synthetic inertia as explained later.
The system will be studied in p.u. quantities. Chosen reference values are listed in table 3.1 here reposted (table 4.1).

Table 4.1: Reference values

Parameter	Value
A_b	$300\ MVA$
V_b	$\sqrt{3}\ 150\ kV$
w_b	$2\pi 50\ rad/s$
$I_b = \dfrac{A_b}{V_b}$	$1.1547\ kA$
$Z_b = \dfrac{V_b}{I_b}$	$225\ \Omega$
$L_b = \dfrac{Z_b}{w_b}$	$716.2\ mH$
$C_b = \frac{1}{Z_b w_b}$	$14.15\ \mu F$

Instead in table 4.2 are reported the p.u. parameter of the system.

We now want to transform the systems equation written previously in per unit. Dividing the equations (4.2) and (4.3) by the reference quantities we obtain

Table 4.2: p.u. parameter of the system

Parameter	Value (p.u.)
$Nominal\ VSC\ power$	1
$Nominal\ AC\ voltage\ (line-to-line)$	1
$Nominal\ angular\ frequency$	1
$Transformer inductance\ L_t$	0.12
$Transformer resistance\ R_t$	0.005
$Nominal\ DC\ voltage\ v_{dcn}$	$\sqrt{2}$
$DC link capacitance\ C_{dc}$	1060

$$v_{inv_d} = v_{g_d} + \frac{L_t}{wb}\frac{di_d}{dt} + R_t i_d - \omega L_t i_q \tag{4.6a}$$

$$v_{inv_q} = v_{g_q} + \frac{L_t}{wb}\frac{di_q}{dt} + R_t i_q + \omega L_t i_d \tag{4.6b}$$

$$\frac{dv_{dc}}{dt} = (i_{wf} - i_{gs})\frac{wb}{C_{dc}} \tag{4.6c}$$

From now on all quantities will be in per unit and the dot over the letter will be omitted. We can rewrite these equations in the form of the state space model

$$\frac{di_d}{dt} = (v_{inv_d} - v_{g_d} - R_t i_d + \omega L_t i_q)\frac{wb}{L_t} \tag{4.7a}$$

$$\frac{di_q}{dt} = (v_{inv_q} - v_{g_q} - R_t i_q - \omega L_t i_d)\frac{wb}{L_t} \tag{4.7b}$$

$$\frac{dv_{dc}}{dt} = (i_{wf} - i_{gs})\frac{wb}{C_{dc}} \tag{4.7c}$$

These are the differential equation of the system. As we can see two of them are coupled. i_q appears in the equations related to d axis and i_d appears in the one related to q axis. This will be taken into account in the control system.

4.4   Vector Control

As suggested in the literature [11] the control system is made in the dq frame. The inner loops controls the d and q currents through the inductor. The outer control loop on d axis controls the DC voltage, instead the outer one on q axis controls the reactive power output.

This is possible since the phase locked loop (PLL) keeps d axis aligned with grid voltage ($v_{g_q} = 0$) and so we can simplify the expression of the power delivered to the grid in the following manner

$$p = v_{g_d} i_{g_d} + v_{g_q} i_{g_q} = v_{g_d} i_{g_d} \tag{4.8a}$$

$$q = v_{g_q} i_{g_d} - v_{g_d} i_{g_q} = -v_{g_d} i_{g_q} \tag{4.8b}$$

Remembering that, through power electronic converter only real power is exchanged between the DC link and AC side, it becomes clear that the DC voltage is influenced only by the power output and so by the d axis current. These are not the only possibilities for the outer loop. As said in [11] instead of giving a DC voltage reference we can directly control power output setting a power reference. Instead with the loop on q axis we can control the voltage at PCC (if it is not stiff as in this case) since the converter is coupled with the grid mainly by an inductor (resistance very small compared with the inductance).
In the following studies the outer controller on q axis is not considered. This because the reactive power and the current i_q are linked by an algebraic equation (see 4.8) and so the reference current for the inner loop can be directly calculated through (4.8). Moreover it has no influence on synthetic inertia.
All the controllers are proportional integrators. In figure 4.2 we can see the complete scheme of the system under investigation.

The control system is made for d and q axis separately, but as we can see from (4.7) and from the figure above there is coupling between d and q axes. This issue is resolved by a feedback decoupling. Measured quantities are introduced in the control scheme in order to be able to operate the control system in a decoupled manner. These signals ($\omega L_t i_d$ and $-\omega L_t i_q$) are visible also in figure 4.2.
In the figures 4.3 and 4.4 the system is divided into d and q axes. As we can see the system is non linear and on d axis there are two loops. So in order to size the controllers we have to linearise the system and separate the two loops on d axis.

To linearise the system we choose to consider the DC link voltage feedback (visible in the model in figure 4.3) constant and equal to the nominal value, the voltage of the grid is kept constant and also the current from the wind farm is kept constant. So with these simplifications we can draw the system in figure 4.5 and 4.6

Looking at the schemes of the system on d axis (4.3 and 4.5) we can note a block -1 right after the PI outer controller. This is necessary because there is also a -1 in the physical system.
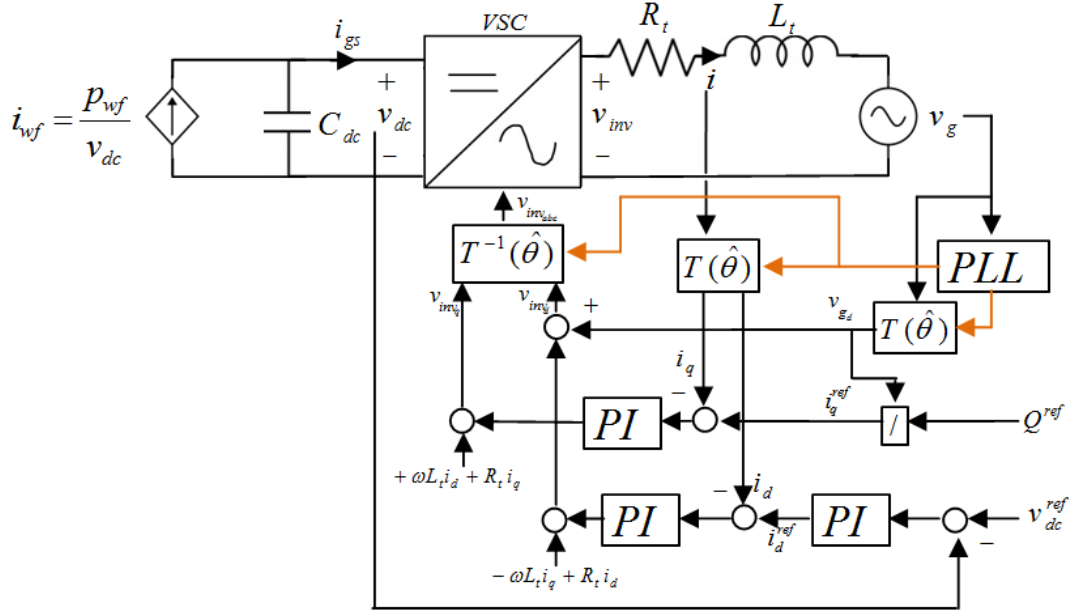
Figure 4.2: System and control scheme

4.4.1 Inner control loops

The dynamics of the inner control loop on d is the same of the one on q axis. In figure 4.5 we can recognise the inner loop of d axis.

Taking into account that the control system has to be much slower than the sampling frequency we choose a passing band of $100Hz$ for the closed loop. The values Kp_{in} and Ki_{in} are calculated using the method in appendix A.

Table 4.3: Inner PI controller parameters

Parameter	Value
Kp_{in}	0.235 p.u.
Ki_{in}	29.25 p.u./s

4.4.2 Outer control loop

The outer control loop on d axis is designed to be much slower than the inner one in order to ensure stability. In figure 4.7 we can see the block diagram of this loop considering the inner one as a unit gain.
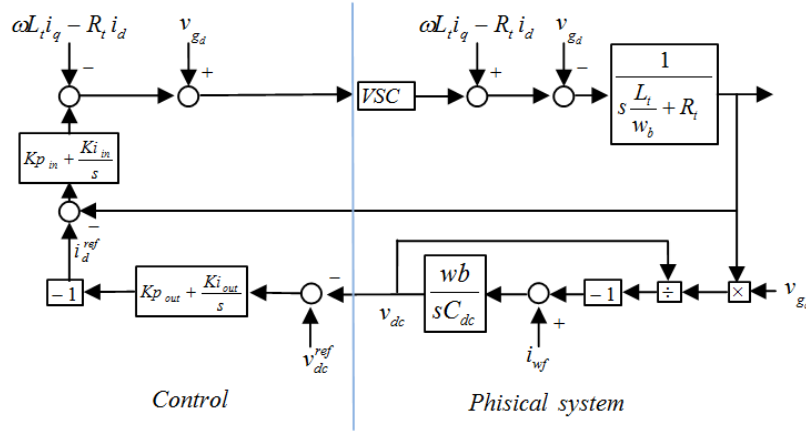
Figure 4.3: System block diagram on d axis
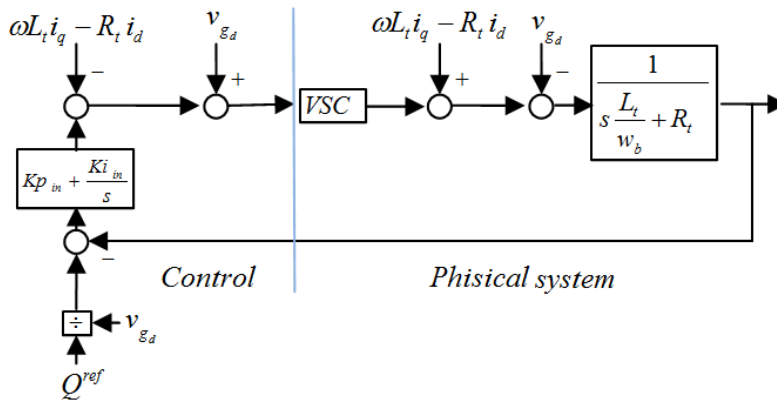
Figure 4.4: System block diagram on q axis

The passing band was chosen equal to $1Hz$ for the closed loop. It has to be much slower than the inner loop to ensure stability. We made this choice also looking at the transfer function between the DC voltage reference and the output reference current. Looking at figure 4.7 we write (4.9) and its Bode plot is in figure 4.8 (line green). In the same figure we can also see the bode plot of the sensitivity control function ($Q_{(s)}$) that is the transfer function between the DC voltage reference and the reference d axis current. The function $Q_{(s)}$ is written in (4.10). We note from the Bode plot that its module is not far from the $0\ db$ axis in the frequency range on interest which is up to around $0.2\ \frac{Hz}{s}$. This since the DC voltage reference depends on grid frequency which we don't expect to vary in a very fast way, $0.1\ \frac{Hz}{s}$ is already a big value (we will talk of this in section
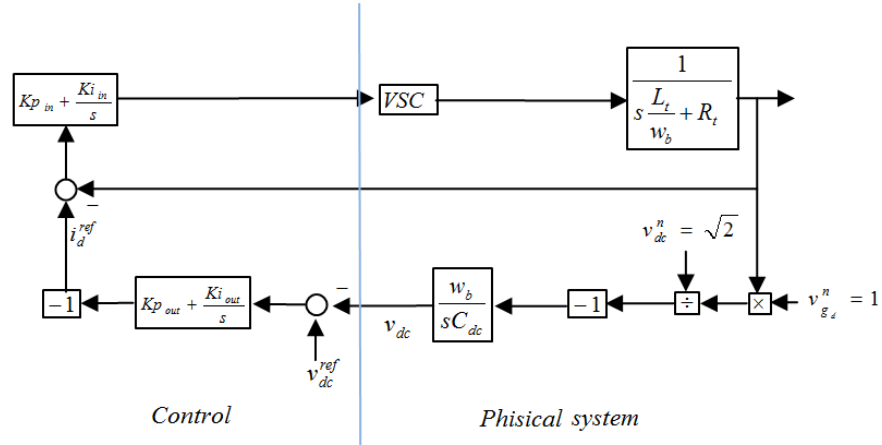
Figure 4.5: Decoupled and linearised block diagram of d axis
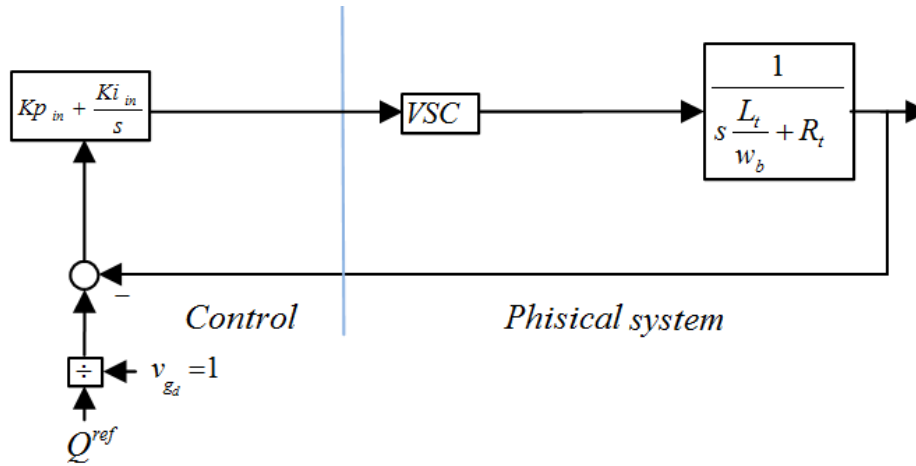
Figure 4.6: Decoupled and linearised block diagram of q axis

5.11.2). Taking this into account we calculated Kp_{out} and Ki_{out} using the method in appendix A.

$$G_{(s)} = \frac{\omega_b}{sC_{dc}} \tag{4.9}$$

$$Q_{(s)} = \frac{R_{(s)}}{1 + R_{(s)}G_{(s)}} \tag{4.10}$$

with
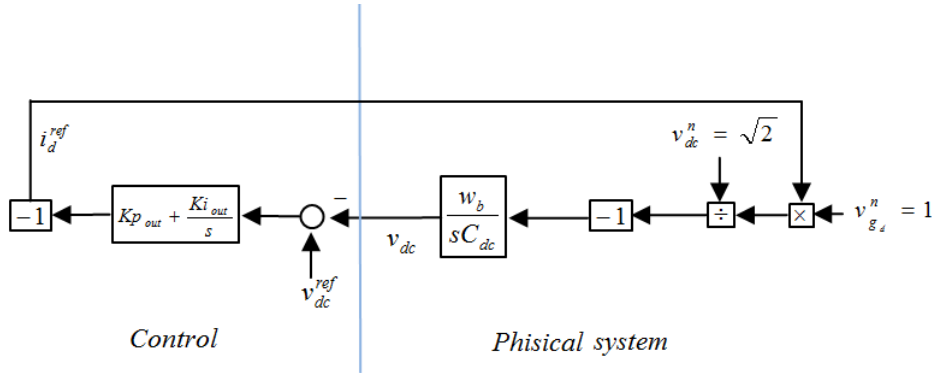
Figure 4.7: Decoupled and linearised block diagram of d axis

Table 4.4: Out PI controller parameters

Parameter	Value (p.u.)
Kp_{out}	28.18
Ki_{out}	64.44

$$R_{(s)} = \frac{Ki_{out}}{s} + Kp_{out} \tag{4.11}$$

4.4.3 PI controller differential equations

Here we will show the differential equations introduced by the controllers in order to develop the complete system differential equation for stability studies. In Laplace domain the PI controller is represented by

$$y_{(s)} = (\frac{K_i}{s} + K_p)u_{(s)} \tag{4.12}$$

where s is the Laplace operator, $y_{(s)}$ is the output and $u_{(s)}$ is the input. We can bring back the equation to time domain (integral initial condition is set to zero)

$$\frac{da}{dt} = K_i u \tag{4.13a}$$

$$y = a + K_p u \tag{4.13b}$$
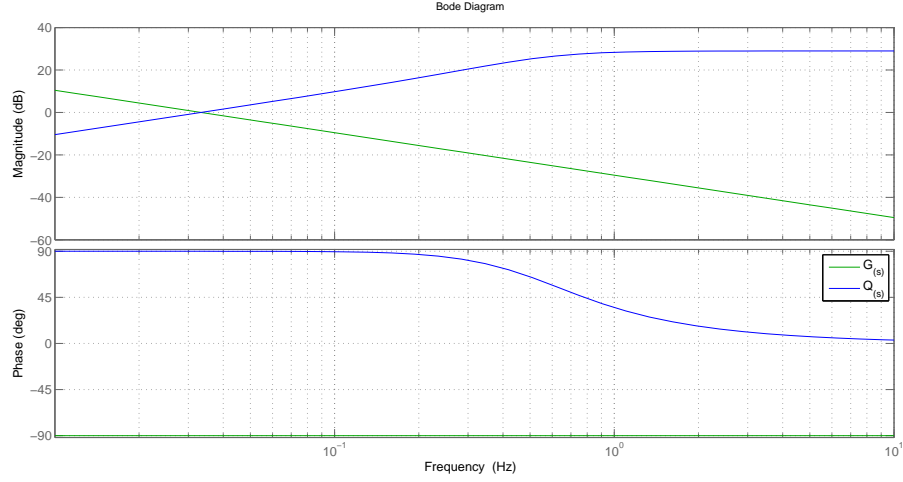
Figure 4.8: Bode plots of the function in (4.9) and in (4.10)

where a is a state variable introduced by the controller. So for each controller a new state variable is introduced: a_d is the one for the PI inner controller on d axis, a_q is the one for the controller on q axis and finally b is the variable introduced by the outer controller on d axis. We can now write all the differential equations of the controllers.

$$\frac{da_d}{dt} = Ki_{in}(i_d^{ref} - i_d) \tag{4.14a}$$

$$\frac{da_q}{dt} = Ki_{in}(i_q^{ref} - i_q) \tag{4.14b}$$

$$\frac{db}{dt} = Ki_{out}(v_{dc}^n - v_{dc}) \tag{4.14c}$$

In order to write the complete system of differential equations we will need also the following equations (the output of the controllers). The complete system of equations will be written in section 4.6 taking into account also the PLL dynamics.

$$i_d^{ref} = b + Kp_{out}(v_{dc}^n - v_{dc}) \tag{4.15a}$$

$$v_{inv_d} = a_d + Kp_{in}(i_d^{ref} - i_d) + v_{g_d} - \omega L_t i_q \tag{4.15b}$$

$$v_{inv_q} = a_q + Kp_{in}(i_q^{ref} - i_q) + v_{g_q} + \omega L_t i_d \tag{4.15c}$$

4.5   Phase locked loop (PLL)

As said before the phase locked loop (PLL) is used to align the control system to the grid voltage and to retrieve the grid frequency. In figure 4.9 we can see the block diagram of the PLL. We had to note that even if the input voltages are in p.u. the estimated $\hat{\omega}$ is in physical value.
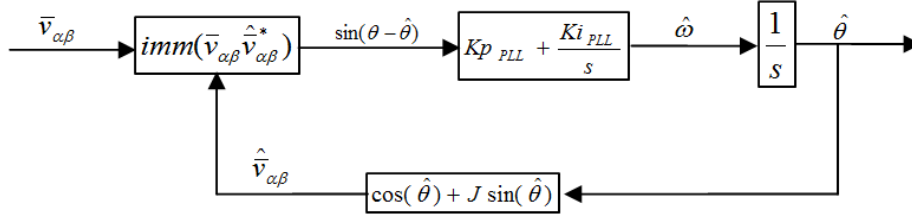
Figure 4.9: PLL blocks diagram

v_α and v_β are the transformation on fixed α and β axes of the voltage to which we want to be aligned, here simply named $\bar{v}$. Matrix used for the transformation is reported in appendix A.The first block of the PLL computes the imaginary part of the complex product of the voltage vector $\bar{v}$ and the complex conjugated of the estimated voltage vector $\hat{\bar{v}}$. This gives the sine of the angle between the two vectors. The control system will minimise this quantity by moving the estimated voltage vector, in such a way we follow the rotating vector $\bar{v}$. In this way we know the position (angle) of the voltage we want to be aligned to. In figure 4.10 there is a representation of this concept, while in the following equations the mathematical aspects will be analysed.

$\bar{v}$ vector can be expressed as $|v|e^{j\theta}$ and estimated $\hat{\bar{v}}$ as $|\hat{v}|e^{j\hat{\theta}}$. In this way we compute the sine of the angle between them:

$$Imm(|v|e^{j\theta}|\hat{v}|e^{-j\hat{\theta}}) = \sin(\theta - \hat{\theta}) \tag{4.16}$$

This shows the relation between the sine of the angle difference and the exponential complex product, but in the control system the operation is implemented using Cartesian coordinates

$$Imm[(v_\alpha + jv_\beta)(\hat{v}_\alpha - j\hat{v}_\beta)] = \sin(\theta - \hat{\theta}) \tag{4.17}$$

In figure 4.9 we can see that the output of the PI controller is marked as $\hat{\omega}$ that is the estimated angular velocity (physical value). Looking at the scheme this results clear because it is the time derivative of the estimated angle, but we need to say that this is true only at steady state. This because $\theta - \hat{\theta} = 0$ only at steady
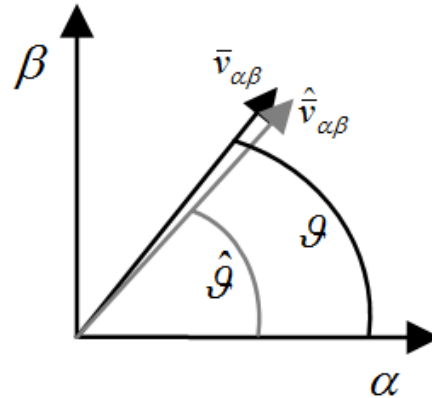
Figure 4.10: Grid voltage vector and estimated voltage vector $(\hat{\bar{v}}_{\alpha\beta})$

state, while during transients the output of the PI is not the actual angular frequency. We will show the mathematical aspect of this concept at the end of this section.

The controller is a PI and the values of its parameters are chosen linearising the loop in figure 4.9. Considering the system around an equilibrium point we can say that $sin(\theta - \hat{\theta}) = \theta - \hat{\theta}$ and so we can draw the linearised closed loop system reported in figure 4.11. Looking at this scheme and with the method in appendix A we find the values for the PI controller (listed in table 4.5). The passing band of the closed loop is chosen equal to 5000 Hz in order to stay always aligned with the grid.
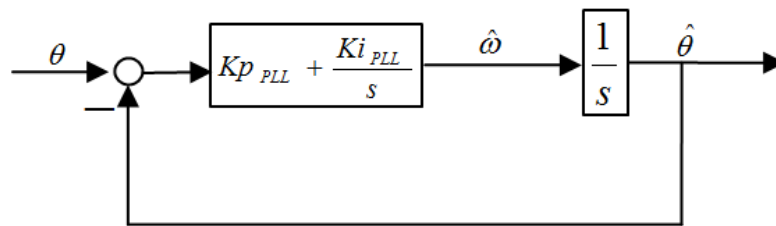
Figure 4.11: Linearised PLL scheme used to compute PI controller parameters

In figure 4.12 we can see the bode plot of the open loop transfer function (written (4.18)). We can see that the passing band of the close loop is 5000 Hz as expected and that the phase margin is 60°. Since the function $L_{(s)}$ has not right half plane zeros and it crosses the 0 db axis only one time, we can apply the Bode

Table 4.5: PLL PI controller parameters

Parameter	Value
Kp_{PLL}	$27.2 \ 10^3 \ \frac{rad}{s}$
Ki_{PLL}	$493.4 \ 10^6 \ \frac{rad}{s^2}$

stability criterion to verify if the system is stable. From (4.18) we can see that the gain is greater than zero and from the graph in figure 4.12 we can verify that the phase margin is greater than zero and moreover the one expected, so we can say that the system is stable.

$$L_{(s)} = (Kp_{PLL} + \frac{Ki_{PLL}}{s})\frac{1}{s} = \frac{Ki_{PLL}}{s^2}(1 + \frac{Kp_{PLL}}{Ki_{PLL}}s) \qquad (4.18)$$
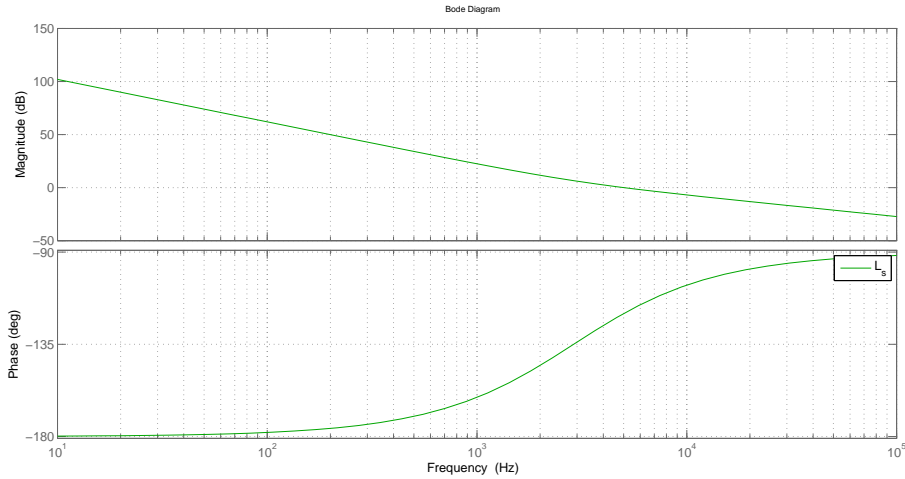
Figure 4.12: Bode diagram of the PLL open loop transfer function 4.18

Let's now analyse why we choose a PI controller. Let's consider the scheme in figure 4.11, and let's name the error $(\theta - \hat{\theta})$ at the input of the PI controller as e . We can now compute the transfer function between the transfer function of the input angle (θ) and the error (e).

$$\frac{e_{(s)}}{\theta_{(s)}} = \frac{1}{1 + L_{(s)}} \qquad (4.19)$$

and so

$$\frac{e_{(s)}}{\theta_{(s)}} = \frac{1}{1 + \frac{Ki_{PLL}}{s^2}(1 + \frac{Kp_{PLL}}{Ki_{PLL}})} = \frac{s^2}{s^2 + Ki_{PLL}(1 + \frac{Kp_{PLL}}{Ki_{PLL}})} \qquad (4.20)$$

Now we apply the final value theorem to find the steady state value of e in the time domain. To do this we need to note that $\theta = \omega t$ (with ω angular frequency) and so its Laplace transformation is

$$\theta_{(s)} = \frac{\omega}{s^2} \qquad (4.21)$$

and so, combining (4.20) and (4.21)

$$\frac{e_{(s)}}{\theta_{(s)}} = \frac{s^2}{s^2 + Ki_{PLL}(1 + \frac{Kp_{PLL}}{Ki_{PLL}})} \frac{\omega}{s^2} \qquad (4.22)$$

Now remembering the final value theorem we can find the steady state value of the error e in the time domain.

$$\lim_{t->\infty} e_{(t)} = \lim_{s->0} s e_{(s)} = \lim_{s->0} s \frac{s^2}{s^2 + Ki_{PLL}(1 + \frac{Kp_{PLL}}{Ki_{PLL}})} \frac{\omega}{s^2} = \omega s = 0 \qquad (4.23)$$

So we demonstrate that the error at steady state is zero. This is due to the PI controller that with the other integrator present in the system can guarantee zero steady state error in presence of a ramp input. This is important since it guarantees that we can stay aligned with the input voltage vector and, as said before, we can say that the output of the PI controller is the angular frequency. At this point a question can emerge, why the PLL? If we measure the voltage we want to be aligned, we made the transformation on α and β axes, we can just compute the inverse tangent of $\frac{v_\beta}{v_\alpha}$ and retrieve the grid angle. This is possible, but it is not accurate since it is very sensible to grid disturbances such as harmonic components. Instead we can use the inverse tangent to initialize the integrator of the PLL when the system is switched on. This will reduce the transient.

4.5.1   Model of PLL for stability analysis

Since we want to include the PLL in the system stability analysis, we have to develop a model of the PLL in d and q axes. To do this we imagine to transform the voltage that we want to follow, instead on fixed α and β axes, on d and q axis that are rotating with a constant angular frequency, ω_b in this case. In this way we consider the reference frame as rotating with a constant angular frequency ω_b. In such a case we see the voltage vector, in absence of grid frequency disturbance, as a static vector. In figure 4.13 we can see a representation of this concept. We can see fixed α and β axes and d and q axes rotating with a constant angular

frequency ω_b. We consider to be on such rotating axes and with the PLL we estimate the angular position that the voltage vector $\bar{v}$ has with respect to the rotating dq frame. In this case we have also to consider that the output of the PI controller is not the estimated angular frequency, but the difference between the actual voltage frequency and the constant angular frequency we use for the dq rotating frame.
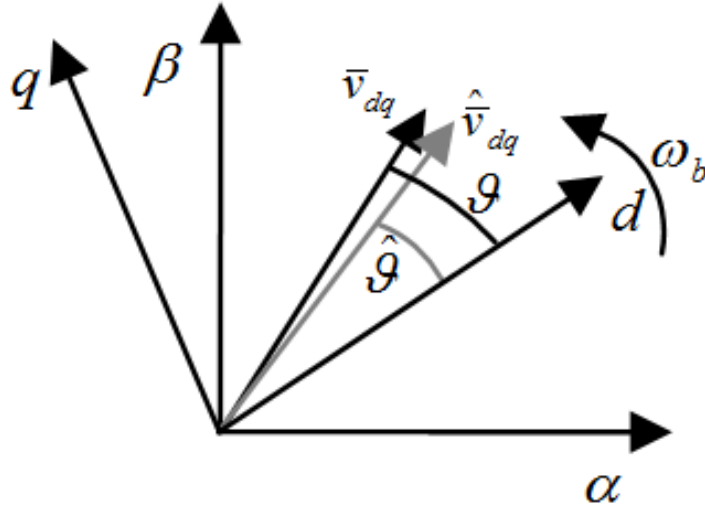
Figure 4.13: Graphical representation of the grid voltage vector, angle θ and $\hat{\theta}$

In this way the input of the system is $\bar{v}$ in dq frame which in the following will be denoted as grid reference frame since we will consider as reference voltage the grid voltage, so $\bar{v} = \bar{v}_g$. We had now to say that a variation in grid frequency is detected here as a variation in the dq components of the grid voltage vector.

4.5.2 PLL differential equations

Now we show the differential equations for the PLL. Looking at figure 4.9 we see two dynamical blocks: the PI controller and an integrator. So two new variables are introduced: $\hat{\theta}$ and ω_i.

$$\frac{d\omega_i}{dt} = Ki_{PLL}sin(\theta - \hat{\theta}) \tag{4.24a}$$

$$\frac{d\hat{\theta}}{dt} = \omega_i + Kp_{PLL}sin(\theta - \hat{\theta}) \tag{4.24b}$$

Considering that the estimated vector has unit module we can say that $\hat{\bar{v}} = cos(\hat{\theta}) + jsin(\hat{\theta})$ and we can compute the value of $sin(\theta - \hat{\theta})$

$$sin(\theta - \hat{\theta}) = Imm(\bar{v_{dq}}(cos(\hat{\theta}) - jsin(\hat{\theta}))) = v_q cos(\hat{\theta}) - v_d sin(\hat{\theta}) \qquad (4.25)$$

4.5.3   Relation between control and grid reference frame

Now that we have derived the differential equations of the system (4.7), the ones of the control system (4.14) and we have described PLL and its equations we have to write the complete system of differential equations. To do this we have to separate the d and q axes of the control and the ones of the grid in which the physical system equations are written. This because we have to take into account the PLL dynamics. So, as explained in 4.5.1 the grid reference frame is defined with a constant frequency transformation ($T(\omega_b)$ in this case) but we don't know its angular position which we retrieve with the PLL (angle $\hat{\theta}$). The relation between the vectors in the control frame (marked with subscript c) and the ones in reference frame is the following

$$\bar{v}^c = \bar{v}e^{-j\hat{\theta}} \qquad (4.26)$$

We can see the representation of this concepts in figure 4.14. We can see the dq grid reference frame that is rotating with a constant angular frequency ω_b, and the control reference frame which is rotating with the estimated angular frequency $\hat{\omega}$

Writing the equation 4.26 for quantities necessary in the control system brings to 4.27

$$v_{g_d}^c = v_{g_d}cos(\hat{\theta}) + v_{g_q}sin(\hat{\theta}) \qquad (4.27a)$$

$$v_{g_q}^c = v_{g_q}cos(\hat{\theta}) - v_{g_d}sin(\hat{\theta}) \qquad (4.27b)$$

$$i_{g_d}^c = i_{g_d}cos(\hat{\theta}) + i_{g_q}sin(\hat{\theta}) \qquad (4.27c)$$

$$i_{g_q}^c = i_{g_q}cos(\hat{\theta}) - i_{g_d}sin(\hat{\theta}) \qquad (4.27d)$$

Then control systems reference values has to be referred to the grid reference frame, again referring to (4.26) we can write in d and q axis
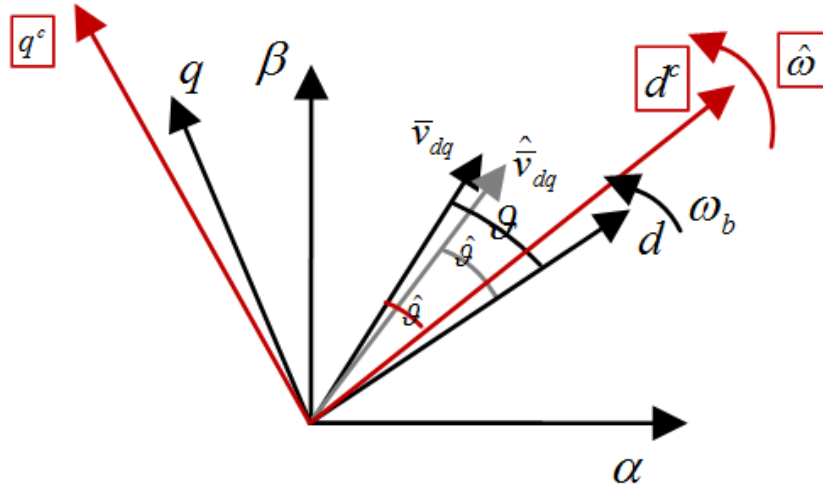
Figure 4.14: Graphic representation of the grid and control d and q axes

$$v_{inv_d} = v_{inv_d}^c cos(\hat{\theta}) - v_{inv_q}^c sin(\hat{\theta}) \tag{4.28a}$$

$$v_{inv_q} = v_{inv_q}^c cos(\hat{\theta}) + v_{inv_d}^c sin(\hat{\theta}) \tag{4.28b}$$

At this point we need to underline htat the grid reference frame is the one in which the equations for the physical system are written . This reference frame is not the one of the control system since we want to take into account the PLL dynamics. The relation between the two frames is in (4.26)

4.6   Complete system of equations

We can now link together all differential equations and write the complete dynamical system considering the equations in (4.7) (4.14), (4.15), (4.24), (4.27) and (4.28). Here for simplicity we report all the equations.

$$\frac{di_d}{dt} = (v_{inv_d} - v_{g_d} - R_t i_d + \omega L_t i_q)\frac{wb}{L_t} \tag{4.29a}$$

$$\frac{di_q}{dt} = (v_{inv_q} - v_{g_q} - R_t i_q - \omega L_t i_d)\frac{wb}{L_t} \tag{4.29b}$$

$$\frac{dv_{dc}}{dt} = (i_{wf} - \frac{v_{g_d}i_{g_d}}{v_{dc}})\frac{wb}{C_{dc}} \tag{4.29c}$$

$$\frac{da_d}{dt} = Ki_{in}(i_d^{ref} - i_{g_d}^c) \tag{4.29d}$$

$$\frac{da_q}{dt} = Ki_{in}(i_q^{ref} - i_{g_q}^c) \tag{4.29e}$$

$$\frac{db}{dt} = Ki_{out}(v_{dc}^n - v_{dc}) \tag{4.29f}$$

$$\frac{d\omega_i}{dt} = Ki_{PLL}sin(\theta - \hat{\theta}) \tag{4.29g}$$

$$\frac{d\hat{\theta}}{dt} = \omega_i + Kp_{PLL}sin(\theta - \hat{\theta}) \tag{4.29h}$$

$$sin(\theta - \hat{\theta}) = v_{g_q}cos(\hat{\theta}) + v_{g_d}sin(\hat{\theta}) \tag{4.30a}$$

$$i_d^{ref} = b + Kp_{out}(v_{dc}^{ref} - v_{dc}) \tag{4.30b}$$

$$v_{inv_d} = a_d + Kp_{in}(i_d^{ref} - i_d) + v_{g_d}^c - \omega L_t i_q \tag{4.30c}$$

$$v_{inv_q} = a_q + Kp_{in}(i_q^{ref} - i_q) + v_{g_q}^c + \omega L_t i_{g_d}^c \tag{4.30d}$$

$$v_{g_d}^c = v_{g_d}cos(\hat{\theta}) + v_{g_q}sin(\hat{\theta}) \tag{4.30e}$$

$$v_{g_q}^c = v_{g_q}cos(\hat{\theta}) - v_{g_d}sin(\hat{\theta}) \tag{4.30f}$$

$$i_{g_d}^c = i_{g_d}cos(\hat{\theta}) + i_{g_q}sin(\hat{\theta}) \tag{4.30g}$$

$$i_{g_q}^c = i_{g_q}cos(\hat{\theta}) - i_{g_d}sin(\hat{\theta}) \tag{4.30h}$$

$$v_{inv_d} = v_{inv_d}^c cos(\hat{\theta}) - v_{inv_q}^c sin(\hat{\theta}) \tag{4.30i}$$

$$v_{inv_q} = v_{inv_q}^c cos(\hat{\theta}) + v_{inv_d}^c sin(\hat{\theta}) \tag{4.30j}$$

The input of the system are v_{g_d}, v_{g_q} and i_{wf} that we set with the values listed in table 4.6

At this point we evaluate the eigenvalues of this system. To find the equilibrium point we use Newton-Raphson method and then we evaluate the eigenvalues of the system linearised around that point. In table 4.7 the values of the state variables at the equilibrium point and in table 4.8 the eigenvalues and the damping

Table 4.6: Input values

Parameter	Value (p.u.)
v_{g_d}	1
v_{g_q}	0
i_{wf}	$1/v_{dc}^n = 1/\sqrt{2}$

factors. As we can see that the system is stable and well dumped. In figure 4.15 we can se a graphical representation of the eigenvalue of table 4.8. An enlargement of the region near the origin is given in figure 4.16 and a further enlargement in figure 4.17. As we can see, the real part of all the eigenvalue is negative, so the system is stable. It is also well dumped since the eigenvalue are very far from the imaginary axis.

Table 4.7: State variables at the equilibrium point

Parameter	Value (p.u.)
i_{d0}	1
i_{q0}	$-1\ 10^{-8}$
v_{dc0}	1.414
a_{d0}	0.005
a_{q0}	0
b_0	1
w_{i0}	0
θ_0	0

Table 4.8: Eigenvalues at the equilibrium point listed in 4.7

Parameter	Value (rad/s)	Damping factor
λ_1	-455.5344	1
λ_2	$-2.8796 + 2.2849i$	$783.3544\ 10^{-3}$
λ_3	$-2.8796 - 2.2849i$	$783.3544\ 10^{-3}$
λ_4	-168.1575	1
λ_5	-464.5945	1
λ_6	-165.0048	1
λ_7	$-13.6035\ 10^3 + 17.562i\ 10^3$	$612.3724\ 10^{-3}$
λ_8	$-13.6035\ 10^3 - 17.5620i\ 10^3$	$612.3724\ 10^{-3}$
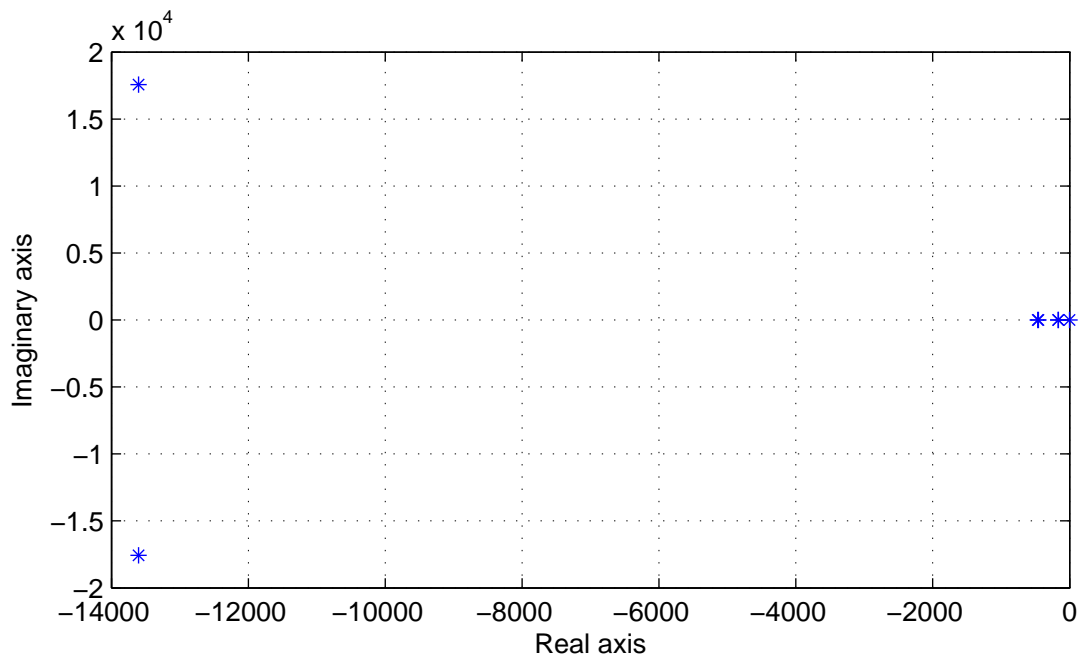
Figure 4.15: Plot of the eigenvalues listed in table 4.8
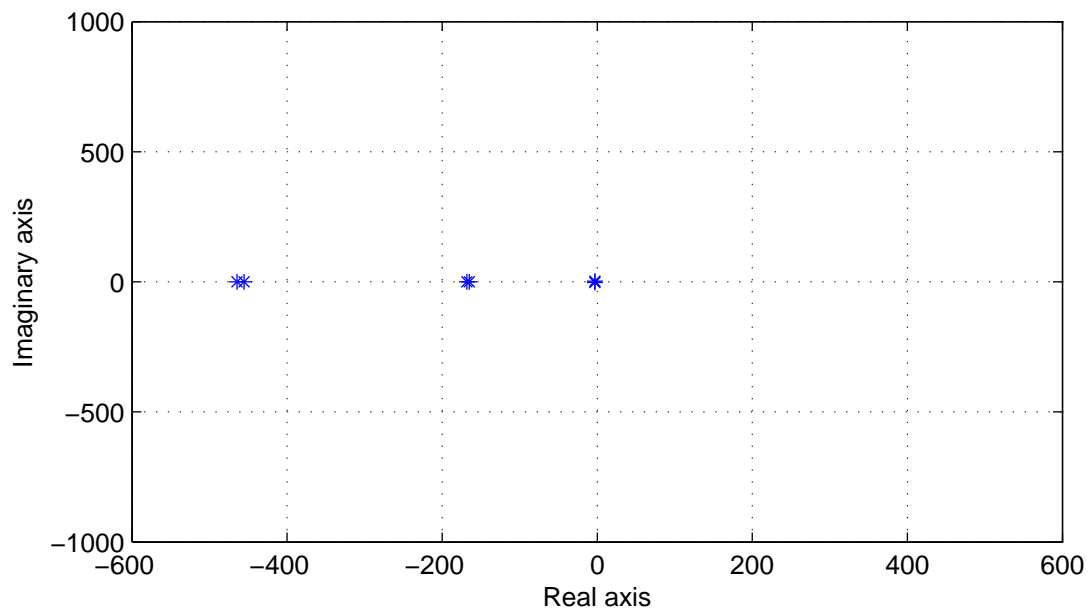
Figure 4.16: An enlargement of the region near the origin of the plot of the eigenvalues listed in table 4.8
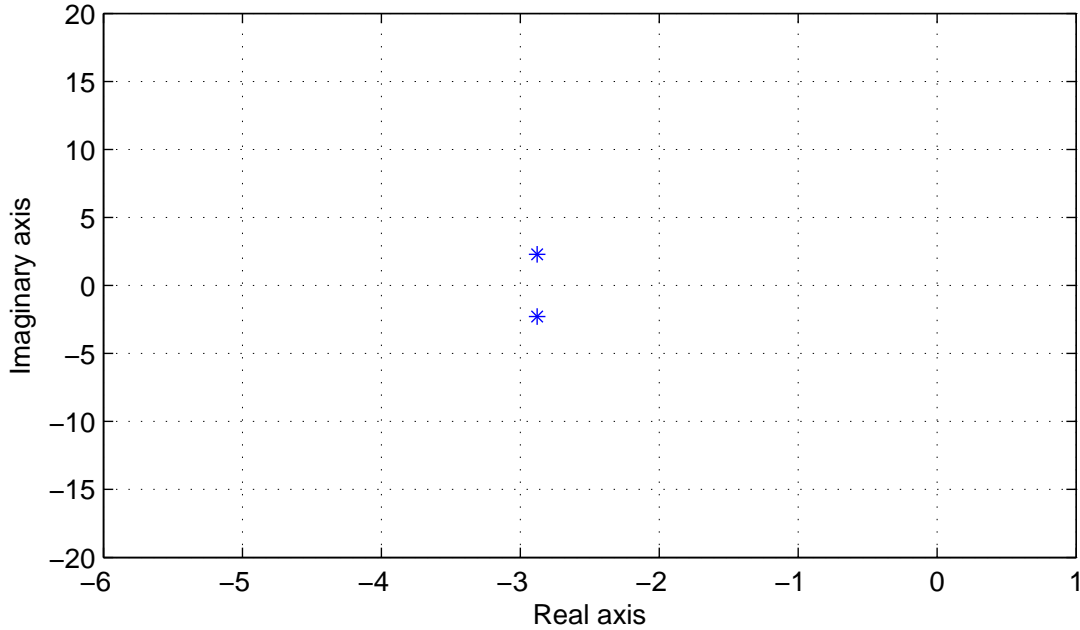
Figure 4.17: A further enlargement of the region near the origin of the plot of the eigenvalues listed in table 4.8

4.7 Inertia emulation with DC voltage droop control

In this section we will introduce in the control system the inertia emulation techniques described in section 2.5.1. DC voltage reference is no more constant, but changes with frequency according to the following law

$$v_{dc}^{ref} = V_{dc}^n + K_{dc}\Delta f \tag{4.31}$$

Detailed derivation of this method is shown in section 2.5.1, here we will perform the stability analysis of the system, we will derive the transfer function between variation of the power (ΔP_{ac}) delivered to the grid and a grid frequency variation (Δf) and we will simulate the system using Matlab Simulink.
The value of K_{dc} is chosen in order to have an inertia constant equal to 6 s, so according to the (2.18): $K_{dc} = 1.26$ $p.u.$

4.7.1 Stability analysis

Modifying the first equation in (4.30) taking into account (4.31) and setting as input the quantities listed in the table 4.6, we can evaluate the equilibrium point of the system using Newton-Raphson method. The equilibrium point and the

eigenvalues are the same of the one reported in table 4.7 and 4.8. This is due to the fact that we modify the DC voltage reference (v_{dc}^{ref}) according to an input (f), this affects A matrix of the system only because the system is non linear. But in this case not in an appreciable manner.

4.7.2   Simulation

We simulate the system using Matlab Simulink implementing in this software tool the mathematical model described by the equations in (4.30) and (4.29). 5 seconds after the simulation has started, when all the state variables have reached the equilibrium and the model is in steady state, we give a grid frequency disturbance. The frequency starts decreasing linearly reaching in 6 seconds a value equal to the 98% of the nominal value (we can see it in figure 4.21). The variation is sensed by the PLL which is very fast acting and the DC voltage reference varies according to (4.31). In the figures below the plots of V_{dc} and power delivered to the main grid following the described frequency disturbance. In figures 4.18 to 4.20 the system modelled in simulink.
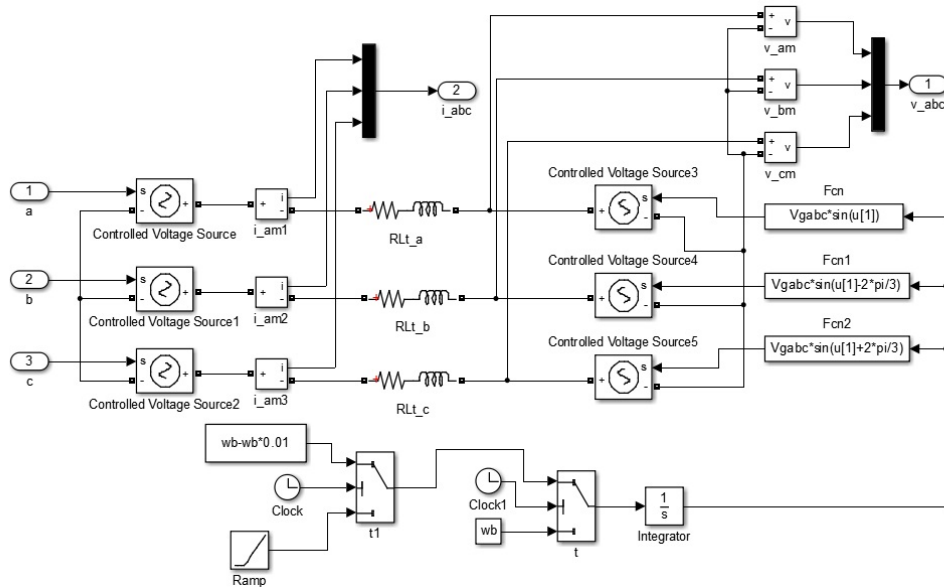

Figure 4.18: Grid interface of the VSC
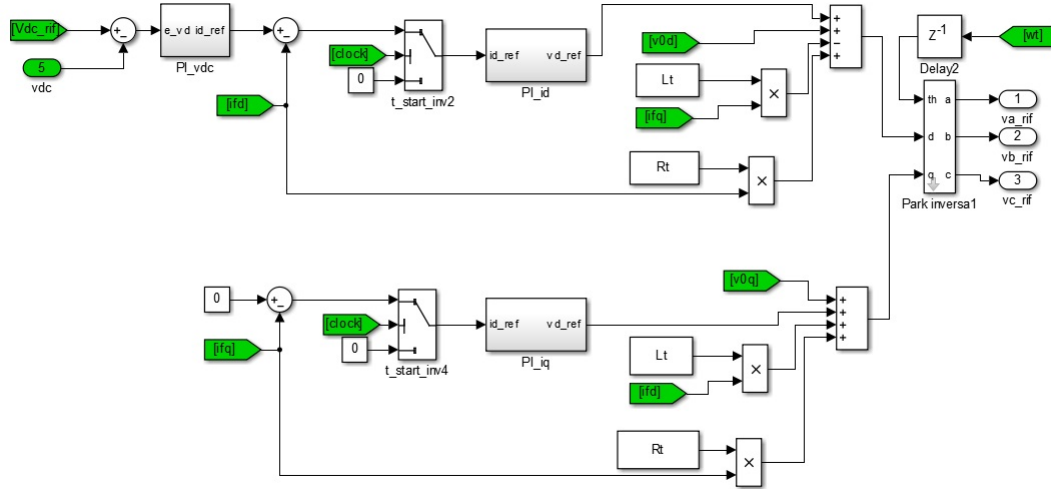
Figure 4.19: Control loops of the system and Park anti-transformation
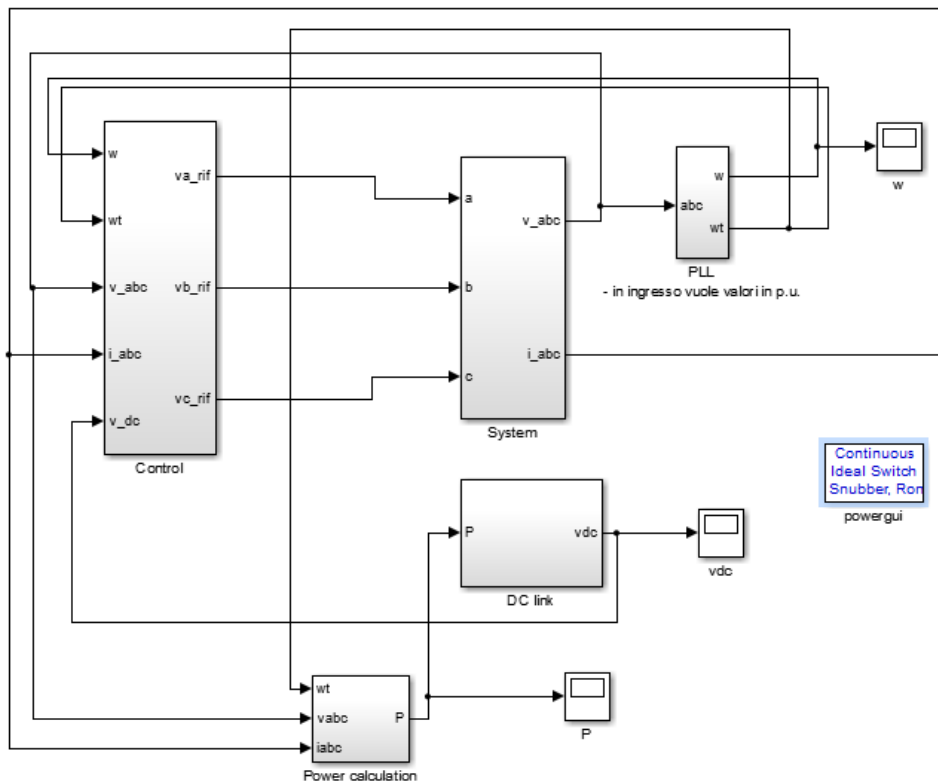
Figure 4.20: The overall system, the blocks in the previous figures are in the subsystems of this figure

In figure 4.21 we can see the frequency disturbance applied to the grid. We recall that the grid is modelled as a voltage source. The slope of the frequency is

0.167 $\frac{Hz}{s}$, this is a value that can take place in the grid, as we will say in section 5.11.2
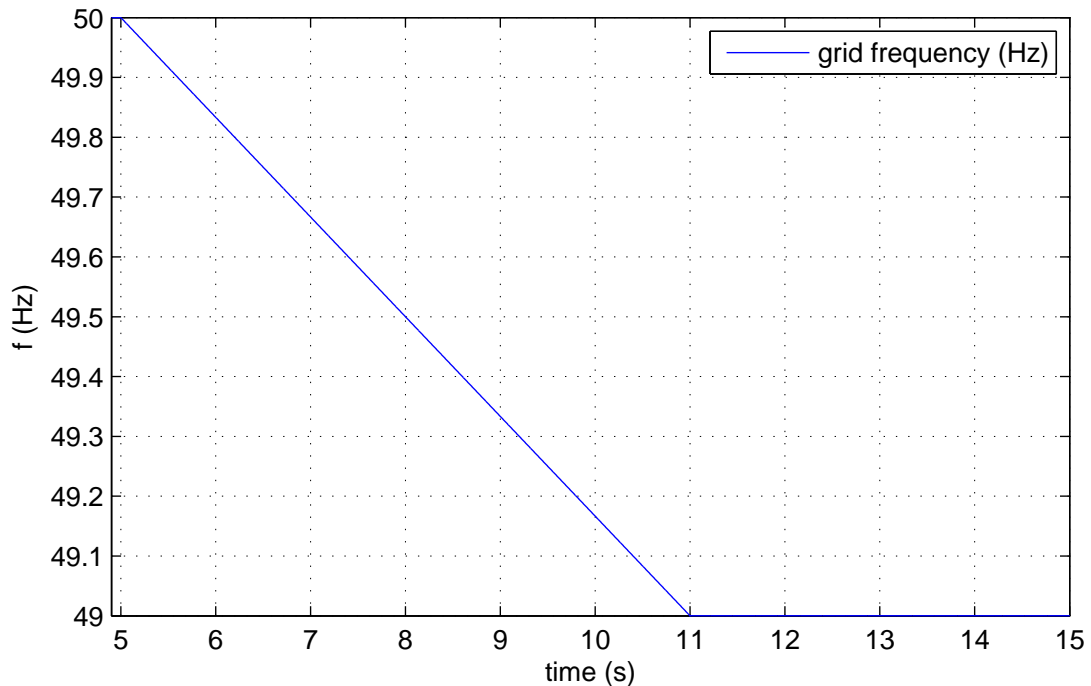
Figure 4.21: Frequency disturbance applied to the grid. The slope of the frequency is 0.167 $\frac{Hz}{s}$, this is a value that can take place in the grid, as we will say in section 5.11.2

In figure 4.22 we can see DC voltage variation (about 0.0242 *p.u.*), when the frequency stops falling (at $t = 11$ *s*) the voltage sets to an other equilibrium point.

In figure 4.23 we can see the output power variation. Since the grid frequency is falling, the output power is incremented. The overshoots are due to the PI outer controller. We can also note that after the frequency stops falling (at $t = 11$ *s*), the output power starts a transient and then it sets again on the value it has before the frequency disturbance. This is due to the fact that through this control we support grid frequency only during its variations.

From figure 4.24 (an enlargement of the area in the rectangle of figure 4.23) we can see that the power output is falling linearly. This thing is not very well appreciable from figure 4.23 since the slope is modest. This behaviour is correct, from figure 4.22 we can see that the DC voltage is falling linearly, so since the delivered power depends on the product between the time derivative of the voltage (that after the first time instants of the transient is constant) and the voltage itself (that is falling linearly), we can conclude that the power has to fall linearly.
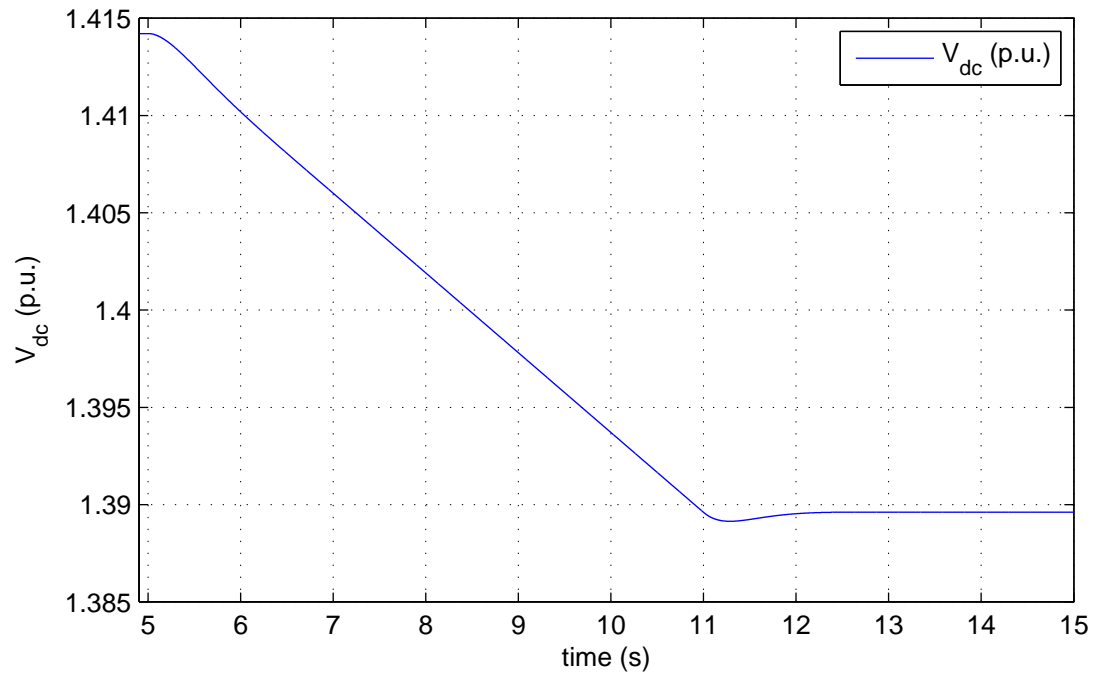
Figure 4.22: DC voltage. When the frequency, after $t = 11\ s$, becomes again constant it stops falling
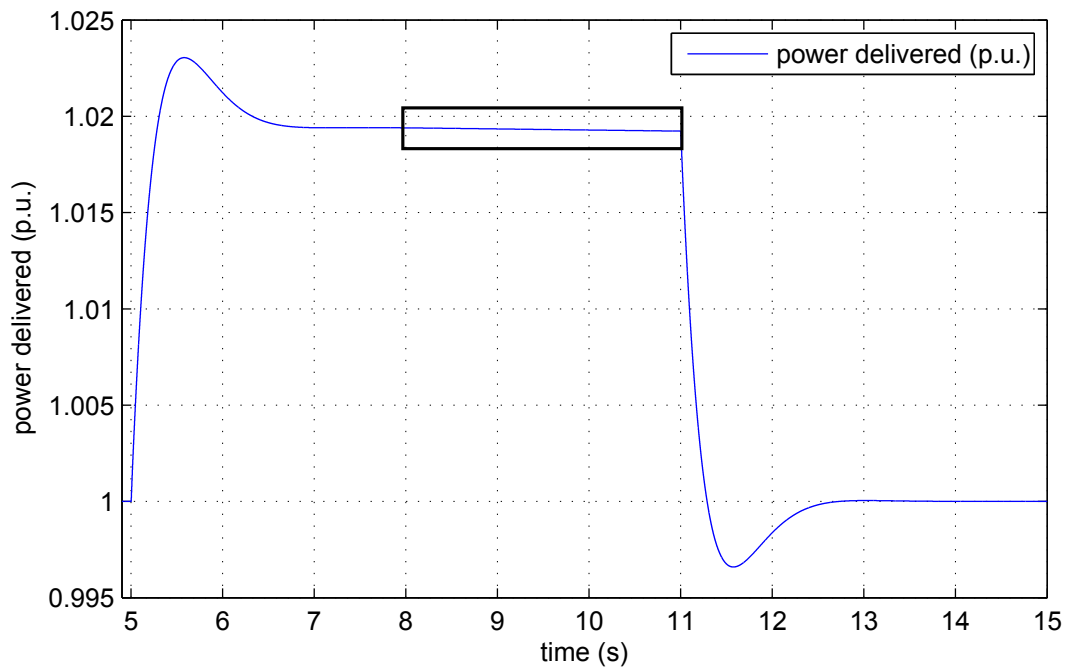
Figure 4.23: Power delivered to the grid. We can note overshoots due to mainly due to the outer loop. In figure 4.24 an enlargement of the part in the rectangle
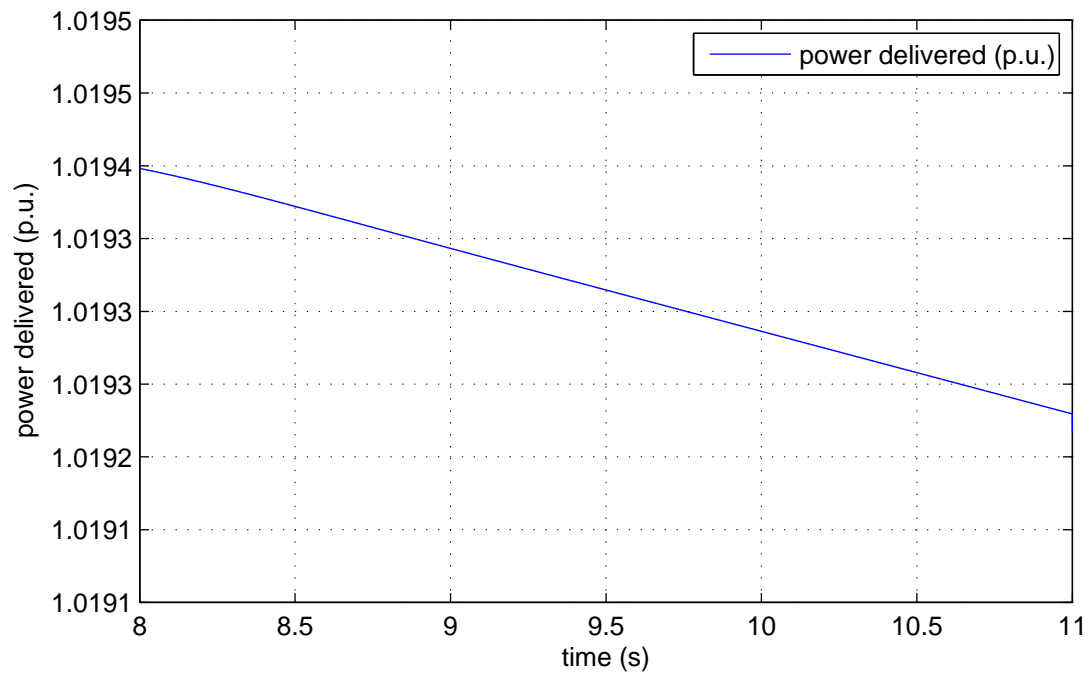
Figure 4.24: Enlargement of a part figure 4.23, we can note that the power delivered decreases linearly

4.7.3 Inertia emulation transfer function

Now we can derive the expression of the transfer function between the grid frequency variation (Δf) and the power (ΔP_{ac}) delivered to the grid.
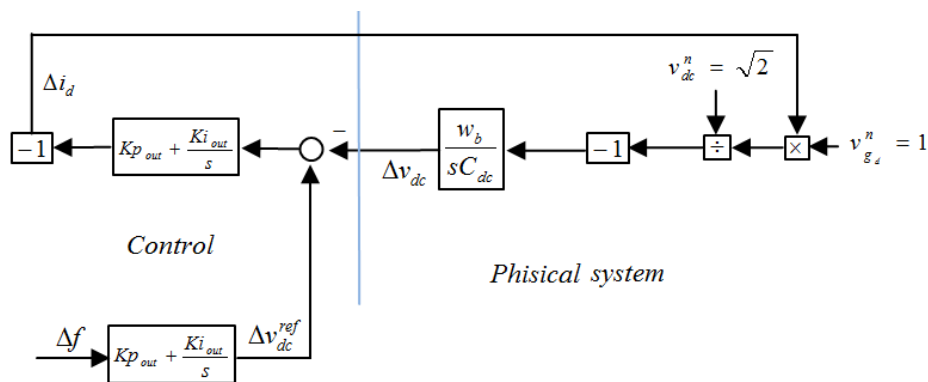
Figure 4.25: Block scheme for the inertia transfer function evaluation

Looking at the figure 4.25 we can see the outer loop on d axis with the voltage reference droop. In this scheme the inner loop is assumed an unit gain. Naming

$$G_{(s)} = \frac{w_b}{sC_{dc}\sqrt{2}} \tag{4.32}$$

$$R_{(s)} = Kp_{out} + \frac{Ki_{out}}{s} \tag{4.33}$$

and considering that the voltage grid is constant ($v_g = 1$ $p.u.$); an output current variation results in an equal output power variation, we can write

$$\frac{\Delta p_{ac}}{\Delta f} = \frac{\Delta i_d}{\Delta f} = \frac{-K_{dc}R_{(s)}}{1 + G_{(s)}R_{(s)}}. \tag{4.34}$$

In figure 4.26 we can see the response of the the power output (p_{ac}) after a grid frequency step disturbance. We can see that the gain is high, but we have to consider that the excitation is a unit step, in practice the frequency will have a significant lower deviation: having a frequency deviation of 1% is already a big value. We can see also that the step response after the transient goes to zero. This is because the new reference value for the DC link voltage is reached and no more power is delivered. This is a consequence of the fact that the primary energy source (in this case P_{wf}) is not modified in consequence of a frequency disturbance.
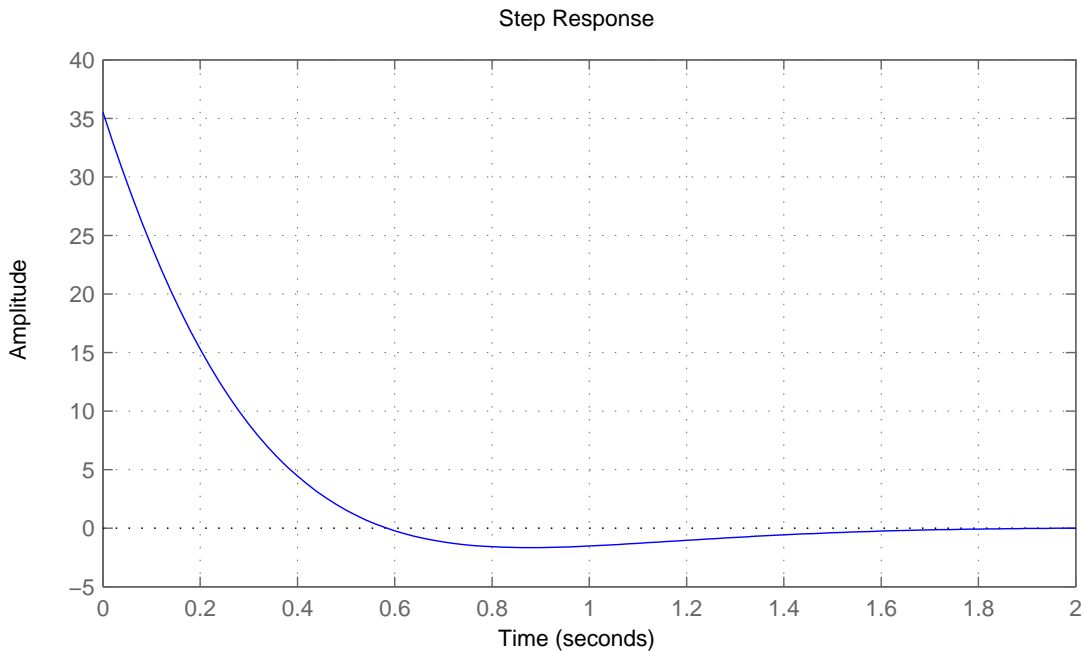
Figure 4.26: Response of the the power output (p_{ac}) after a grid frequency step disturbance
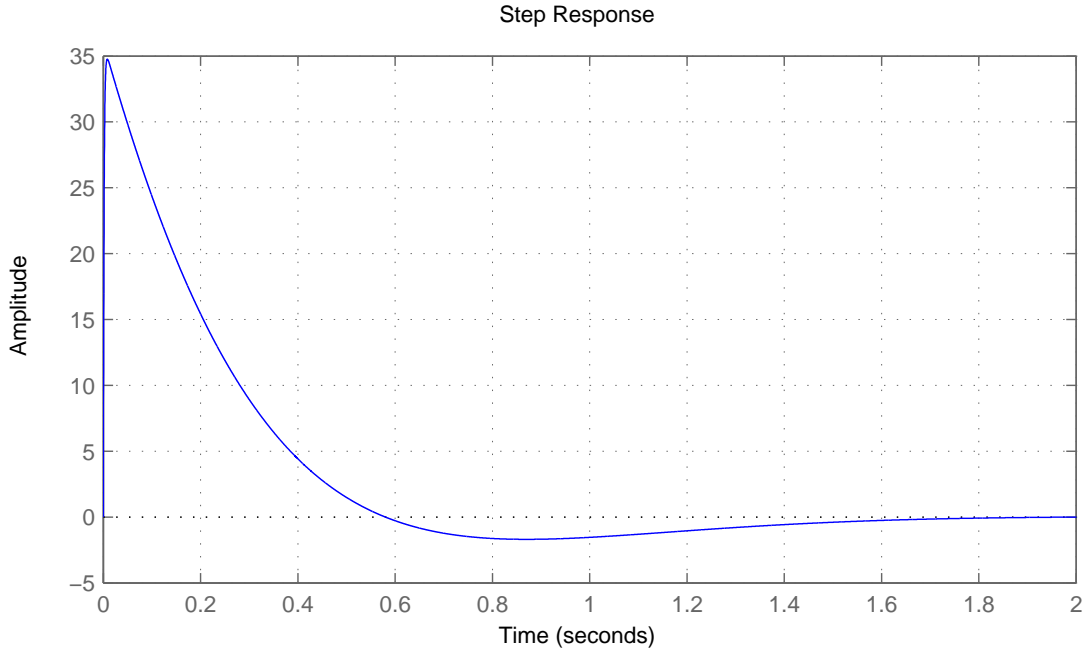
Figure 4.27: Response of the the power output (p_{ac}) after a grid frequency step disturbance considering also the inner current loop

If we consider also the inner current loop the response is pretty much the same, we can see it in figure 4.27. The only difference we can note is a non instantaneous reaction after the step input: this is due to the inner loop time constant, but it is very thin.

4.8 DC voltage square root control method

We now implement the method explained in section 2.5.2. We modify the first equation in (4.30) taking into account (2.21) here reported

$$v_{dc}^{ref} = \sqrt{\frac{4H_{dc}f}{T_c} - K_2} \qquad (4.35)$$

The value of H_{dc} is chosen equal to $6s$ in order to compare the obtained results with the ones obtained in section 4.7. We set as input the quantities listed in the table 4.6.
We can evaluate the equilibrium point of the system using Newton-Raphson method. In tab. 4.9 the values of the state variables at the equilibrium point that is the same we found in section 4.6. Instead in table 4.10 the eigenvalues for this system. We can see that they are the same of the base system (section 4.6),

this as the previous case because we modify only an input equation. We ca see
that the system is stable and well dumped.

Table 4.9: State variables at the equilibrium point

Parameter	Value
i_{d0}	1
i_{q0}	$-1\ 10^{-8}$
v_{dc0}	1.414
a_{d0}	0.005
a_{q0}	0
b_0	1
w_{i0}	0
θ_0	0

Table 4.10: Eigenvalues at the equilibrium point listed in table 4.9

Parameter	Value (rad/s)	Damping factor
λ_1	-455.5344	1
λ_2	$-2.8796 + 2.2849i$	$783.3544\ 10^{-3}$
λ_3	$-2.8796 - 2.2849i$	$783.3544\ 10^{-3}$
λ_4	-168.1575	1
λ_5	-464.5945	1
λ_6	-165.0048	1
λ_7	$-13.6035\ 10^3 + 17.562i\ 10^3$	$612.3724\ 10^{-3}$
λ_8	$-13.6035\ 10^3 - 17.562i\ 10^3$	$612.3724\ 10^{-3}$

As we can see from figures 4.28, 4.29 and 4.30; the results are close to the
one obtained before, in section 4.7.2. This since we choose to control DC voltage
with respect to frequency deviation in order to obtain an inertia constant H_{dc} of
6 s in both cases. Moreover the frequency deviation is small and so the method
previously used (section 4.7) which relies on a linearisation (see section 2.5.1), is a
good approximation of the one here adopted that does not rely on a linearisation.
The comments to the figure are the same of the ones done in the previous section
(see section 4.7).
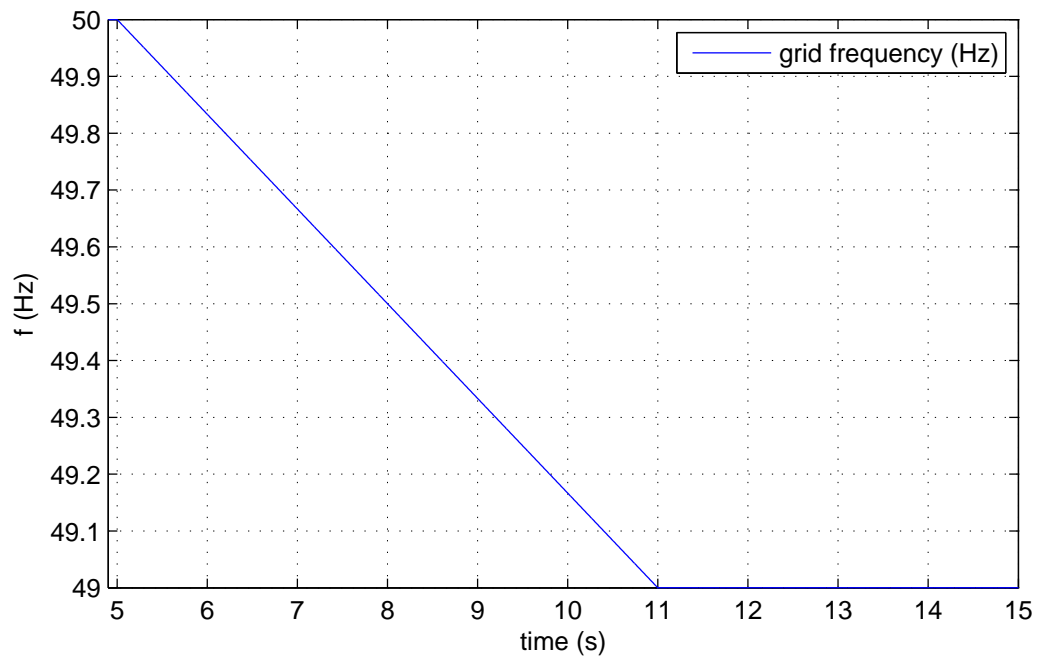
Figure 4.28: Frequency disturbance applied to the grid. The slope of the frequency is 0.167 $\frac{Hz}{s}$, this is a value that can take place in the grid, as we will say in section 5.11.2
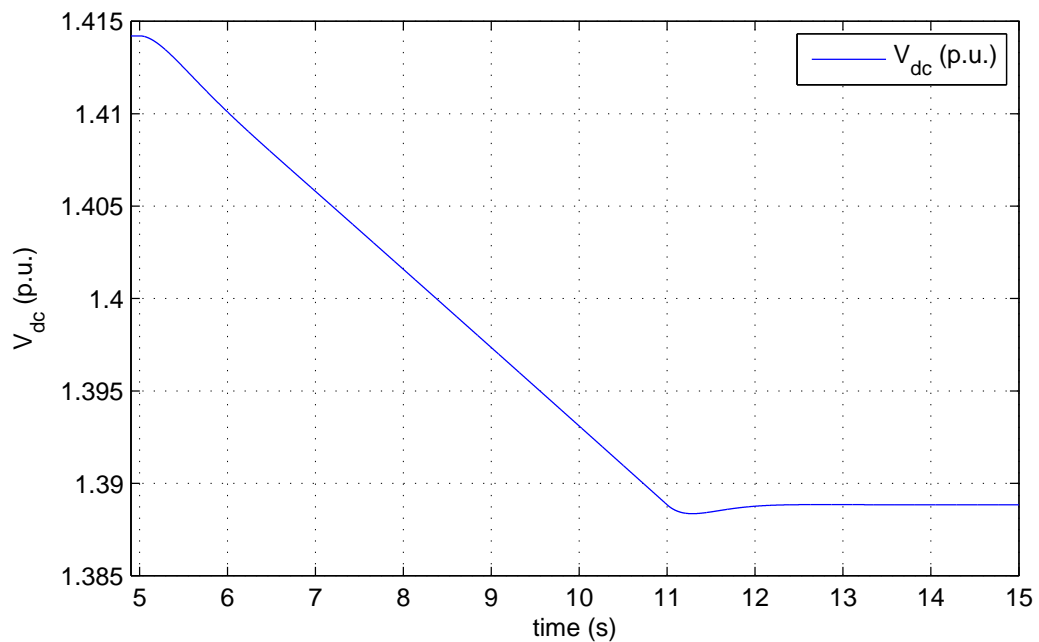
Figure 4.29: DC voltage. When the frequency, after $t = 11$ s, becomes again constant it stops falling
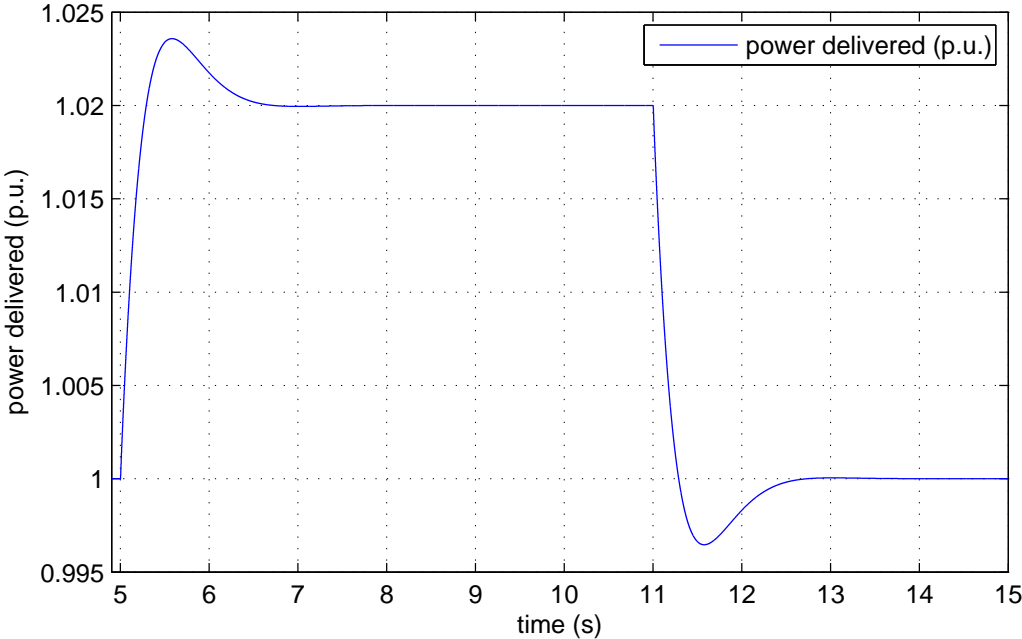
Figure 4.30: Power delivered to the grid. We can note overshoots mainly due to the outer loop.

Chapter 5

DFIG

5.1 Introduction

Figure 5.1 shows a typical configuration for a doubly fed induction generator (DFIG). The induction machine wound rotor is supplied by a power electronic converter that acts as a variable frequency voltage source. In this way we can control the frequency of the rotor currents, and so the rotating speed of the rotor magnetic field. This permits a large variation of the mechanical speed, up to 33 % of the nominal value, the precise range depends on the size of the rotor converters since the power that passes through the rotor circuit depends on the slip as explained in section 5.4. In this way we can extract the maximum wind power available at different wind speed as we will explain later.
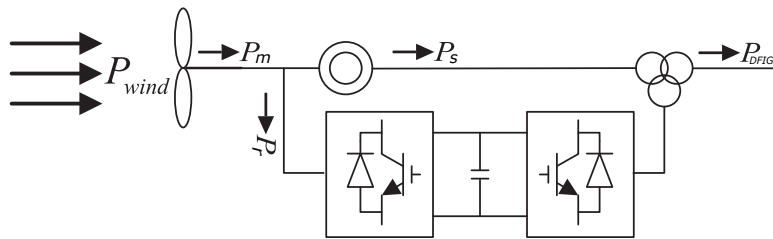
Figure 5.1: Typical configuration for a doubly fed induction generator (DFIG)

5.2 Turbine characteristics

The mathematical expression of the power available from the wind is the following

$$P_{wind} = \frac{\rho}{2}\pi R^2 v_w^3 C_{p(\lambda,\beta)} \tag{5.1}$$

where ρ is the air density, R is the turbine radius, v_w is the actual velocity of the wind and C_p is the aerodynamic efficiency of the turbine. This last term is a function of λ and β. λ is known as *tip speed ratio*, that is the ratio between the velocity of the tip of the blade and the wind velocity $\left(\frac{\Omega_{wt}R}{v_w}\right)$, while β is the pitch angle. We name Ω_{wt} the physical angular speed of the wind turbine, Ω_m the p.u. speed. In figure 5.2a we can see how C_p varies with respect to λ, various curves are drown for specified value of β. Instead in figure 5.2b there is a plot of the available power at the turbine shaft as function of Ω_m (rotational speed of the turbine in p.u.) for different wind velocity (in p.u. of the base power). We refer to horizontal axis turbines.
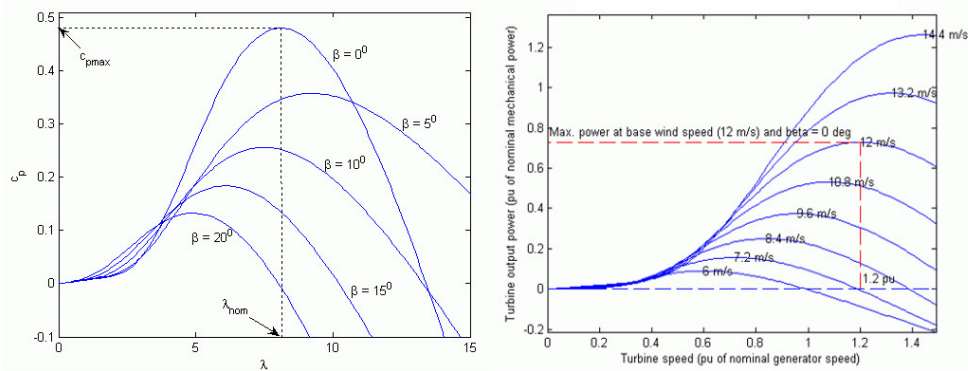
Figure 5.2: C_p as function of λ and β; available power at the turbine shaft as function of Ω_m

Even in turbines where it is expected to modify the pitch angle, generally it is kept constant until the maximum power of the electrical generator is reached. Only then it is used to decrement efficiency in order to operate even when power from the wind is too high (in figure 5.2a we can see that incrementing the pitch angle the efficiency decreases). This because the regulation of blade angle is delicate and slow. So, to operate at the maximum C_p, considering that wind speed is not constant, we need to accept to work with different rotor speeds. From now on we consider to operate with fixed pitch angle.

5.3   Turbine tracking curve

Generally the system operates to extract the maximum power available until rated limits are reached. DFIGs are able to control electrical power output, so we need to find an optimum power characteristic to track. Usually wind velocity is not measured since the measure is not accurate and reliable because the wind turbine itself disturbs the measurement and also wind velocity can vary along the

surface that the wind turbine covers; so a precise estimation of the power coming from the wind is difficult. Instead the rotor speed Ω_m is measured, so the power tracking characteristic is a function of Ω_m. We can see an example of power tracking characteristic in figure 5.3 (red curve). Before point A (correspondent to the cut in velocity) wind is too low, no power is extracted, between A and B (low wind velocity region) the power is varied linearly with Ω_m, than there is the MPPT region where we follow the maximum power until we reach point C. After point C there is the high speed region where, in the first part (between C and D), the power is varied linearly with Ω_m, then, when it is reached the maximum power deliverable by the electrical generator, the output power is kept constant by means of the pitch angle.
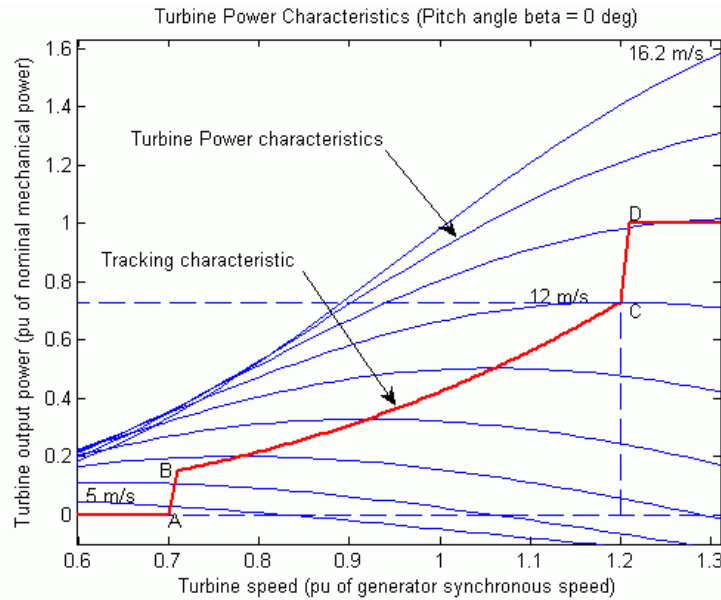
Figure 5.3: DFIG tracking characteristic

In this way we control the power output as a function of the rotor speed, which varies according to the power imbalance between the power from the wind and the electrical power we deliver, following the law in (5.2); it is just a power balance, like the one we described in (2.30) (H_t is the overall inertia constant of the turbine).

$$2H_t\Omega_m\frac{d\Omega_m}{dt} = p_{wind} - p_{wf} \tag{5.2}$$

So the operational rotor speed, the one for which the power tracking curve and the curve of the power coming from the wind meet each other, will be automatically reached (the system is stable; if the power set point is higher than wind

power, the speed decreases, which causes a decrement of power set point until the power delivered matches the one coming from the wind).

In the MPPT region the power tracking characteristics has the following expression (P_{DFIG}^{ref} stands for electric power reference)

$$P_{DFIG}^{ref} = \frac{0.5\rho\pi R^5 \Omega_{wt}^3 C_p^*}{\lambda^{*3} P_b} \tag{5.3}$$

the expression is derived by substituting v_w in (5.1). The value of C_p^* and λ^{*3} are the optimal ones or other values if other strategies than MPPT are adopted. Since the control system will be in p.u. we divide by P_b, the base power.

Generally in the control system we don't use a power reference signal, but a torque reference T_e^{ref}. Its expression is obtained dividing the P_{DFIG}^{ref} by Ω_m, so

$$T_e^{ref} = \frac{0.5\rho\pi R^5 \Omega_{wt}^2 C_p^*}{\lambda^{*3} T_{b_m}} \tag{5.4}$$

where T_{b_m} is the base mechanical torque.

5.4 Active power relation in steady state

Looking at the arrows in figure 5.1 we can write the power balance for a DFIG in steady state (in this section (5.4) all variables are in physical values)

$$P_s = P_m - P_r \tag{5.5}$$

Where P_m is the mechanical power delivered by the turbine, P_r is the electrical power exiting the rotor windings, P_s is the power delivered by the stator.

Taking into account also losses (P_{ls} and P_{lr} are respectively stator and rotor losses.), we can define $P_s' = P_s + P_{ls}$ and $P_r' = P_r + P_{lr}$ and rewrite the above equation

$$P_s' = P_m - P_r' \tag{5.6}$$

We can now transform the equation using torque and rotational speeds. T_m and T_e are the mechanical and electrical torque respectively, Ω_m and Ω_s are mechanical and electrical rotational speed

$$T_e\Omega_s = T_m\Omega_m + P_r' \tag{5.7}$$

rearranging the equation

$$P'_r = T_m\Omega_m - T_e\Omega_s \tag{5.8}$$

introducing now the slip s, defined as $s = \frac{\Omega_s - n\Omega_m}{\Omega_s}$ where n is the number of pole pair of the machine, and remembering that also mechanical and electrical torque are related by the number of pole pairs

$$P'_r = T_e(s\Omega_s) \tag{5.9}$$

combing (5.6) and (5.9) we can write

$$P_m = (1 - s)P'_s \tag{5.10}$$

so

$$P'_s = \frac{P_m}{1 - s} \tag{5.11}$$

and taking into account (5.6)

$$P'_r = -\frac{sP_m}{1 - s} \tag{5.12}$$

then bringing in evidence losses

$$P_s + P_{ls} = \frac{P_m}{1 - s} \tag{5.13}$$

$$P_r + P_{lr} = -\frac{sP_m}{1 - s} \tag{5.14}$$

Looking at the equation we can say that if mechanical power is positive, surely P'_s is positive. This because s can change sign, but it is always $|s| < 1$ (for a DFIG we can reach s up to $\pm\, 0.33$). Instead P'_r depends on s sign.

5.5   Four parameter induction machine equivalent model

We will now briefly recall the four parameter, *Park model* of an induction machine referred to rotating axes, with transient inductance on rotor side. We will use this

model since we want to control the machine with a field oriented vector control. The equations will be written in p.u., except for w_s (rotating speed of stator flux ψ_s) and w_b is the base electrical speed

$$\bar{v}_s = r_s\bar{i}_s + \frac{p\bar{\Psi}_s}{w_b} + j\frac{\omega_s}{w_b}\bar{\Psi}_s \tag{5.15a}$$

$$\bar{v}_r = r_r\bar{i}_r + \frac{p\bar{\Psi}_r}{w_b} + j\frac{\omega_r}{w_b}\bar{\Psi}_s \tag{5.15b}$$

$$p\Omega_m = \frac{1}{2H_t}(T_e - T_m) \tag{5.15c}$$

$$\omega_r = \omega_s - \Omega_m\omega \tag{5.15d}$$

Where variables with subscript $"s"$ are referred to the stator instead the subscript $"r"$ indicates rotor quantities. Moreover H_t is the inertia constant of the machine and the wind turbine, T_m is the prime mover torque (in this case the one from the wind) and T_e is the electrical torque. The sign convention for the variables in the equations is the one illustrated in figure 5.4 (the arrows indicate positive values)
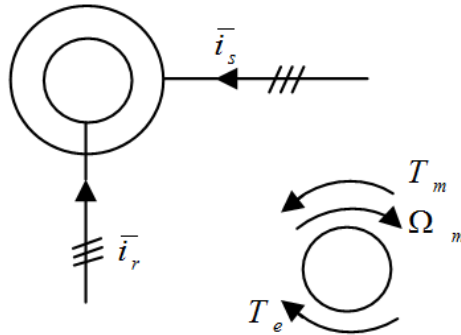
Figure 5.4: Sign convention for the DFIG

Now we have to consider also the link between fluxes and currents and the expression for the electromagnetic torque (* indicates the complex conjugate)

$$\bar{\Psi}_s = L_s(\bar{i}_s + \bar{i}_r) \tag{5.16a}$$

$$\bar{\Psi}_r = \bar{\Psi}_s + L_{kr}\bar{i}_r \tag{5.16b}$$

$$T_e = Re\frac{(\bar{v}_s\bar{i}_s^* + \bar{v}_r\bar{i}_r^*)}{\Omega} = -\Psi_{s_d}i_{s_q} + \Psi_{s_q}i_{s_d} \tag{5.16c}$$

where

$$L_{kr} = L_s(\frac{L_s L_r}{L_m^2}) \tag{5.17}$$

Now we choose as state variables $\bar{\Psi}_s$ and $\bar{i}_r$ and we rewrite the equations in (5.15) as function of these quantities also taking into account the relations in (5.16)

$$\frac{d\Psi_{s_d}}{dt} = (v_{s_d} - \frac{R_s}{L_s}\Psi_{s_d} + R_s i_{r_d})w_b \tag{5.18a}$$

$$\frac{d\Psi_{s_q}}{dt} = (v_{s_q} - \frac{w_s}{w_b}\Psi_{s_d} + R_s i_{r_d})w_b \tag{5.18b}$$

$$\frac{di_{r_d}}{dt} = (v_{r_d} - v_{s_d} - (R_r + R_s)i_{r_d} + \frac{R_s}{L_s}\Psi_{s_d} + \omega_r\frac{w_b}{L_{kr}}i_{r_q})\frac{wb}{L_{kr}} \tag{5.18c}$$

$$\frac{di_{r_q}}{dt} = (v_{r_q} - v_{s_q} - (R_r + R_s)i_{r_q} + (\omega_s - \omega_r)\frac{\Psi_{s_d}}{w_b} - \omega_r\frac{L_{kr}}{w_b}i_{rd})\frac{wb}{L_{kr}} \tag{5.18d}$$

$$\frac{d\Omega_m}{dt} = \frac{1}{2H_t}(T_m - T_e) \tag{5.18e}$$

5.6 Control system

The control of the machine is made through the rotor converter which gives the voltage $\bar{v}_r$. The inverter is assumed as ideal, so reference quantities given by the control system are supposed instantaneously applied. We will use a field oriented control (FOC). We choose a synchronous reference frame aligned with the stator flux which will always lie on d axis. Considering this we can say that $\Psi_{s_q} = 0$ and we can retrieve the value of ω_s from (5.18b) which results

$$\omega_s = \frac{v_{s_q} + R_s i_{r_d}}{\Psi_{s_d}}w_b \tag{5.19}$$

Sine d axis is not tied with the grid angular frequency w, but it depends on the orientation of the stator flux, and so on the machine dynamics, we need another state variable (which we name μ) to link the flux angle to the grid voltage angle. Let's consider the grid phase voltages that are (physical values)

$$v_a = \sqrt{2}V\cos(\omega t) \tag{5.20a}$$

$$v_a = \sqrt{2}V\cos(\omega t - \frac{2}{3}\pi) \tag{5.20b}$$

$$v_a = \sqrt{2}V\cos(\omega t + \frac{2}{3}\pi) \tag{5.20c}$$

with dq transformation on rotating axes with angular velocity equal to $\dot{\theta}_s = \omega_s$ the equations become

$$v_d = \sqrt{3}V\cos(\dot{\theta}_s - \omega t) \tag{5.21a}$$
$$v_q = \sqrt{3}V\sin(\dot{\theta}_s - \omega t) \tag{5.21b}$$

and considering line to line voltage as base voltage, we can transform the equations in p.u.

$$v_{d_{p.u.}} = V_{p.u.}\cos(\theta_s - \omega t) \tag{5.22a}$$
$$v_{q_{p.u.}} = V_{p.u.}\sin(\theta_s - \omega t) \tag{5.22b}$$

In the following the subscript $p.u.$ will be omitted. Let's now define the new variable μ

$$\mu = \int_0^t (\dot{\theta}_s - \omega)dt + \mu_0 \tag{5.23}$$

that becomes

$$\mu = \theta_s - \theta_{s0} - \omega t + \mu_0 \tag{5.24}$$

and so

$$\theta_s - \omega t = \mu + \theta_{s0} - \mu_0 \tag{5.25}$$

Now we can substitute this expression in 5.22

$$v_d = V\cos(\mu + \theta_{s0} - \mu_0) \tag{5.26a}$$
$$v_q = V\sin(\mu + \theta_{s0} - \mu_0) \tag{5.26b}$$
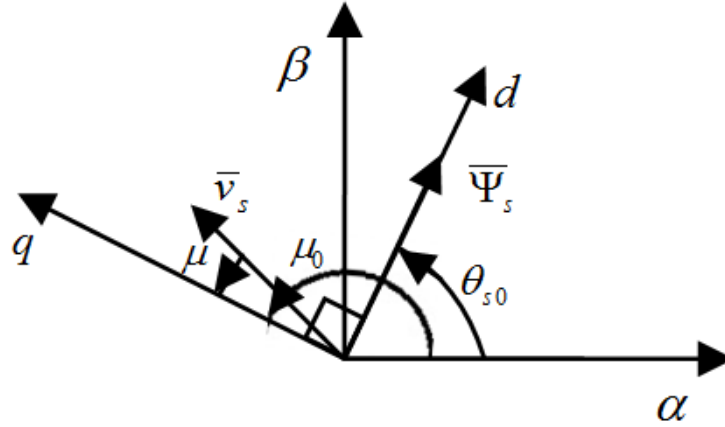
Figure 5.5: Representation of the vectors and angle described in this section

We can see in figure 5.5 a vectorial representation of these equation and concepts.

We choose μ_0 to satisfy the following equation

$$\theta_{s0} - \mu_0 = -90° \tag{5.27}$$

in this way

$$\mu_0 = \theta_{s0} + 90° \tag{5.28}$$

and so we can say that at the instant $t = 0$ the d axis is pointed by θ_{s0} and q axis by μ_0.
Now substituting (5.27) into (5.26) gives

$$v_d = V\cos(\mu - 90°) = V\sin(\mu) \tag{5.29a}$$
$$v_q = V\sin(\mu - 90°) = V\cos(\mu) \tag{5.29b}$$

In the following v_d and v_q of (5.29) will be named v_{sd} and v_{sq} since they are the stator voltages of the machine. And so

$$v_{s_d} = V sin(\mu) \tag{5.30a}$$

$$v_{s_q} = V cos(\mu) \tag{5.30b}$$

So in this way we found how to describe the grid voltage vector in the reference frame given by the stator flux. The operation is made through the angle μ which is defined in (5.23) through an integral, so we need to introduce another differential equation. This is done deriving with respect to time (5.23), which gives

$$\frac{d\mu}{dt} = \dot{\theta}_s - \omega \tag{5.31}$$

5.6.1   PI controllers

We choose a closed loop control equipped with a PI controller for each axis rotor current, the reference d axis current is set to zero ($i_{r_d}^{ref} = 0$) since we do not want to supply reactive power. The reference q axis current is obtained from (5.35) The controller are the same on d and q axis since the physical system is the same on d and q axes. In figure 5.6 and 5.7 we can see a block diagram of the current loops. To find the value of the proportional and integral coefficient we use the method explained in appendix A. The transfer function of the physical system ($G_{(s)}$) is the Laplace transform of (5.18c) neglecting coupling and compensated terms

$$G_{(s)} = \frac{1}{((R_r + R_s) + s\dfrac{L_{kr}}{w_b})} \tag{5.32}$$

Considering that such function crosses the 0 db axis at approximately 200 Hz we choose a passband for the closed loop equal to 100 Hz and a phase margin of 80 degrees. This to avoid to reach high values of the control variable which implies an high power for the actuator. With this condition we found the value listed in table 5.1

As explained in section 4.4.3 for the VSC, we introduce a differential equation for each PI controller, the introduced state variable are h_d and h_q

Table 5.1: Parameters of DFIG current loop PI controller

Parameter	Value
K_p	67.54 $p.u.$
K_i	0.523 $p.u./s$
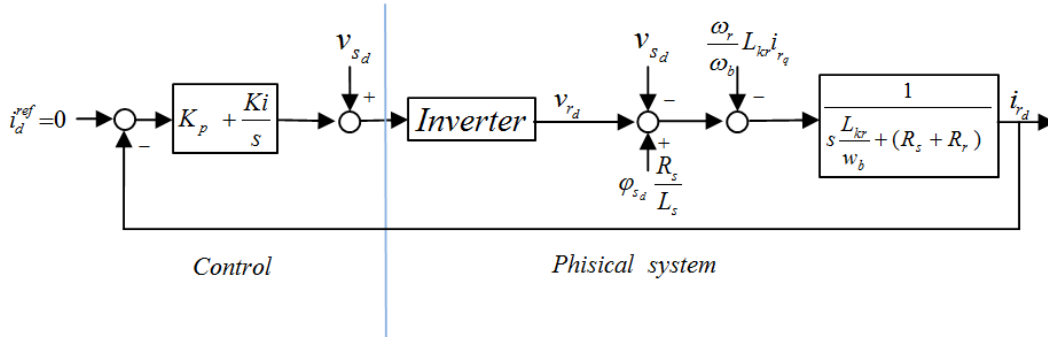
Figure 5.6: Current loop on d axis of the DFIG

$$\frac{dh_d}{dt} = K_i(i_{r_d}^{ref} - i_{r_d}) \tag{5.33a}$$

$$\frac{dh_q}{dt} = K_i(i_{r_q}^{ref} - i_{r_d}) \tag{5.33b}$$

Instead the reference rotor voltages are

$$v_{r_d} = h_d + Kp(i_{r_d}^{ref} - i_{r_d}) + v_{s_d} \tag{5.34a}$$

$$v_{r_q} = h_q + Kp(i_{r_q}^{ref} - i_{r_q}) + v_{s_q} \tag{5.34b}$$

The DC link between the two rotor converters is assumed as ideal, like the inverter that feeds the rotor. So the reference rotor voltages are assumed instantaneously applied. i_q^{ref} current reference that shows up in the equations is obtained from the torque reference taking into account the electrical torque expression in (5.16)c and that $\psi_{s_q} = 0$

$$i_q^{ref} = \frac{-T_e^{ref}}{\psi_{s_d}} \tag{5.35}$$
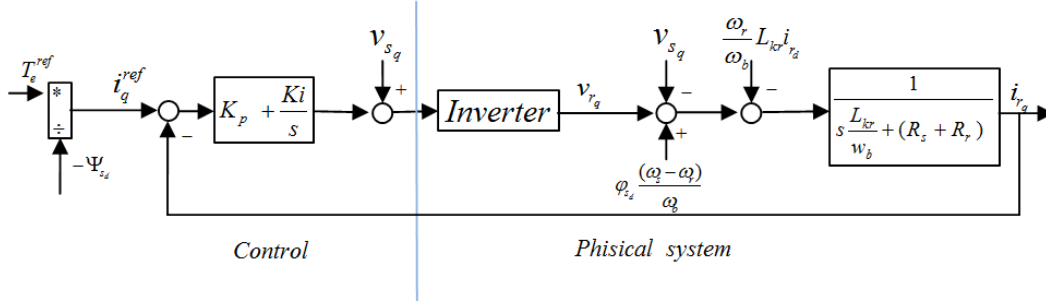
Figure 5.7: Current loop on q axis of the DFIG

5.7   System data

We decide to study a power plant of $1MW$, which is assumed as base power for the system. The data for the induction generator and the wind turbine are listed in table 5.2 and 5.3 respectively. Data are given already in p.u.

Table 5.2: Induction generator p.u. data. R_s: stator resistance, L_s: stator inductance, R_r: rotor resistance, L_{kr}: short circuit rotor side inductance

Parameter	Value (p.u.)
R_s	0.01
L_s	4
R_r	0.005
L_{kr}	0.267

Table 5.3: Wind turbine data. R: turbine radius, Ω_n: nominal rotating speed, H_t: inertia constant, v_w. rated wind velocity

Parameter	Value
R	$35.6\ m$
Ω_n	$2.4\ \frac{rad}{s}$
H_t	$6\ s$
v_{w_n}	$10\ \frac{m}{s}$

For the analysis we will need the value of the rotating speed of the blades in physical value. So the base mechanical speed: $\Omega_b = \Omega_n = 2.4\frac{rad}{s}$. We can now derive the expression of the mechanical base torque which will be also useful in future: $T_{b_m} = \frac{P_b}{\Omega_b}$ with $P_b = 1MW$.

5.7.1   Power coefficient Cp

In order to develop our studies we need an expression for the curve $C_p - \lambda$. We will use a polynomial approximation of a real turbine power curve. The polynomial is a fifth order polynomial given here

$$C_p = -10.4E^{-6}\lambda^5 + 491E^{-6}\lambda^4 - 8.34E^{-3}\lambda^3 + 53.23E^{-3*}\lambda^2 - 31E^{-3}\lambda - 147.3E^{-3} \tag{5.36}$$

In figure 5.8 the plot of $C_p - \lambda$ curve. Blue circulars represents the points of the real curve that we have used to estimate the polynomial curve. For a good approximation we will consider that λ will never decrease below 2 because at that value the polynomial curve is not a good approximation of the real one. This is not a problem since during normal operation λ is very far from 2.
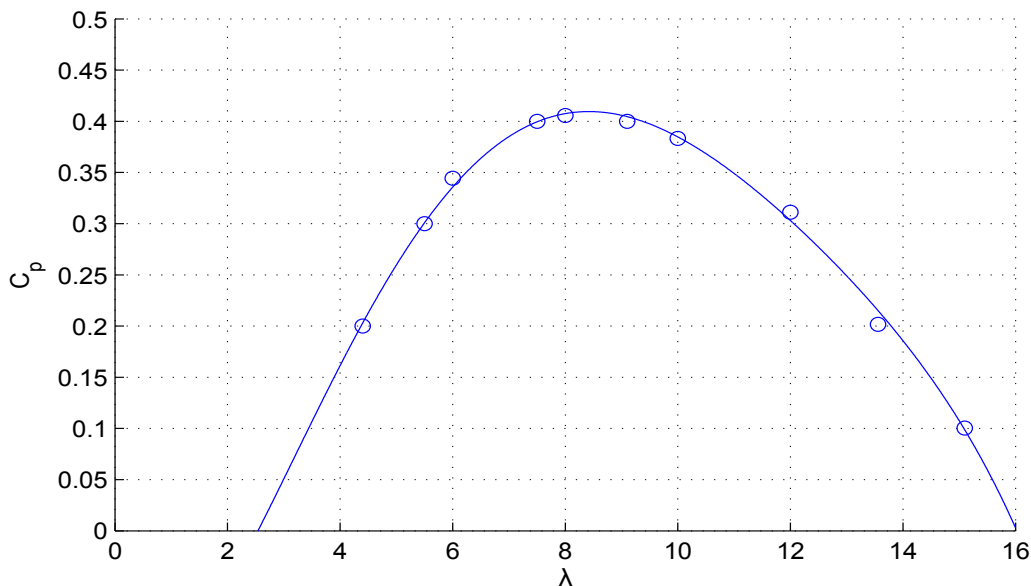

Figure 5.8: Power coefficient C_p as a function of the tip-speed ratio λ for the analysed wind turbine

5.8   Complete system of differential equations and eigenvalues

Here we write the complete system equations (gathering the various equations written in the previous sections). In (5.37) the differential equations and in (5.38)

the others. We point out that the expressions for P_{wind} gives physical value.

$$\frac{d\Psi_{s_d}}{dt} = (v_{s_d} - \frac{R_s}{L_s}\Psi_{s_d} + R_s i_{r_d})w_b \tag{5.37a}$$

$$\frac{di_{r_d}}{dt} = (v_{r_d} - v_{s_d} - (R_r + R_s)i_{r_d} + \frac{R_s}{L_s}\Psi_{s_d} + \omega_r\frac{L_{kr}}{w_b}i_{r_q})\frac{wb}{L_{kr}} \tag{5.37b}$$

$$\frac{di_{r_q}}{dt} = (v_{r_q} - v_{s_q} - (R_r + R_s)i_{r_q} + (\omega_s - \omega_r)\frac{\Psi_{s_d}}{w_b} - \omega_r\frac{L_{kr}}{w_b}i_{rd})\frac{wb}{L_{kr}} \tag{5.37c}$$

$$\frac{d\Omega_m}{dt} = \frac{1}{2H_t}(T_e - T_m) \tag{5.37d}$$

$$\frac{d\mu}{dt} = \omega_s - \omega \tag{5.37e}$$

$$\frac{dh_d}{dt} = K_i(i_{r_d}^{ref} - i_{r_d}) \tag{5.37f}$$

$$\frac{dh_q}{dt} = K_i(i_{r_q}^{ref} - i_{r_d}) \tag{5.37g}$$

$$v_{s_d} = V sin(\mu) \tag{5.38a}$$

$$v_{s_q} = V cos(\mu) \tag{5.38b}$$

$$\omega_s = (v_{s_q} + R_s i_{r_d})\frac{w_b}{\psi_{s_d}} \tag{5.38c}$$

$$\omega_r = \omega_s - \Omega_m\omega \tag{5.38d}$$

$$T_e^{ref} = -(\frac{\rho}{2}\pi R^5(\Omega_m\Omega_b)^2\frac{C_p^*}{\lambda^{*3}})/T_b \tag{5.38e}$$

$$i_{r_q}^{ref} = -\frac{T_e^{ref}}{\psi s_d} \tag{5.38f}$$

$$v_{r_d} = h_d + K_p(i_{r_d}^{ref} - i_{r_d}) + v_{s_d} \tag{5.38g}$$

$$v_{r_q} = h_q + K_p(i_{r_q}^{ref} - i_{r_q}) + v_{s_q} \tag{5.38h}$$

$$\lambda = \frac{\Omega_m\Omega_b R}{v_w} \tag{5.38i}$$

$$C_p = -10.4E^{-6}\lambda^5 + 491E^{-6}\lambda^4 - 8.34E^{-3}\lambda^3 + 53.23E^{-3*}\lambda^2 - 31E^{-3}\lambda - 147.3E^{-3} \tag{5.38j}$$

$$T_m = -\frac{P_{wind}}{\Omega_m P_b} = -\frac{\frac{\rho}{2}\pi R^3 v_w^2 C_p}{\lambda P_b} \tag{5.38k}$$

$$i_{r_q}^{ref} = -\frac{T_e^{ref}}{\psi s_d} \tag{5.38l}$$

The inputs (table 5.4) for the system are the grid voltage magnitude V which is set

equal to 1 $p.u.$, the grid frequency $2\pi f = \omega$ (under normal operation $f = 50Hz$), and the wind velocity v_w. The only coefficient not set in the equation are now C_p^* and λ^* which are used to find the reference torque as explained in section 5.3

Table 5.4: Input data for the DFIG, grid voltage magnitude V which is set equal to 1 $p.u.$ and grid frequency $2\pi f = \omega$ (under normal operation $f = 50Hz$)

Parameter	Value
V	$1\ p.u.$
Ω	$2\pi 50\ \frac{rad}{s}$

5.9 DFIG primary reserve

As explained in section 2.2 the primary reserve stops the frequency deviation and balance load and generation. Traditionally wind power plants do not take part in this regulation, but as said in section 2.2.1 Ireland and Great Britain renewable energy power plants are already requested to take part in primary regulation and this, in the future, may also happen in other countries. Traditionally primary reserve control is made by the so called droop control. This means that the prime mover power is adjusted according to the frequency deviation following a law like

$$P_g^{ref} = P_g^n - K_{droop}\Delta f \tag{5.39}$$

where P_g^n is the power reference under normal operating conditions. In figure 5.9 we can see a block diagram of the primary control. H_g is the overall time constant of the grid, P_l is the power drawn by the loads and P_g is the generated power (we assume by traditional power plants). This scheme is representative of one machine system or of a multi-machine system but only considering that synchronism is never lost, not even during transient. In the figure 5.9 we can also see the block representing the turbine delay here represented as a first order transfer function. This takes into account the time to change the primary mover power output. Taking into account this delay means that the power output is not instantaneously modified after a frequency variation.

The description above is valid for traditional power plants, but with DFIG the things are pretty much different. First off all the primary energy source is not controllable, and second, we can modify power output in a fast way. In fact the power is given by the product between the rotational speed and the electric
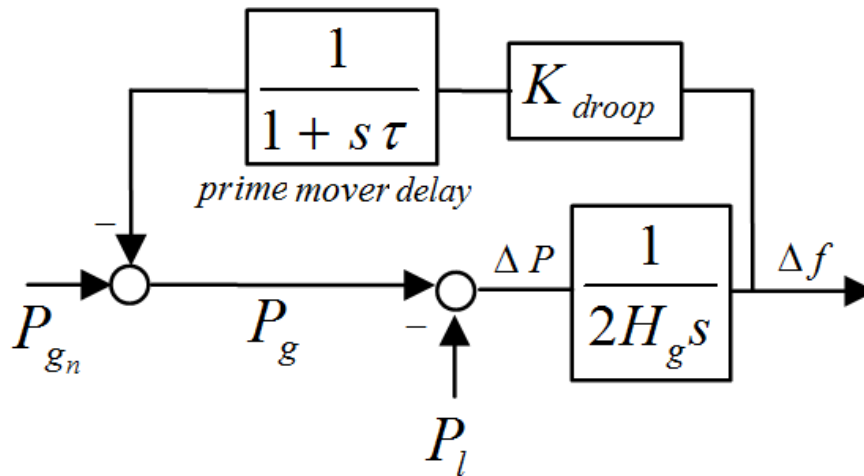
Figure 5.9: Block diagram of the primary control taking into account prime mover delay. The overall system inertia is represented by H_g. P_l is the power drawn by the loads and P_g is the generated power (we assume by traditional power plants).

torque. The rotational speed varies slowly, but not the electrical torque that is controlled through q axis current which has a high passing band (100 Hz as said in section 5.6.1). So we can modify power output with a prompt response by the only mean of a torque modification.

In a wind power plant, to overcome the first mentioned issue and be able to increase permanently power output after a frequency variation the only way is to run the power plant not following the maximum power point tracking (MPPT) strategy, but extract less power from the wind than the available one. To do this we have two ways

- acting on pitch angle, running the turbine at normal operation with a pitch angle different form the optimal one. In this way we extract less power than the one that is coming from the wind and if it is needed we can modify the pitch angle to extract some more power. Regarding this regulation it is worth to say that modifying pitch angle is not an easy and fast action, and generally we try to maintain pitch angle as constant as possible also because the mechanism is delicate.

- acting on angular velocity, that is running the turbine at a speed higher than the optimal one. In this way if more power is needed we can increase power output in a very fast way incrementing electrical torque. This will cause a droop in the angular speed of the turbine which will cause an increase in generated power due to the reaching of a higher efficiency region. In figure 5.10 we can see in green the MPPT power tracking curve and in red the

de-loaded power tracking curve. In this case it correspond to the 95% of the available power.
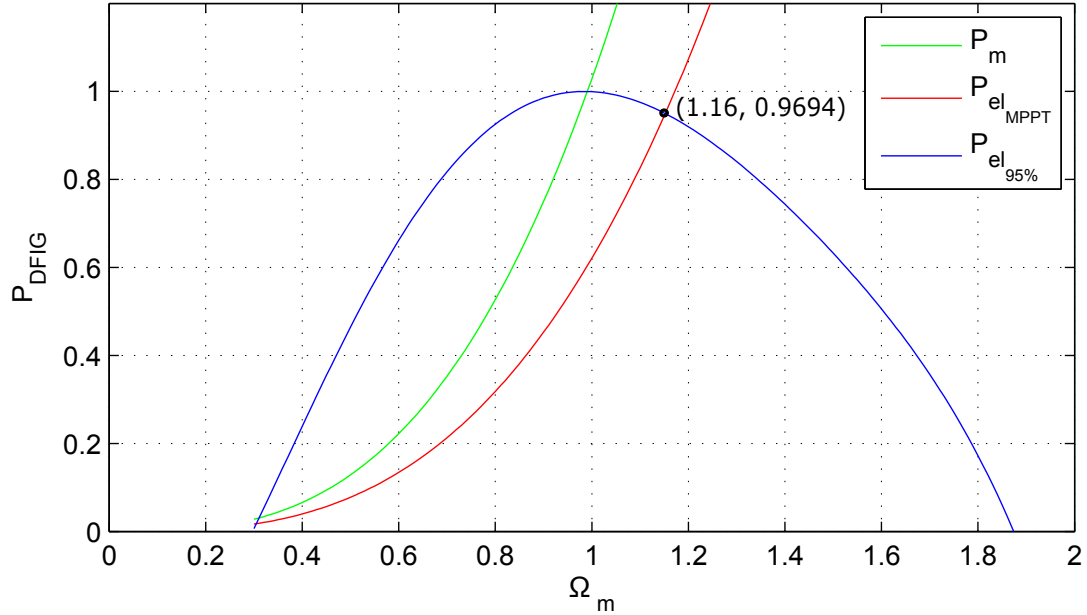
Figure 5.10: Mechanical power (in blue), MPPT curve (green) and de-loaded power tracking curve (red)

In this work we will consider the pitch angle always constant and we will exploit the second method. We will use as reference power tracking curve the red one in figure 5.10 it has the equation reported in (5.3) with

$$C_p^* = 0.3889 \tag{5.40a}$$

$$\lambda^* = 9.85 \tag{5.40b}$$

Instead the MPPT curve has

$$C_p^{MPPT} = 0.4095 \tag{5.41a}$$

$$\lambda^{MPPT} = 8.47 \tag{5.41b}$$

5.9.1   stability analysis of the de-loaded system

We now compute the operating point and the eigenvalues for the system adopting a de-loaded reference curve described in the section above. The equations of the system are the ones listed in (5.37) and (5.38) taking into account (5.40). At this point, applying the Newton-Raphson method we find the equilibrium point of the system. Then for the linearised system around that point we evaluate the eigenvalues. The results are in the tables and figures below.

Table 5.5: State variables at the equilibrium point (case $v_w = 10 \ m/s$)

Parameter	Value (p.u.)
$\psi_{s_d 0}$	0.9999
$i_{r_d 0}$	0
$i_{r_q 0}$	0.824
Ω_{m0}	1.152
μ_0	0.0025
h_{d0}	−0.0309
h_{q0}	−1.139

We can see that Ω_m is greater than one even if wind velocity is $v_w = 10 \ m/s$ which is the nominal wind speed. This because we are using a de-loaded reference power curve, the red one in figure 5.10 and the intersection with the mechanical power available from the wind is at a velocity higher than the nominal one.

Table 5.6: Eigenvalues of the linearised system around the equilibrium point (case $v_w = 10 \ m/s$)

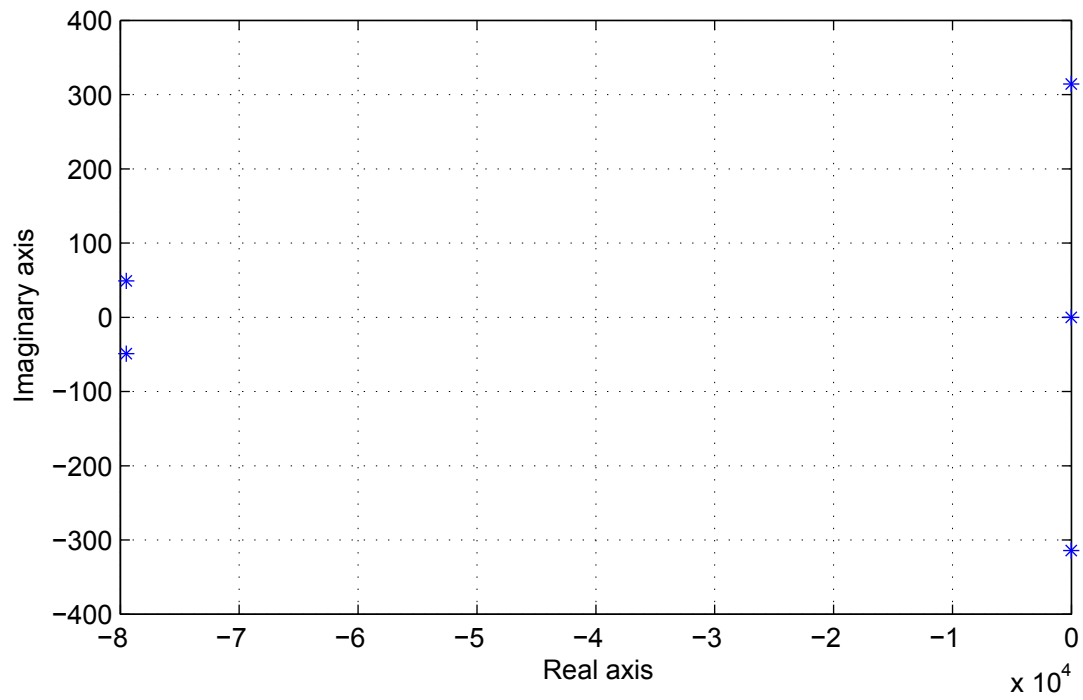| Parameter	Value (rad/s)	Damping factor
λ_1	$-79.4908 \ 10^3 + 49.0075i$	≈ 1
λ_2	$-79.4908e \ 10^3 - 49.0075i$	≈ 1
λ_3	$-789.6947 \ 10^{-3} + 314.1636i$	0.0025136
λ_4	$-789.6947 \ 10^{-3} - 314.1636i$	0.0025136
λ_5	$-220.9105 \ 10^{-3}$	1
λ_6	$-7.7466e \ 10^{-3}$	1
λ_7	$-7.7006e \ 10^{-3}$	1

Figure 5.11: Eigenvalues in the complex plane (case $v_w = 10 \; \frac{m}{s}$)
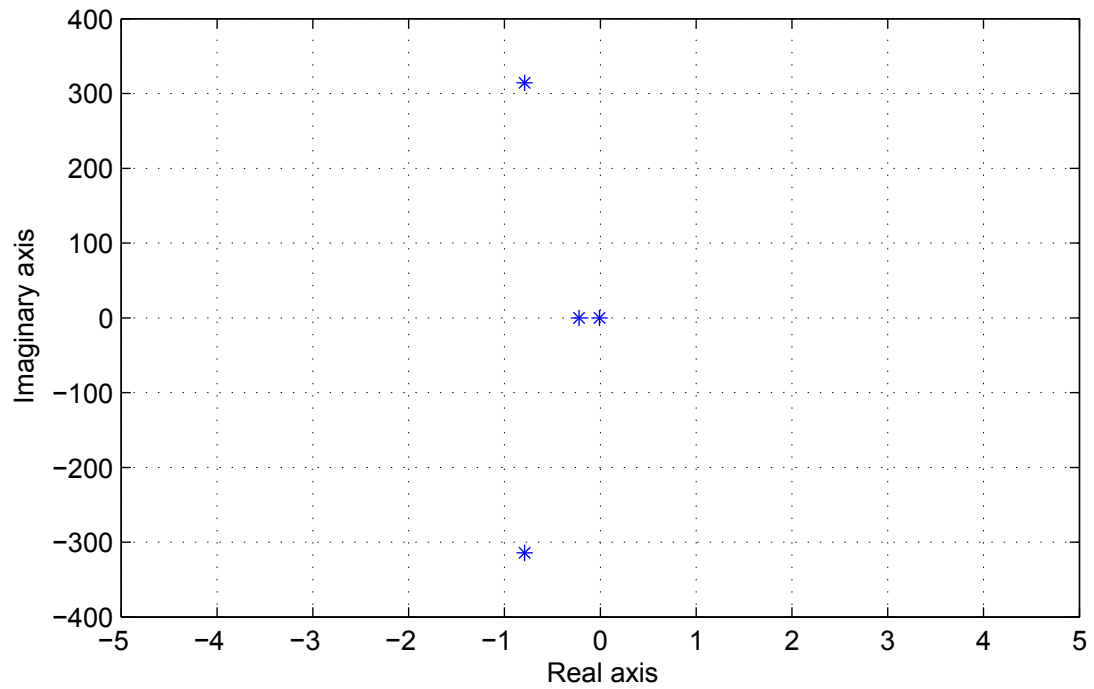

Figure 5.12: An enlargement of the plot of the complex plane in figure 5.11 near the origin (case $v_w = 10 \; \frac{m}{s}$)

As we can see from the figures the system is stable, but has two eigenvalues not well dumped (λ_3 and λ_4). The damping ratio (σ) of such eigenvalue is

$$\sigma = \frac{-Re(\lambda)}{\sqrt{Re(\lambda)^2 + Imm(\lambda)^2}} = 0.00248 \qquad (5.42)$$

These are two critical eigenvalues since a low damping ratio can lead to instability. We now try to find to which variables these eigenvalues are related. We compute the participation factors [15]. We compute this for the case $v_w = 10\frac{m}{s}$.

Table 5.7: Participation factors (absolute value) of the state variables to the eigenvalues

State variable	Participation factor for λ_3	Participation factor for λ_4
ψ_{s_d}	0.5	0.5
i_{r_d}	$76.457 10^{-9}$	$76.457 10^{-9}$
i_{r_q}	$13.556 10^{-9}$	$13.556 10^{-9}$
Ω_m	$135.695 10^{-12}$	$135.695 10^{-12}$
μ	0.5	0.5
h_d	$476.958 10^{-12}$	$476.958 10^{-12}$
h_q	$1.836 10^{-12}$	$1.836 10^{-12}$

As we can see from table 5.7 the state variables that most influence the position of λ_3 and λ_4 are ψ_{s_d} and μ.

5.9.2   Analysis varying v_w and V

We now compute the eigenvalues for different wind velocities v_w and grid voltages V. Wind velocity is varied between 5 m/s and 13 m/s with steps of 0.5 m/s (keeping $V = 1$ $p.u.$), grid voltage between 0.9 $p.u.$ and 1.1 $p.u$ with steps of 0.01 $p.u$ (keeping $v_w = 10$ m/s). In addition to eigenvalues we plot here also the values of the state variable μ and ψ_{s_d} and the electrical power output for each case, in the figures where these are plotted, on x axis there is the related value of grid voltage or wind velocity. The results are reported in the following figures. As we can see the angle μ does not vary in both cases. Instead as expected the electrical power output varies if wind velocity varies (we can recognise from figure 5.15 that it varies with the cubic power of v_w), instead it does not vary if grid voltage is varied. Instead the flux ψ_{s_d} varies only with the grid voltages. Looking at the eigenvalues we can see that they do not vary so much their position. So we can conclude that the operating point does not influence very much the stability.
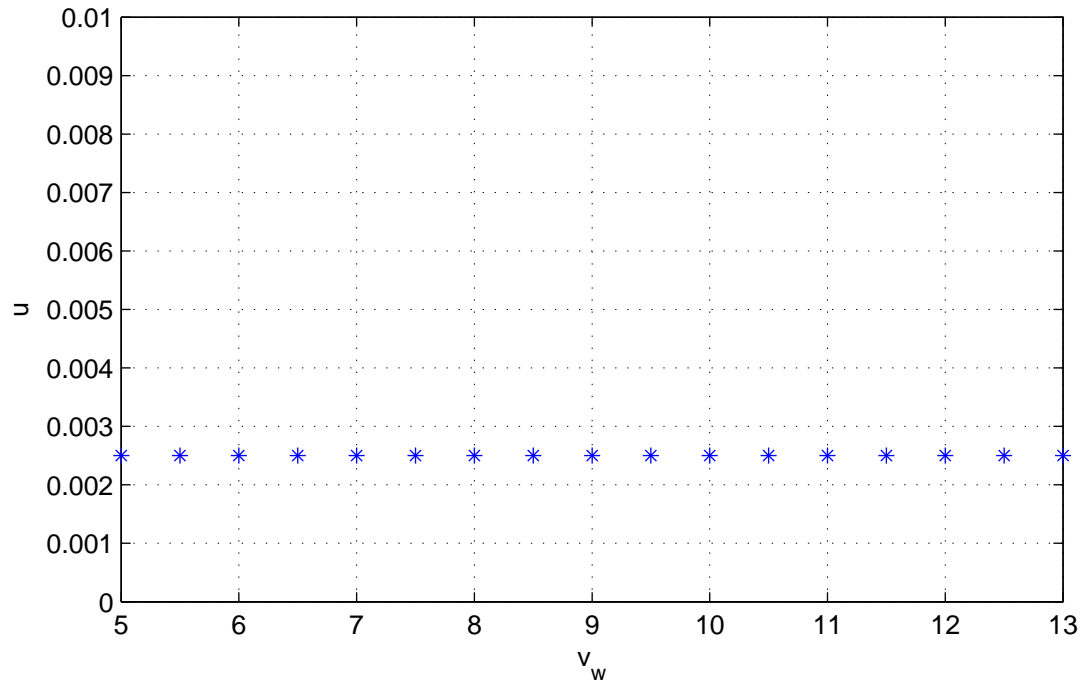
Figure 5.13: Values of the state variable μ for different wind velocity values
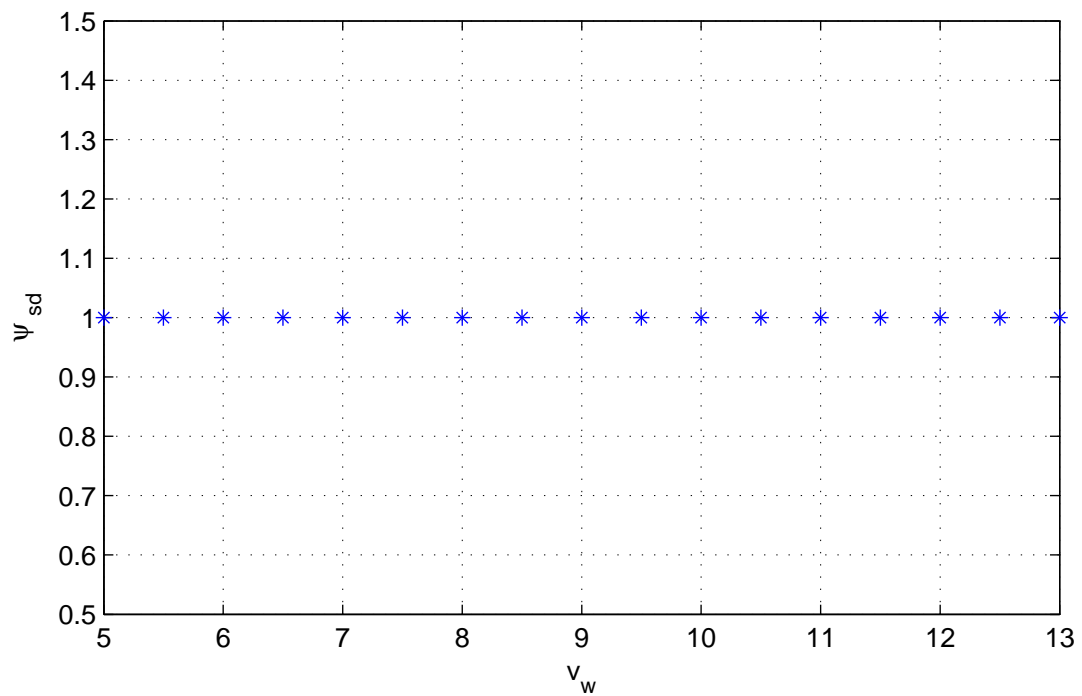
Figure 5.14: Values of the state variable ψ_{sd} for different wind velocity values
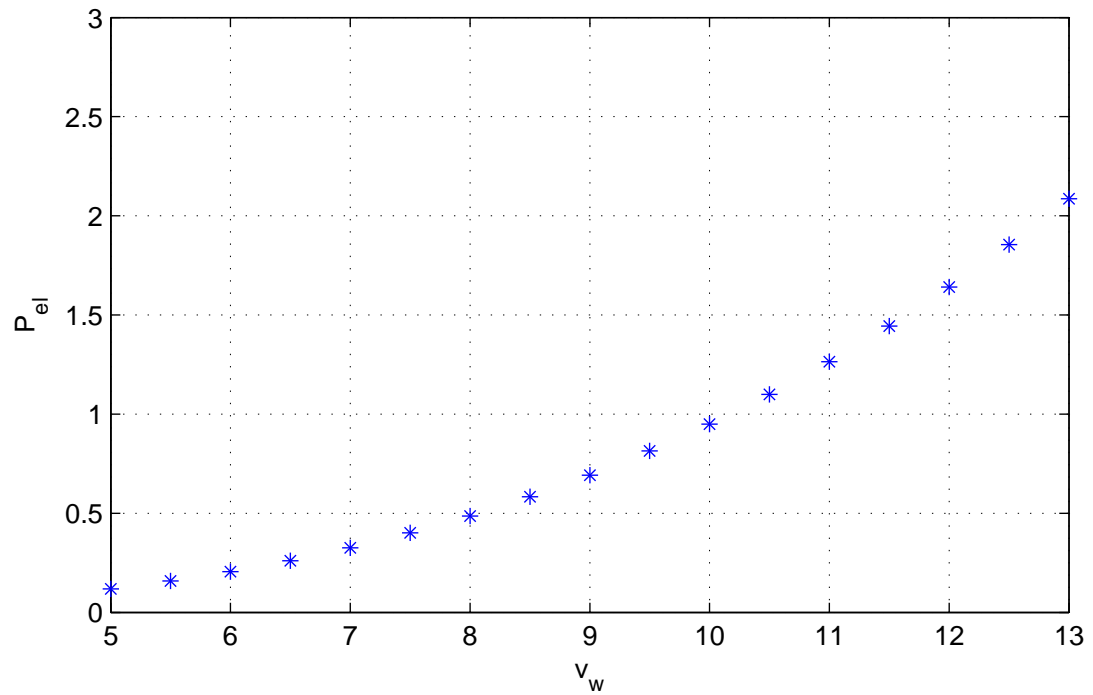
Figure 5.15: Values of the power output for different wind velocity values

Figure 5.16: Eigenvalues for different wind velocity values (the two most distant eigenvalues from the real axis are not plotted)

Figure 5.17: Values of the state variable μ for different grid voltage values

Figure 5.18: Values of the state variable ψ_{sd} for different grid voltage values

Figure 5.19: Values of the power output for different grid voltage values

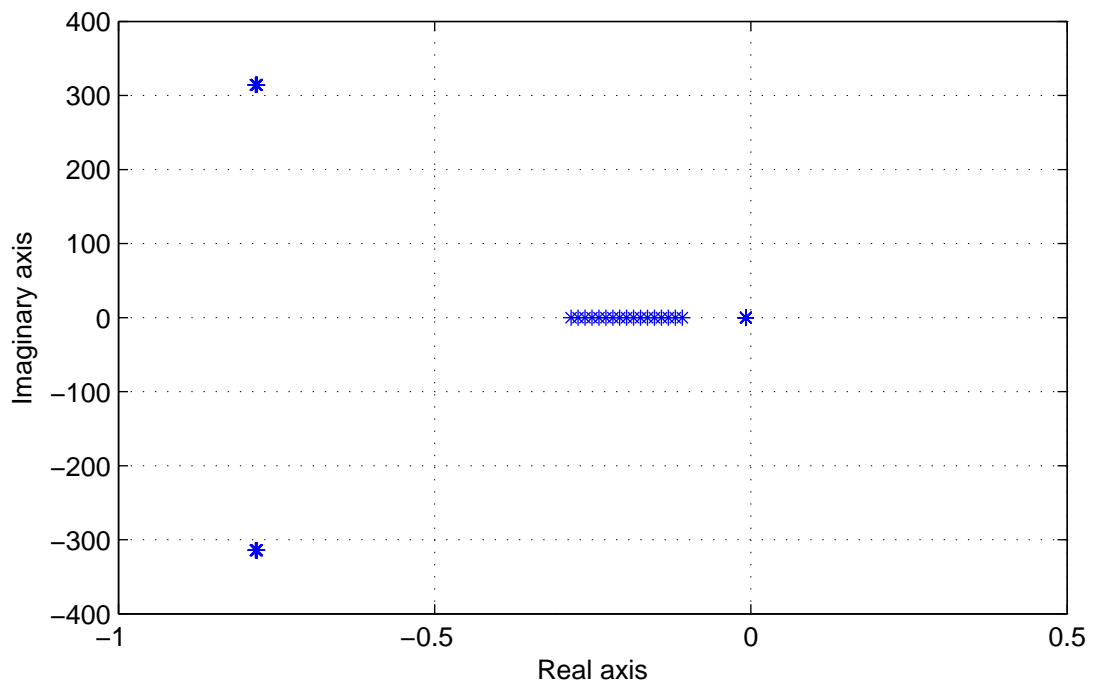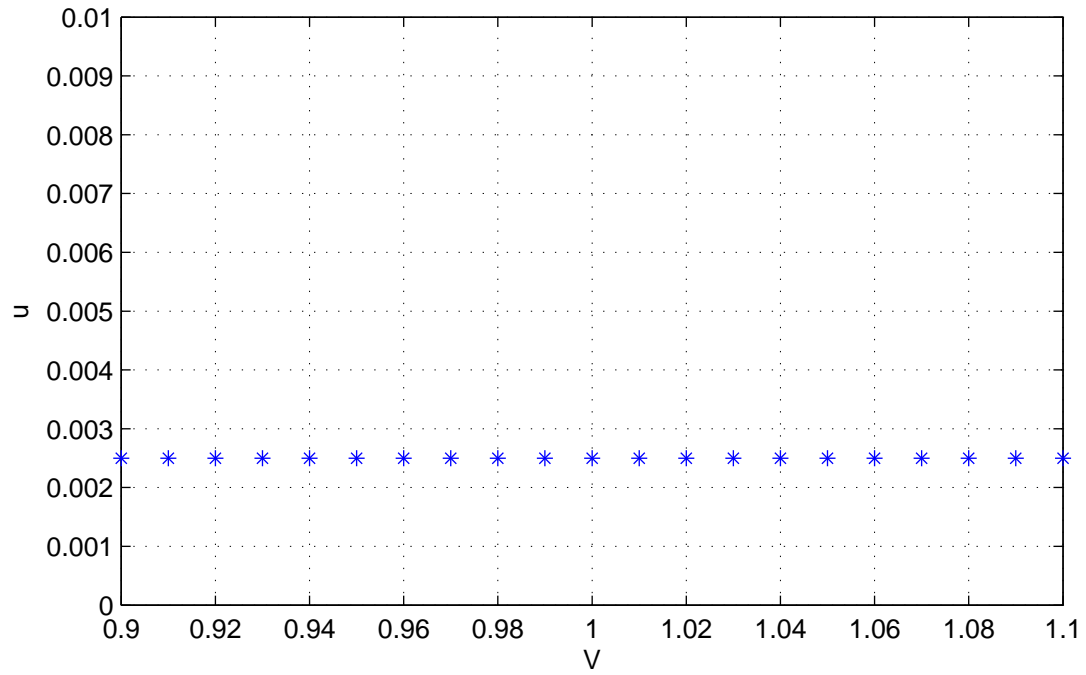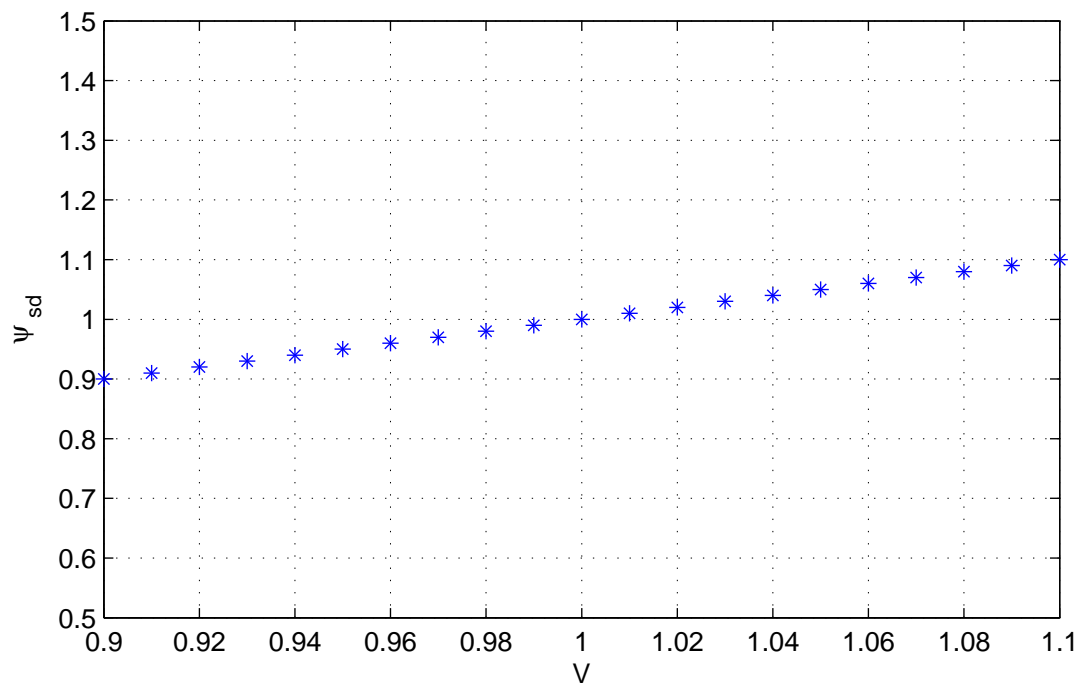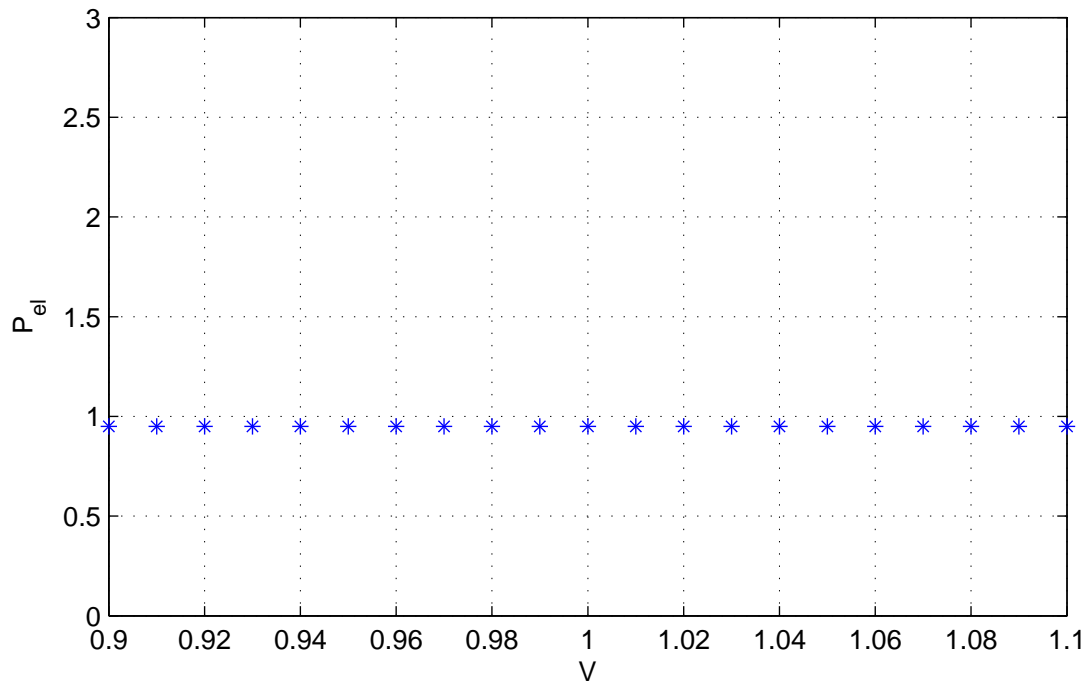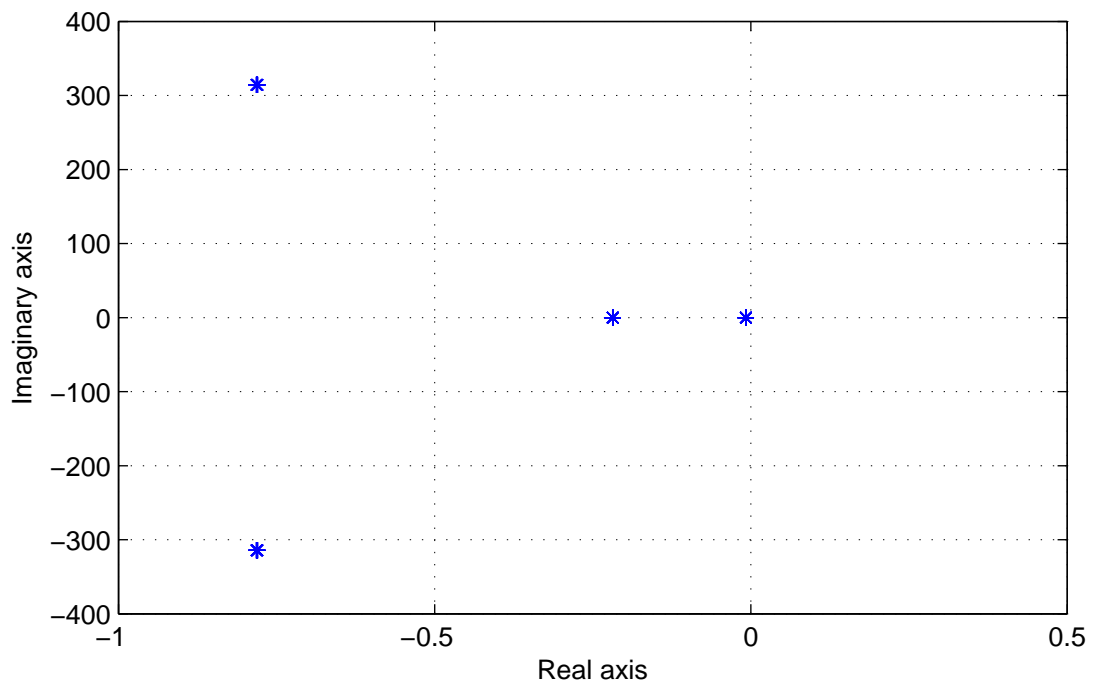Figure 5.20: Eigenvalues for different grid voltage values (the two most distant eigenvalues from the real axis are not plotted)

5.10 DFIG primary reserve - Moving reference power curve

We will now implement the primary droop control. As said before, we consider to run the wind farm not through MPPT strategy, but at 95% of the available power, so in every moment we are able to increase power output of 5% as a response to frequency grid disturbances. We have to highlight that in this way the power reserve is not constant, but it depends on the power output of the wind farm. The power we are able to extract from the wind depends on the coefficient C_p as explained in section 5.2. Here we recall the formula for the wind power

$$P_{wind} = \frac{\rho}{2}\pi R^2 v_w^3 C_{p(\lambda,\beta)} \tag{5.43}$$

Our goal is to extract at whatever wind condition the 95% of the available wind power in absence of grid frequency deviation and to modify linearly the power output with the grid frequency deviation. Looking at the above equation it seems easy, the power depends linearly on C_p so we can modify the C_p coefficient according to grid frequency deviation and obtain a droop control, so the value of C_p^* is settled. But in our control system we have the equation

$$T_e^{ref} = (\frac{\rho}{2}\pi R^5(\Omega_m\Omega_b)^2\frac{C_p^*}{\lambda^{*3}})/T_b \tag{5.44}$$

where shows up also λ^*. We have to retrieve it from the value of C_p^*. In (5.36) we approximate the $C_p - \lambda$ function by means of a fifth order polynomial, so to retrieve the value of λ^* starting from C_p^* we need to find the roots of a fifth order polynomial equation and choose the one of interest. Doing this numerically is not a problem, but for eigenvalues computation we need a closed formula of the solution which doesn't exist for such polynomial equation. So we change the approximation, instead of using a fifth order polynomial we will use a second order one. In this case we know the exact solution of the polynomial equation and we can introduce it in the stability study. In figure 5.10 we can see a plot of the $C_p - \lambda$ curve approximated with a second and a fifth order polynomial. The small blue circles are the points retrieved from the actual curve. We can say that the point are a bit farther from the curve, but in the region of interest it can be considered a good approximation.

The second order polynomial is

$$C_p = -9.3154E^{-3}\lambda^2 + 162.6299E^{-3}\lambda - 303.2498E^{-3} \tag{5.45}$$

Looking at (5.43) we can say that to extract the 95% of the wind power we need
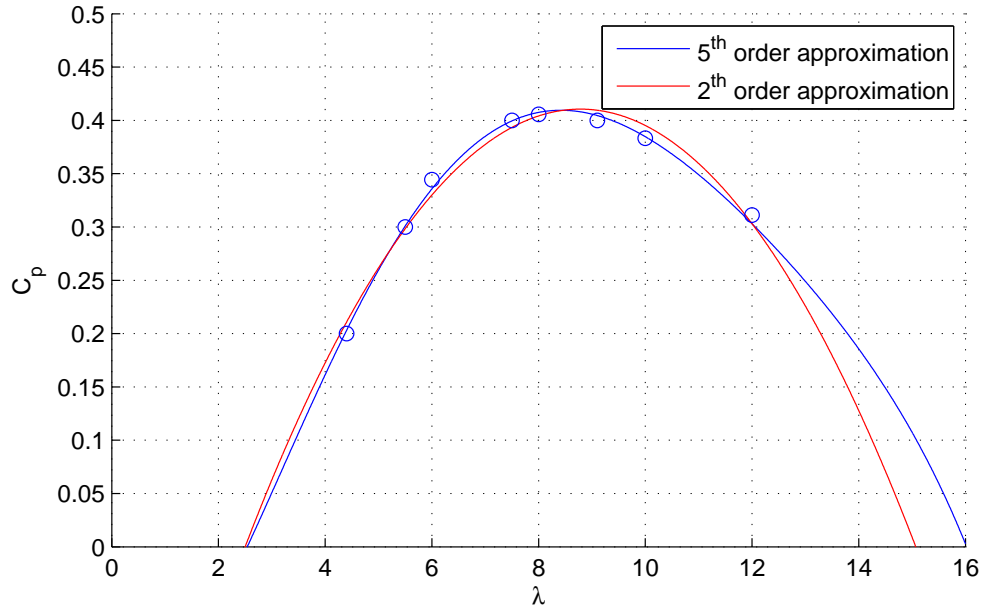
Figure 5.21: $C_p - \lambda$ curve, in red the approximation with a second order polynomial, the small blue circulars are the point retrieved from the actual curve.

to work with a C_p equal to the 95% of the maximum one achievable. Looking at figure 5.21 we can find that the maximum available C_p is equal to 0.406. Considering now that we want to modify power reference according to grid frequency deviation we can write that reference C_p is

$$C_p^* = (0.95 - K\Delta f)C_p^{max} \tag{5.46}$$

where f is the frequency in p.u. and $C_p^{max} = 0.406$. Once we have computed this value we have to find the value of lambda which permits to have such value, we need to solve

$$C_p^* = -9.3154E^{-3}\lambda^{*^2} + 162.6299E^{-3}\lambda^* - 303.2498E^{-3} \tag{5.47}$$

The equation has two solution, the ones pointed out in figure 5.22 with red crosses. We always choose the right solution, since the left one would not be a stable. In fact in case of the left solution, if we deliver more power that the one that is coming from the wind and so Ω_m decreases, this will cause a reduction in the power we are able to extract from the wind since we go to a less efficiency region. This will cause another speed reduction and so on.
So with the solution formula for the second order equation we find the value of λ^*.
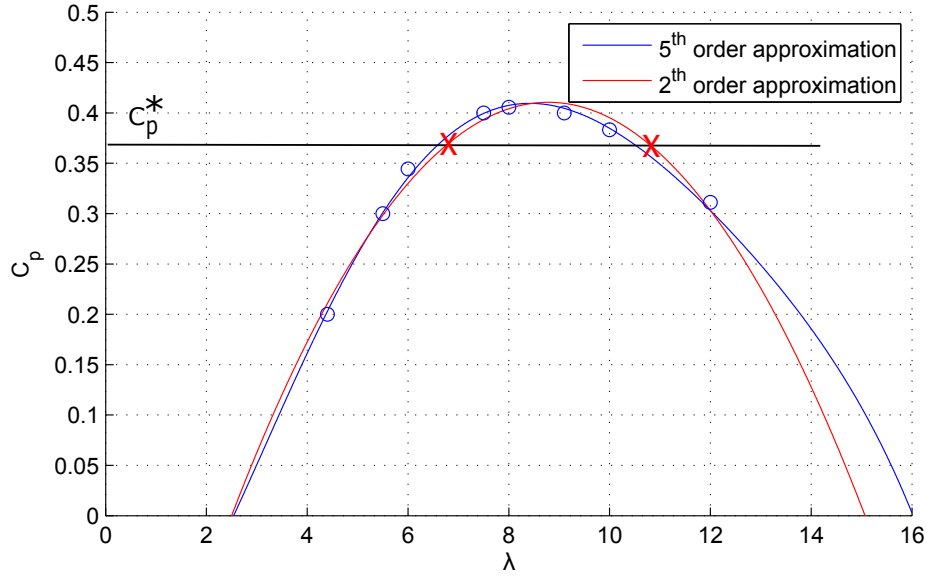
Figure 5.22: The red crosses indicates the solution of the equation (unknown λ^*)

At this point we only have to choose the value of K in (5.46). We made the choice considering to deliver all the power reserve in presence of a grid frequency deviation of 1%. So $K = 5$. Now that we have all the elements we can compute again with Newton-Raphson method the equilibrium point and than the eigenvalues. The equations for the system are the one in 5.37 and 5.38 taking into account that C_p^* and λ^* are no more constant values, but are calculated as previously described. In table 5.9 there are the state variables at the equilibrium point and in table 5.10 the eigenvalues. As input we use again the one in table 5.4

Table 5.8: State variables at the equilibrium point (case $v_w = 10 \ m/s$ and C_p^* found according to 5.46)

Parameter	Value (p.u.)
ψ_{s_d0}	0.9999
i_{r_d0}	0
i_{r_q0}	0.7875
Ω_{m0}	1.1960
μ_0	0.0025
h_{d0}	-0.0437
h_{q0}	-1.207

Table 5.9: State variables at the equilibrium point (case $v_w = 10 \ m/s$ and C_p^* found according to (5.46))

Table 5.10: Eigenvalues of the linearised system around the equilibrium point (case $v_w = 10\ m/s$ and C_p^* found according to (5.46))

Parameter	Value (rad/s)	Damping factor
λ_1	$-79.4909\ 10^3 + 62.7491i$	≈ 1
λ_2	$-79.4909e\ 10^3 - 62.7491i$	≈ 1
λ_3	$-789.2935e\ 10^{-3} + 314.1632i$	0.0025124
λ_4	$-789.2935\ 10^{-3} - 314.1632i$	0.0025124
λ_5	$-206.4342\ 10^{-3}$	1
λ_6	$-7.7467\ 10^{-3}$	1
λ_7	$-7.6973\ 10^{-3}$	1

5.10.1 Grid model and simulation with DFIG constant power output

We will now simulate using Matlab-simulink the previously described DFIG wind turbine connected to an electrical grid. in figure 5.23 the scheme of the system. We model the electrical network as described in section 5.9. In figure 5.24 the block scheme used for the simulation, with respect to the one in figure 5.9 we can see we have added the power produced by the DFIG (P_{DFIG}).
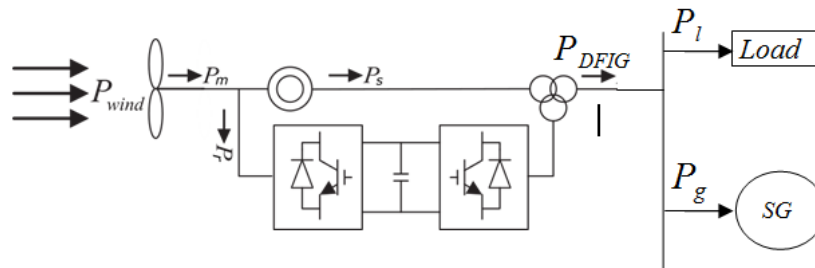

Figure 5.23: Grid model for the simulation

The DFIG, which nominal power is equal to 1 $p.u.$ is inserted in a grid that supply a load of 5 $p.u.$. The overall inertia constant of the grid is $H_g = 5s$. The time constant of the prime mover of the traditional power plant (τ) is chosen equal to 500 ms. We think to deal with a hydroelectric power plant, much more faster that a thermal power plant whose turbine time constant can reach values of around 10 s [16]. K_{droop} is chosen equal to 40 $p.u.$. We made this choice considering that the primary reserve of the plant is equal to 10 % of the nominal power (which in this case is approximately equal to $P_{gn} \approx 4\ p.u$) is totally delivered in presence of a grid frequency deviation of 1 %. Let's now consider the DFIG power output

as a constant to see how the grid reacts if the load is instantaneously increased of 1% after 1 s the simulation is started. The DFIG power output is constant and equal to 0.95 $p.u.$. In figure 5.25 we can see the power drawn by the load, instead in figure 5.26 the power produced by the traditional power plant. Eventually in figure 5.27 we can see how the frequency evolves in time. We can note in the frequency an oscillation due to the delay introduced by the prime mover delay. This simulation will be compared with the one with the DFIG power output regulated in the next sections. We will refer to this case as "base case"
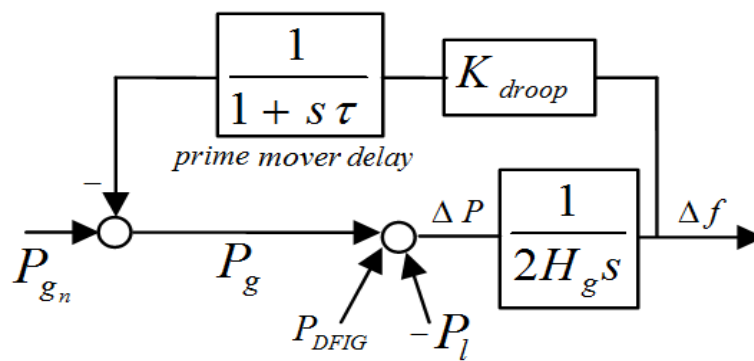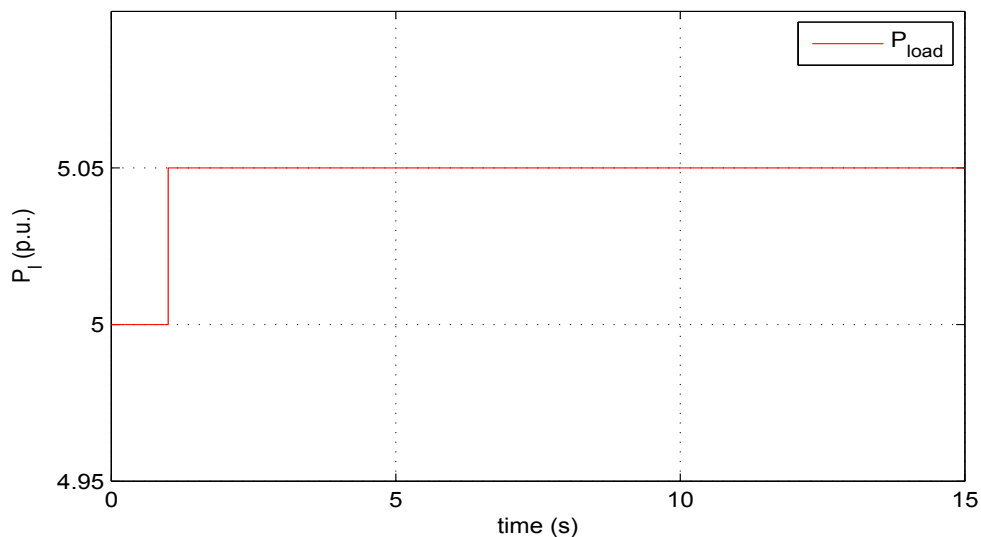

Figure 5.24: Grid model for the simulation

Figure 5.25: Power drawn by the load, at $t = 1$ s the imposed step increase of 0.05 $p.u.$.
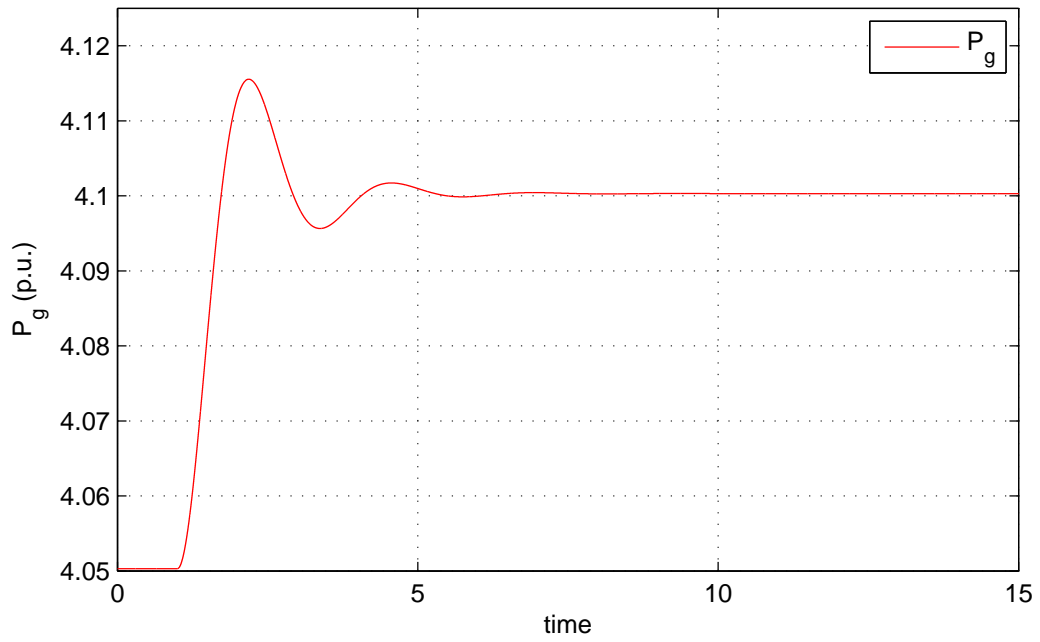
Figure 5.26: Power delivered by the traditional power plant. The transient is due to the load variation reported in figure 5.25
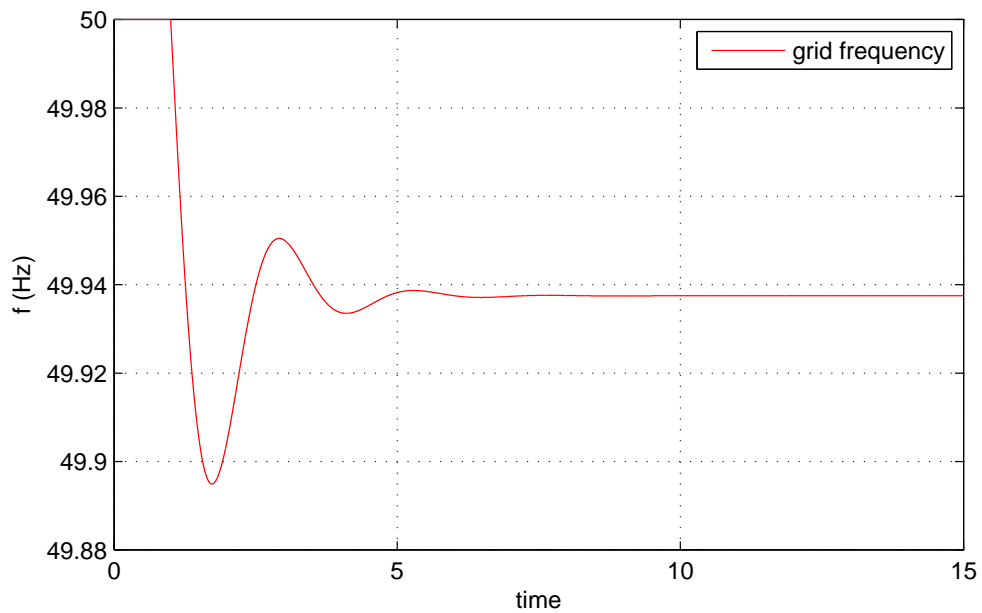

Figure 5.27: Grid frequency behaviour due to the load variation reported in figure 5.25

5.10.2 Simulation with DFIG equipped with primary reserve

In the following simulation the DFIG power output is not kept constant, but adjusted according to grid frequency as explained in the first part of section 5.10. Here we see how the system behaves in presence of the DFIG primary reserve and that this primary reserve behaves in a similar way of an inertia except for the first part time interval after the load disturbance.

The load variation is the same of the previous case (figure 5.25). In the following figures we can see some important variable of the system and for some of them we can do a comparison between this case and the previous one described in section 5.10.1. In figure 5.28 we can see the grid frequency and in figure 5.29 we can see in the same plot the frequency behaviour for this case and the base case (section 5.10.1). We can note that it has a smaller oscillation than the one we can observe in the base case, moreover its steady state value is higher than the one of the case before. But we can note that the transient in the base case is much faster.The difference in the setting time is due to the DFIG behaviour, let's analyse this.

After the load imbalance the frequency starts to fall. So the droop control of the traditional power plant and the power control of the DFIG begin to act. The frequency deviation is stopped in a shorter way with respect to the previous case, in fact we can see that in the previous case it reaches a lower peak value . This is due to the DFIG action. Then the frequency starts to increase and then after an oscillation starts to decrease monotonically setting to a steady state value with a transient time very large if compared with the one it has in the base case. This is due to the DFIG. To explain this let's look at figure 5.30 and at figure 5.31 (an enlargement of the interesting area). The blue curve is the power coming from the wind, the red curve the power tracking characteristic that we were following before the disturbance and the green one is the actual power delivered during the simulation (the arrow indicates the direction with respect to time). Let's look at point A, it is reached at time $t = 1.5\ s$. We retrieve the time value from the graph of the power delivered by the DFIG (figure 5.32), we note also that at this time the frequency stops to fall. But this is not a stable operating point since it is not the intersection between the power coming from the wind and the one delivered. So the mechanical speed starts to fall. This causes a reduction in power set point since we are using a power reference proportional with the third power of the angular speed. This causes a continuous unbalance between generation and load which causes the frequency ongoing falling. This happens in a slowly manner due to the fact that the angular velocity of the DFIG changes slowly since the power imbalance that he sees is not high (it is the difference between the blue and the green curve in figure 5.31 for a specific value of Ω_m). Than the transient will end when the delivered electrical power reachs the one coming from the wind in point B.
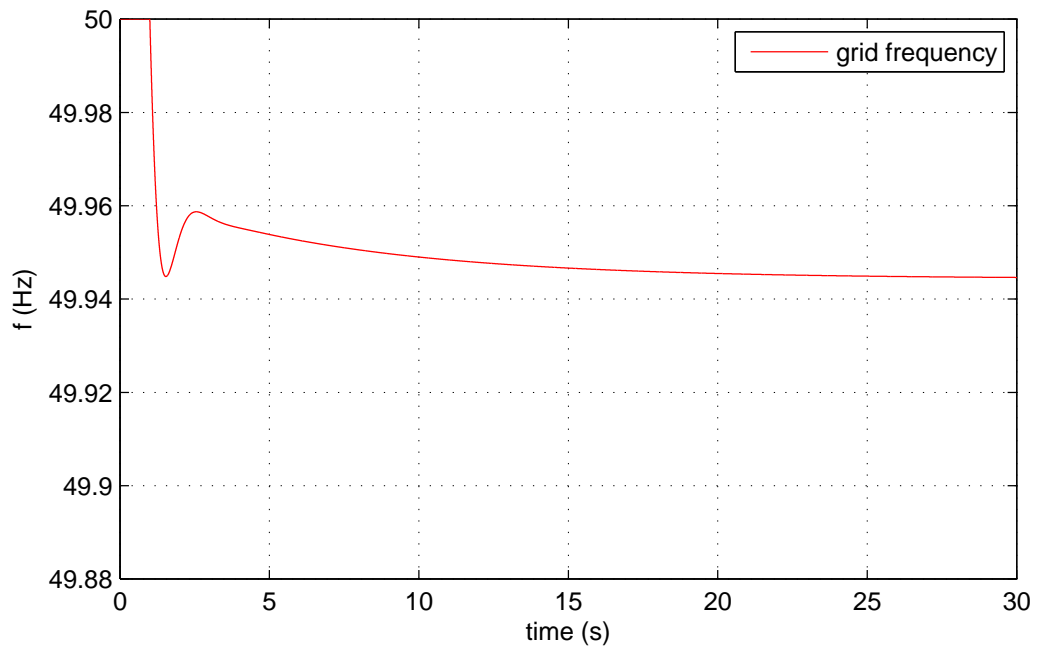
Figure 5.28: Grid frequency behaviour due to the load variation in figure 5.25 considering the DFIG equipped with primary power reserve
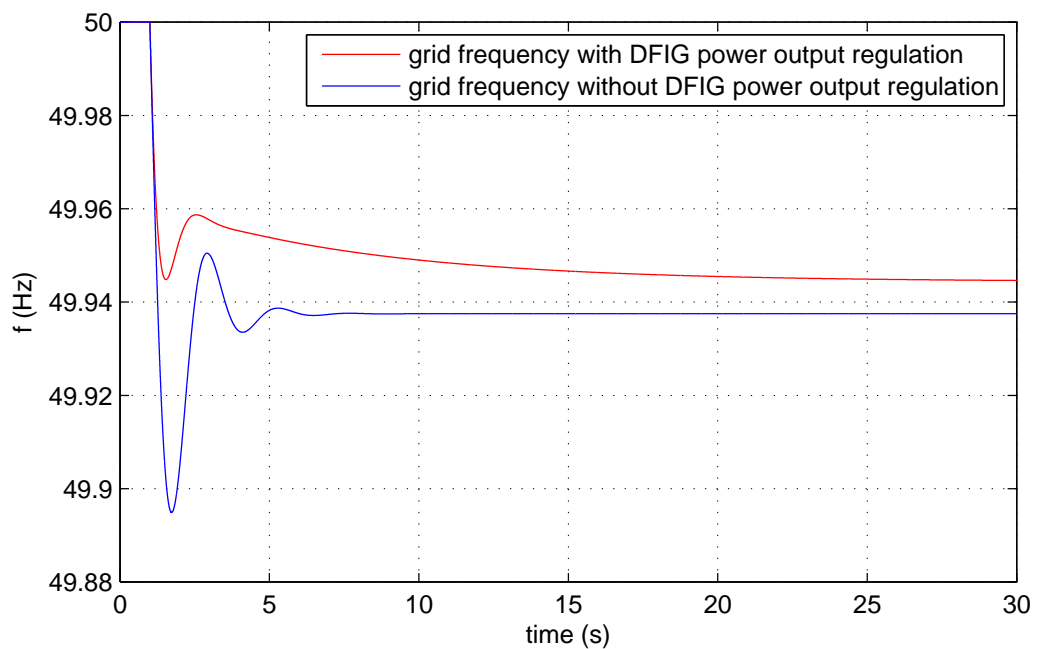
Figure 5.29: Grid frequency comparison between the base case and the one described in this section
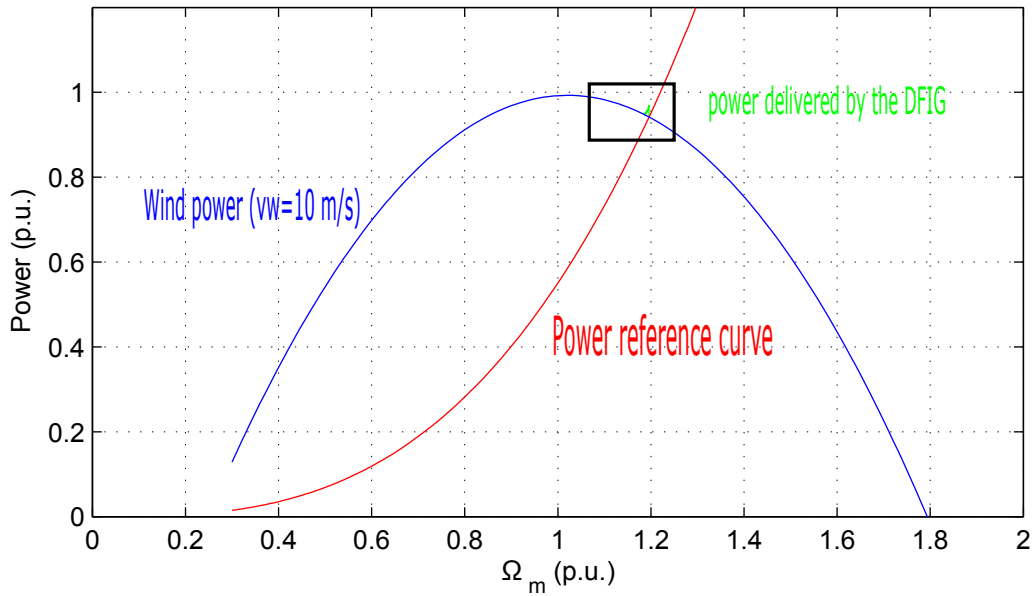
Figure 5.30: In blue the power coming from the wind (considering $v_w = \ s$), in red the power tracking curve and in green power output trajectory with respect to Ω_m
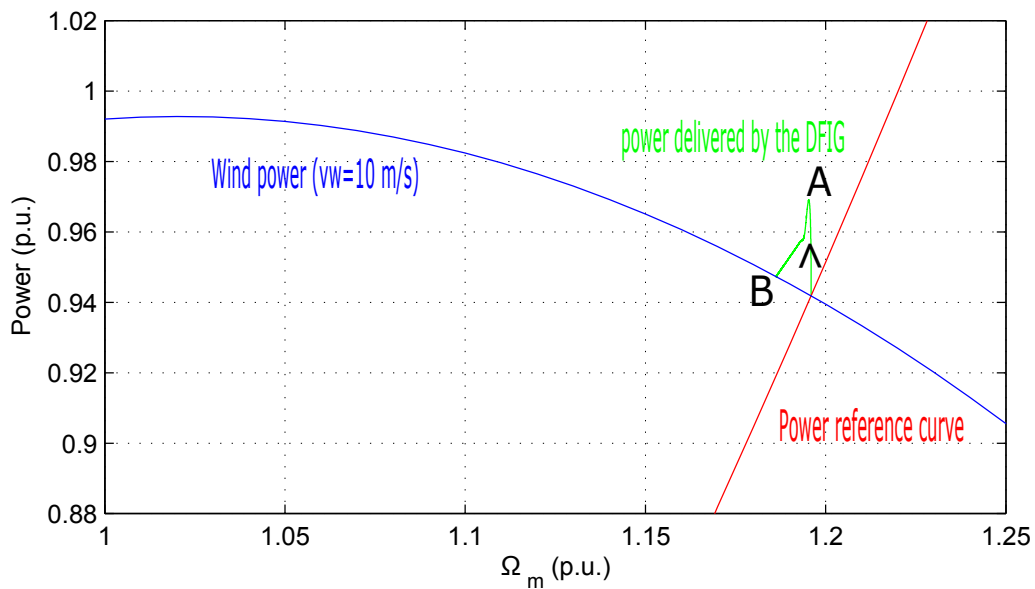
Figure 5.31: An enlargement of figure 5.31
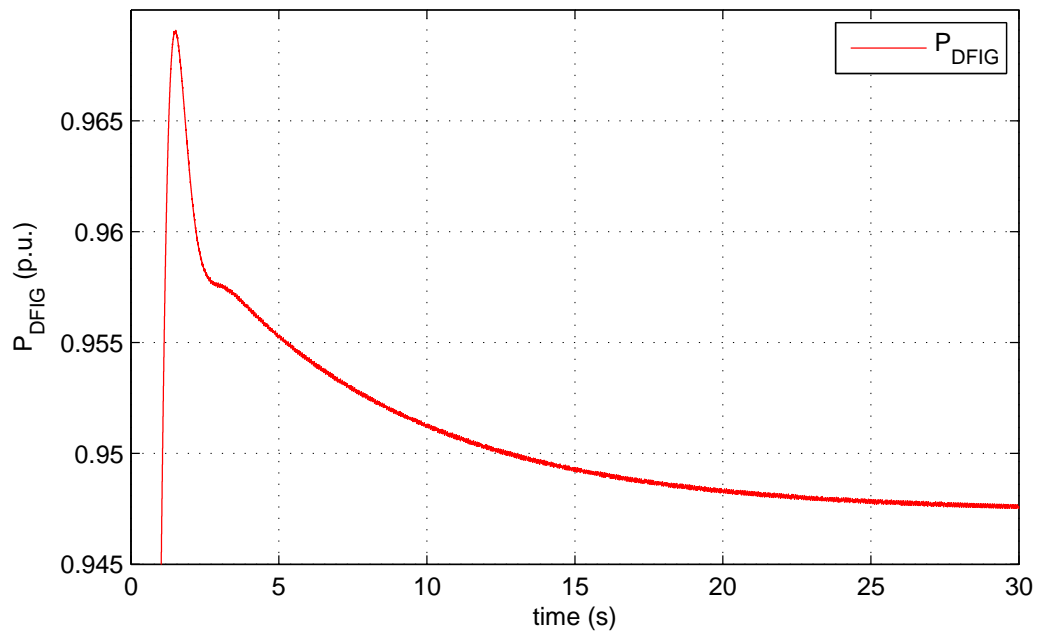
Figure 5.32: Power delivered by the DFIG after the load variation in figure 5.25 considering the DFIG equipped with primary power reserve
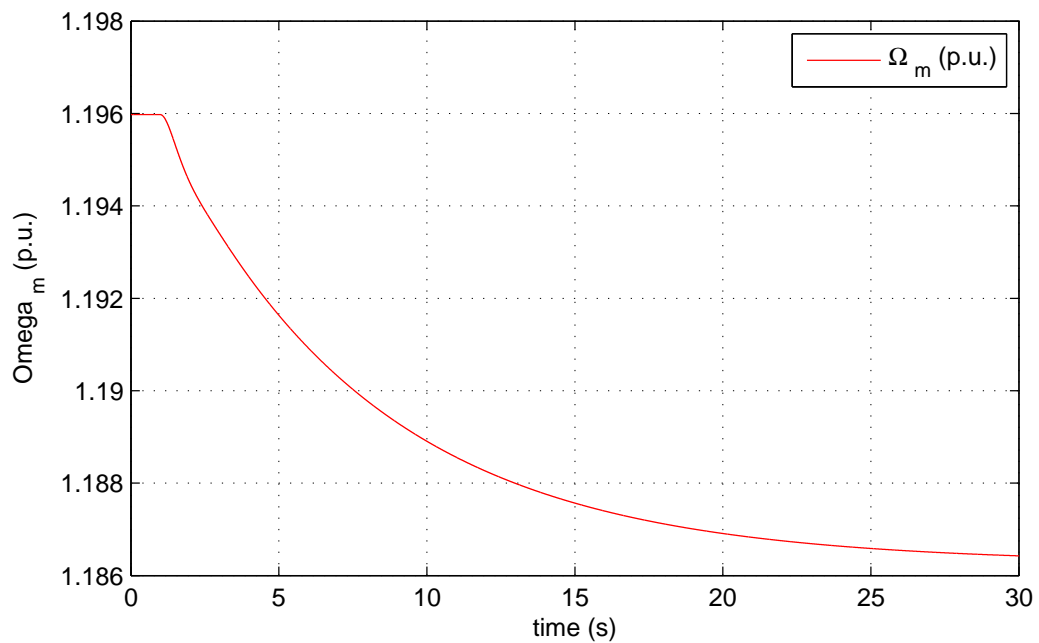
Figure 5.33: Mechanical angular speed after the load variation in figure 5.25 considering the DFIG equipped with primary power reserve

In section 2.5.3 we related the variation in mechanical angular speed to the

ability to supply inertia. Here we can find an example of this. Through this control we are able to supply inertia and also have a primary power reserve.

From (2.32) (replacing ω_d with Ω_m since in section 2.5.3 we used ω_d to indicate the p.u. mechanical speed) we can say that the inertia we are able to supply to the grid H_w is

$$H_w = \frac{H_t \Omega_{m0} \Delta \Omega_m}{\Delta_f} \tag{5.48}$$
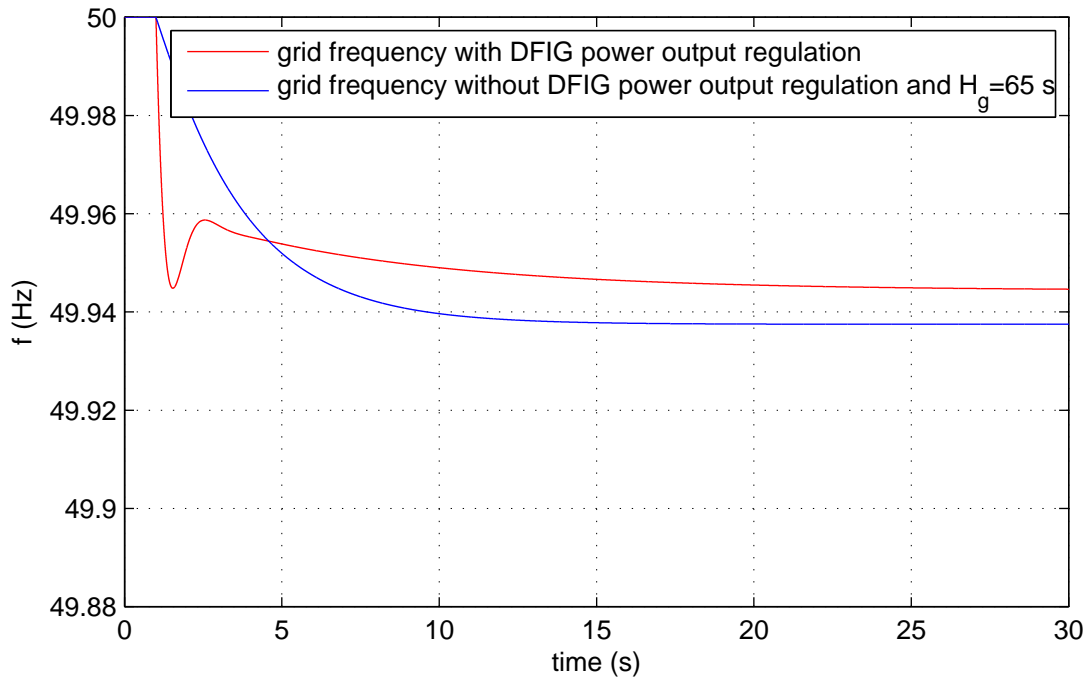
Figure 5.34: Grid frequency comparison

where H_t is the physical inertia constant of the turbine we already use in the equations. We can compute its value for this simulation. We retrieve form the graphs the values of $\Omega_{m0} = 1.196$, $\Delta \Omega_m = 0.01$ and $\Delta_f = 0.055/50$ and we remember that $H_t = 6$.

$$H_w \approx 65 \ s \tag{5.49}$$

It seems a very high value, but as we can see from figure the frequency transient time is very high. To verify that the value make sense we simulate again the system with a constant DFIG power output described in section 5.10.1, but with a grid inertia constant $H_g = 65 \ s$. The frequency behaviour in this case with the

one with the DFIG power support are reported in figure 5.34. We can see that except for the steady state value and the first part of the transient the slope is similar. So we can say that it is like we have a grid with an inertia equal to 65s. It si worth to underline that the situation is not the same since in the first part of the transient with the DFIG power support the frequency drops quickly in any case, but this is due to the fact that the power support is made through a control that relies on the grid frequency deviation and not on the grid frequency time derivative. We will see in section 5.11.2 a support that relies on the derivative of the grid frequency and we will analyse the difference in the frequency behaviour.

5.11 Adding power signal

We now implement two other solutions to supply inertia. In the first we rely on the grid frequency deviation, instead the second one on the time derivative of the grid frequency. We will now describe these two methods, for each one we will do the stability analysis, a simulation and we will propose some comments.
We will consider a DFIG equipped with a power control described in section 5.9.

5.11.1 Inertia emulation - droop control

Here we explain a method similar to the one described for the DC link (section 2.5.1), the main difference is that here we do not directly control the variable responsible of the inertia, in this case Ω_m. The method is proposed by some articles as [12].
With this method we vary power output according to the grid frequency deviation. In figure 5.35 we can see a block scheme which gives the reference quadrature axis current (f is the p.u. frequency).

We consider for this analysis the DFIG system described in section 5.9. So we again follow the de-loaded power characteristics and we deliver to the grid the 95 % of the available power from the wind, the moving reference curve described in sect. 5.10 is not implemented since we want to see the effect of this added droop control on the base system.
We choose droop controller coefficient (k_{dr})considering that in presence of a grid frequency variation of 1% we deliver all the primary power reserve which is 5%. So

$$k_{dr} = \frac{\Delta_p}{\Delta_f} = \frac{0.05}{0.01} = 5 \ p.u. \tag{5.50}$$

We made the stability analysis for this system, the equation are the one listed in 5.38 except for the 5.38e that becomes (f is the p.u. frequency)
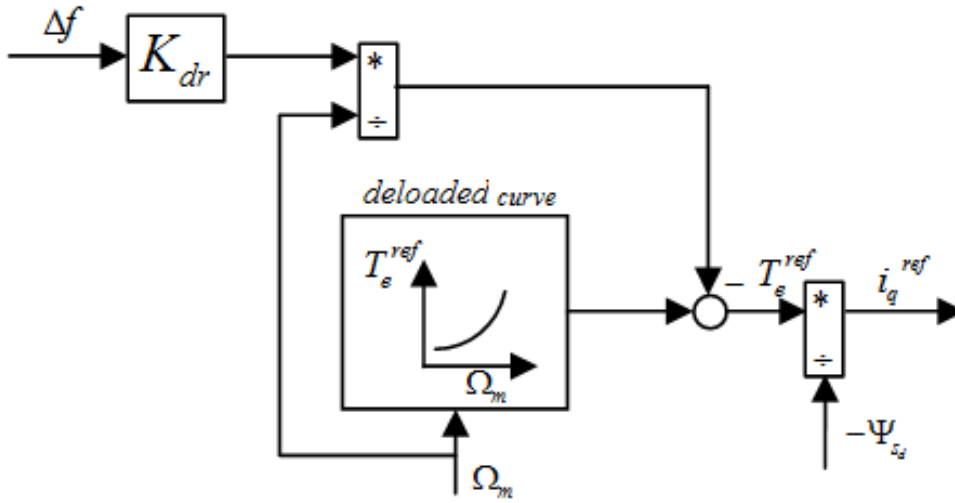
Figure 5.35: Droop control block scheme, i_q^{ref} is used to as reference fo the current loop (see figure 5.7)

$$T_e^{ref} = (\frac{\rho}{2}\pi R^5(\Omega_m\Omega_b)^2\frac{C_p^*}{\lambda^{*3}})/T_b - \frac{K_{dr}\Delta f}{\Omega_m} \tag{5.51}$$

Input variable are the same used for the stability analysis made before ($v_w = 10\ \frac{m}{s}$ and $V = 1\ p.u.$.). Here we do not report the value of the state variables at the equilibrium point and the eigenvalues since they are the same of the one in table 5.5 and table 5.6. This happens because in our system grid frequency is an input and it influences the eigenvalues only because of non linearity of the system, and in this case not in an appreciable manner. If the system were linear the input coefficients (such in this case K_{dr}) wouldn't enter the A matrix. But even if droop control does not influence small signal stability it greatly influences outputs as we can see from the simulation.
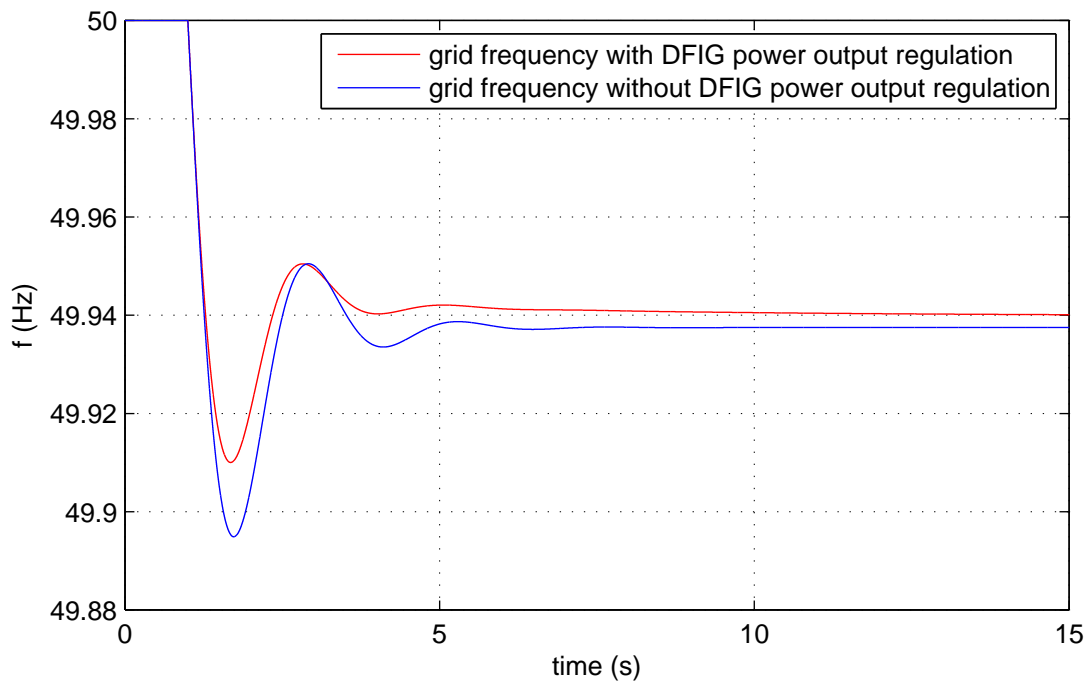
Figure 5.36: Grid frequency comparison

Simulation is carried out considering the DFIG interacting with a grid as done in section 5.10.2.

In figure 5.36 we can see the grid frequency in the base case with DFIG constant power output and in case of a DFIG equipped with droop control. We can see that in the second case the grid frequency oscillation is less high and the steady state value is a bit higher. But also in this case we can make the comment we made before in the last part of section, id est in the first instants of the transient the shape of the frequency behaviour is the same with respect to the base case, and as said before this is due to the fact that we rely on grid frequency deviation to give power support.

We ca also say that this method is similar the one we described before. In fact in both cases we modify power output in presence of a grid frequency deviation, the main difference is that in this case the modification is not durable, instead in the case of the primary reserve the output power (after its transient) sets to another value.

5.11.2 Inertia emulation - time derivative of the frequency measurement

We now implement the method described in 2.6. With this method we vary power output according to the grid frequency time derivative. In figure 5.37 we can see a block scheme which gives the reference quadrature axis current (f is the p.u.
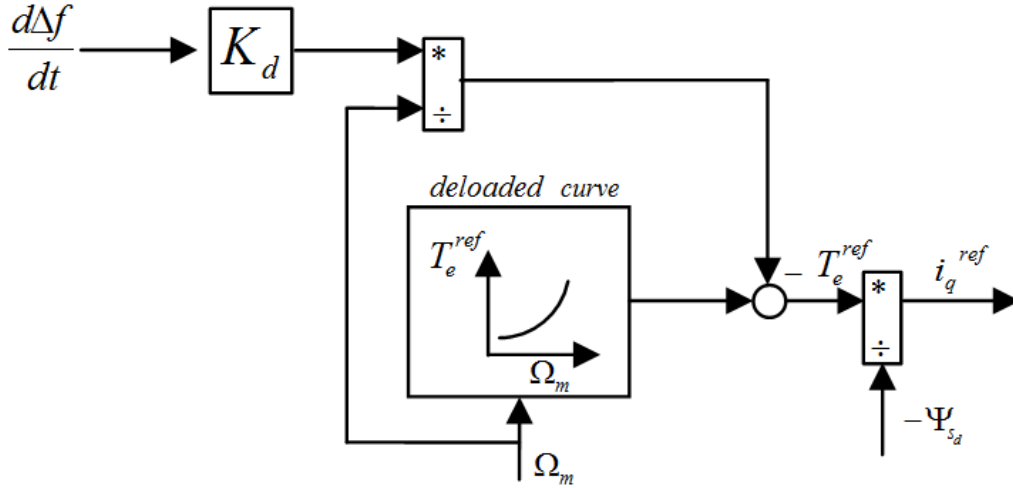
frequency).

Figure 5.37: Control block scheme, i_q^{ref} is used to as reference fo the current loop (see figure 5.7)

The measurement of the time derivative of the grid frequency is needed. This is not exactly achievable in practice, since to compute time derivative at time t we have to know the value of the signal at time $t + \Delta t$. The time derivative operation has the function s as Laplace transform. To make the transfer function achievable we have to add a pole, so the function becomes

$$G_{(s)} = \frac{s}{p_d s + 1} \tag{5.52}$$

In terms of state space model frequency measurement system has the following equations

$$\frac{dx}{dt} = -\frac{x}{p_d} + u \tag{5.53}$$

$$y = -\frac{x}{p_d^2} + \frac{u}{p_d} \tag{5.54}$$

in our case the input u is the frequency, the output y is the frequency time derivative approximation and x is the new state variable introduced. p_d is a parameter, we choose $p_d = 0.01\ s$ thinking that this choice will not degrade very much the time derivative of the grid frequency measurement. In fact the pole is at approximately $16\ Hz/s$ and such derivative is never reached in real grid measurement.

This value is 100 times the admitted derivatives for the grid frequency. It is reported [17] that in Italy there are three thresholds for load shedding due to excessive derivative in grid frequency: the first one is at 0.1 Hz/s the second one is at 0.17 Hz/s and the third one is at 0.50 Hz/s. At each step more load is shed. It is also to say that this kind of load shedding take place only if the frequency falls under 49.6 Hz.

The equation according to which we modify the wind farm power output in 2.34 is here reported (f is the p.u. frequency)

$$\Delta P_{DFIG} = -K_d \frac{d\Delta f}{dt} \tag{5.55}$$

We have now to choose the value of K_d. As pointed out in section 2.5.3 the inertia we are able to supply depends on the actual rotational speed and speed variation we can accept. We consider to have the turbine rotating at nominal speed, so $\Omega_m = 1$. Then we consider that we can slow down the turbine of 10%. This is a reasonable value, we can see from figure 5.10 that at wind velocity near the nominal one the MPPT curve and the de-loaded one are distant approximately 10 to 15 % with respect to Ω_m. We now compute the energy (E) we have at disposal from the slowing down of the turbine of 10% starting from $\Omega_m = 1$

$$\frac{1}{2}J\Omega_{wt}^2 - \frac{1}{2}J(0.9\Omega_{wt})^2 = E \tag{5.56}$$

where Ω_{wt} is the physical rotating speed and J is the turbine inertia moment. Now we bring the equation in p.u.

$$\frac{\frac{1}{2}J\Omega_{wt}^2 - \frac{1}{2}J(0.9\Omega_{wt})^2}{P_b} = \frac{E}{P_b} \tag{5.57}$$

which some manipulation gives

$$H_t - H_t 0.9^2 = \frac{E}{P_b} \tag{5.58}$$

and so

$$E = 0.19 H_t P_b \tag{5.59}$$

We now consider that our synthetic inertia has to last a least 10 seconds with a frequency time derivative equal to 0.1 Hz/s (which corresponds to 0.1/50 $p.u$). We choose such value for the time derivative of the frequency since it a threshold under which in Italy [17] begins load shedding. So if the frequency time derivative

is constant also the ΔP given by the controller is constant, so we can write

$$10\Delta P P_b = E \tag{5.60}$$

$$-K_d \frac{0.1}{50} P_b = E \tag{5.61}$$

$$-K_d \frac{0.1}{50} P_b = 0.19 H_t P_b \tag{5.62}$$

and so

$$K_d = -(1.9 H_t)50 \tag{5.63}$$

But this is a big value. In fact if we consider to be in presence of a grid frequency time derivative of 0.1 Hz/s according to (5.64) and considering $\Omega_m = 1$ $p.u.$ we need to deliver an additional torque approximately 1.2 times the nominal one. This is too high since it implies a rotor current 2.2 times the nominal one. So the value of K_d in (5.63) can be seen as a limit. We will use instead $K_d = 50$ $p.u.$. We made the choice considering that in presence of a grid frequency time derivative of 0.1 Hz/s we increase power output (and so reference torque) by 10 %.
We now made the stability analysis for this system, the equation are the one listed in 5.38 except for the 5.38e that becomes

$$T_e^{ref} = (\frac{\rho}{2}\pi R^5 (\Omega_m \Omega_b)^2 \frac{C_p^*}{\lambda^{*3}})/T_b - \frac{K_d}{\Omega_m}\frac{d\Delta f}{dt} \tag{5.64}$$

The equilibrium point (for a wind velocity equal to 10 $\frac{m}{s}$) is the one listed in table 5.11, instead the eigenvalues are listed in 5.12

As we can see there is one more eigenvalue with respect to the system without the derivative measurement but the other haven't vary their position.
We made also a simulation the system. In In figure 5.38 we can see how the grid frequency varies in time. In the same plot there is also the frequency behaviour in the base case.

Table 5.11: State variables at the equilibrium point (case $v_w = 10$ and C_p^* found according to 5.46)

Parameter	Value
ψ_{s_d}	0.9999
i_{r_d}	0
i_{r_q}	0.7875
Ω_m	1.1960
μ	0.0025
h_d	-0.0437
h_q	-1.207
x	3.14

Table 5.12: Eigenvalues of the linearised system around the equilibrium point

Parameter	Value (rad/s)	Damping
λ_1	$-79.493412 \ 10^3 + 60.2810 \ i$	≈ 1
λ_2	$-79.4934 \ 10^3 - 60.2810 \ i$	≈ 1
λ_3	$-781.4301 \ 10^{-3} + 314.1553 \ i$	$2.4874 \ 10^{-3}$
λ_4	$-781.4301e \ 10^{-3} - 314.1553 \ i$	$2.4874 \ 10^{-3}$
λ_5	$-203.8704e \ 10^{-3}$	1
λ_6	$-7.7444 \ 10^{-3}$	1
λ_7	$-7.7963 \ 10^{-3}$	1
λ_8	-100	1

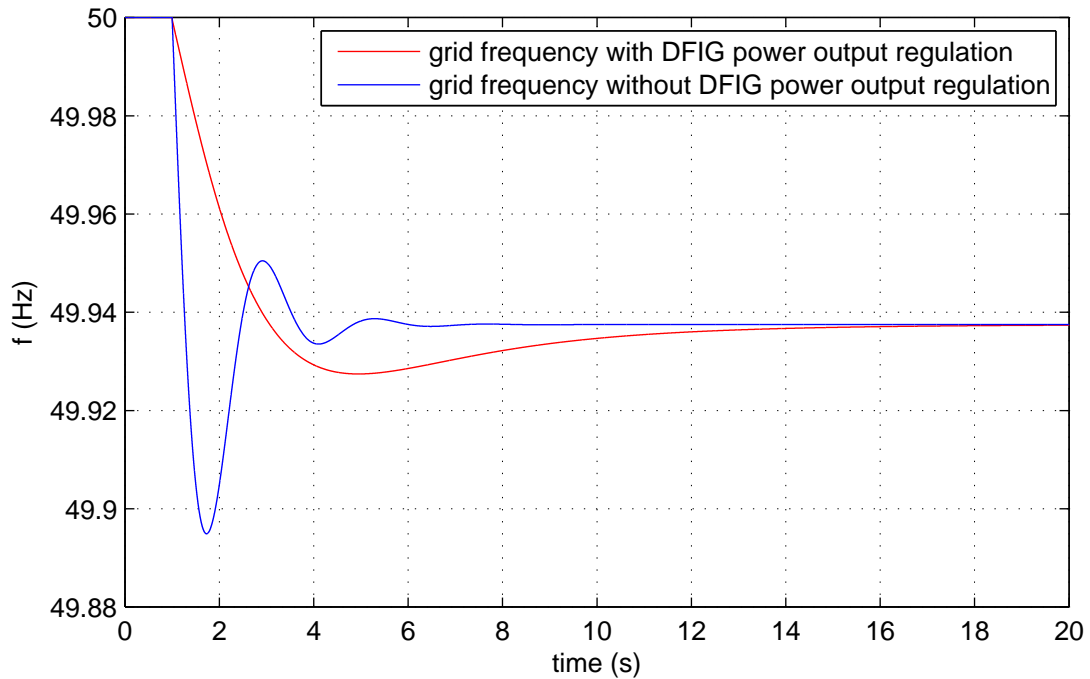
Figure 5.38: Grid frequency comparison

We can see that in this case the transient is different from the one without DFIG control also in the first instant after the load change. The frequency varies smoothly, this is due to the power support as function of the grid frequency time derivative. In this case we can say that we have added synthetic inertia from the very beginning of the transient.

Conclusions

In this thesis we have seen the synthetic inertia in HVDC connections and wind power plants equipped with DFIGs. Both these systems, due to the presence of power electronic converters, cannot naturally use the mechanical inertia of generators to sustain grid frequency.

We have analysed and sized the control system for the HVDC connection dealing with the synthetic inertia realization, represented by the inertia constant H we want to obtain. The synthetic inertia is obtained by changing the dc voltage as a function of the change of the grid frequency. We have made the stability analysis and simulations implementing the model in Matlab-Simulink to see how it behaves in presence of grid frequency disturbances.

Then we have studied a wind turbine equipped with a DFIG connected to the grid, through a seventh order mathematical model made by differential equations. The control system has been developed and the stability check has been analytically performed. Then by implementing the mathematical model in Matlab-Simulink, some simulations have been done for the various cases here briefly summarized. We have firstly implemented the primary reserve considering to run the wind turbine not following the MPPT strategy. Then we have studied the interaction of this DFIG with a traditional generator, represented by an inertia constant and a load; the inertial behaviour of the DFIG is obtained through various strategies. In order to change the frequency of the grid, the load was suddenly increased to see the system behaviour and compare it between various cases.

Firstly we have compared the situation, in which the power output of the wind plant is kept constant, with the case in which the wind power plant is equipped with primary reserve. We have seen how the frequency evolves in the two cases: in the first part of the transient it has different peak values but the same shape, but after a while the system acts differently in presence of wind turbine primary reserve. In fact the frequency sets to the steady state value more slowly: this can be interpreted as a inertia behaviour, so we can say that only introducing a primary reserve the wind power plant can introduce synthetic inertia in the system.

Then we have implemented the synthetic inertia relying on the grid frequency deviation and on the grid frequency time derivative: this signal works on the

reference torque of the electrical machine. We again did the stability analysis and simulations. In both cases there is a frequency support: the frequency steady state value is higher and the transient oscillations are lower with respect to the case in which the DFIG power output is constant, but the main difference between these two methods is that the one that relies on the grid frequency time derivative actually modifies the frequency transient from the very beginning making it softer. This is due to the derivative action not present in the other method. We can say that even if the grid support is present in different methods, the real inertial behaviour is obtained only with a derivative action.

Appendix A

PI controller synthesis

In this appendix we will show the method used to find the values of the proportional and integral gains (K_p and K_i) of the controllers. We suppose to have a system with transfer function $G_{(s)}$ and a negative feedback as in figure A.1.
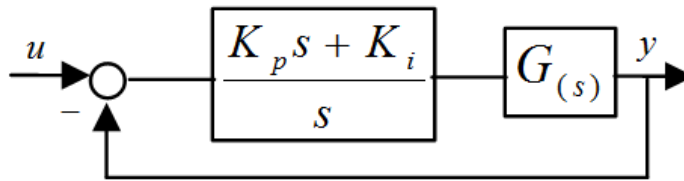

Figure A.1: PI controller and process typical close control loop

The open loop transfer function is

$$L_{(s)} = \frac{K_p s + K_i}{s} G_{(s)} \tag{A.1}$$

We have two parameters to find, so we need two constraints. These are:

1. the passing band of the closed loop system (w_p), witch is the frequency at which the closed loop transfer function ($F_{(s)} = \frac{L_{(s)}}{1+L_{(s)}}$) module is equal to $-3\ db$;

2. the phase margin φ_m;

Considering these two constraints we can write

$$|L_{(s)}|_{(s=jw_p)} = 1 \tag{A.2a}$$

$$\angle(L_{(s)})_{(s=jw_p)} = -\pi + \varphi_m \tag{A.2b}$$

witch leads to

$$|\frac{K_p s + K_i}{j w_p}| = \frac{1}{G_{(j w_p)}} \tag{A.3a}$$

$$\angle(\frac{K_p s + K_i}{j w_p}) = -\pi + \varphi_m - \angle(G_{(j w_p)}) \tag{A.3b}$$

Now considering that a complex number can be written as

$$a + jb = |a + jb| \cos(\angle(a + jb)) + j|a + jb| \sin(\angle(a + jb)) \tag{A.4}$$

we can find from equation A.3 the expression for K_p and K_i as a function of the system transfer function $G_{(s)}$ and the desired phase margin and passing band

$$K_p = \frac{1}{|G_{(j w_p)}|} \cos(-pi + \varphi_m - \angle(G_{(j w_p)})) \tag{A.5a}$$

$$K_i = \frac{-j w_p}{|G_{(j w_p)}|} \sin(-pi + \varphi_m - \angle(G_{(j w_p)})) \tag{A.5b}$$

$$\tag{A.5c}$$

Appendix A

Transformation matrices

A.1 $dq0$ transformation

It is a rotational matrix that can be applied to a set of three variables and gives three other variables. The angle θ is a function of the time.

$$T_\theta = \sqrt{\frac{2}{3}} \begin{bmatrix} \cos(\theta) & \cos(\theta - \frac{2}{3}\pi) & \cos(\theta + \frac{2}{3}\pi) \\ -\sin(\theta) & -\sin(\theta - \frac{2}{3}\pi) & -\sin(\theta + \frac{2}{3}\pi) \\ \frac{1}{\sqrt{2}} & \frac{1}{\sqrt{2}} & \frac{1}{\sqrt{2}} \end{bmatrix}$$

A.2 $\alpha\beta0$ transformation

It is a particular case as the previous described transformation, with $\theta = 0$.

$$T = \sqrt{\frac{2}{3}} \begin{bmatrix} 1 & -\frac{1}{2} & -\frac{1}{2} \\ 0 & \frac{\sqrt{3}}{2} & -\frac{\sqrt{3}}{2} \\ \frac{1}{\sqrt{2}} & \frac{1}{\sqrt{2}} & \frac{1}{\sqrt{2}} \end{bmatrix}$$

Bibliography

[1] Eu energy policy to 2050, european wind energy association, available online: http://www.ewea.org/publications/reports/eu-energy-policy-to-2050/.

[2] www.terna.it.

[3] Bruce Dunn et al. Electrical energy storage for the grid: A battery of choices. *Science*, 2011, no:334, pp: 928-935.

[4] Egido I et al. An ultra-capacitor for frequency stability enhancement in small-isolated power systems: Models, simulation and field tests. *Elsevier, Appl Energy*, 2014.

[5] G. Malarange G. Delille, B. François. Dynamic frequency control support by energy storage to reduce the impact of wind and solar generation on isolated power systems inertia. *IEEE Transactions on sustainable energy*, October 2012, vol. 3, no. 4, pp: 931-939.

[6] Ying Zhu Ming Cheng. The state of the art of wind energy conversion systems and technologies: A review. *Elsevier, Energy Conversion and Management*, 2014, vol. 54, pp: 244-254.

[7] Luisa Frosio. Droop control for interface inverters of hybrid power plants connected to isolated microgris, 2013, Phd Thesis Politecnico di Milano.

[8] Karel De Brabandere. Voltage and frequency droop control in low voltage grids by distributed generators with inverter front-end, 2006, Phd Thesis Katholieke Universiteit Leuven.

[9] Andreas Sumper Oriol Gomis-Bellmunt Francisco Díaz-González, Melanie Hau. Participation of wind power plants in system frequency control: review of grid code requirements and control methods. *Elsevier, Renewable and Sustainable Energy Reviews*, 2014, vol. 34, pp: 551-564.

[10] Entso-e entso-e network code for requirements for grid connection applicable to all generators, available online: https://www.entsoe.eu/.

[11] Grain P. Adam Andrew J. Roscoe Jiebei Zhu, Campbell D. Booth and Chris G. Bright. Inertia emulation control strategy for vsc-hvdc transmission systems. *IEEE Transactions on power systems*, May 2013, vol. 28, no. 2, pp: 1277-1287.

[12] Yong Yang Yingyi Li Hairong Chen Zheng Xu Yujun Li, Zeren Zhang. Coordinated control of wind farm and vschvdc system using capacitor energy and kinetic energy to improve inertia level of power systems. *Elsevier, Electrical Power and Energy Systems*, 2014, vol. 59, pp: 79-92.

[13] Zhilei Yao Xing Wei, Lan Xiao and Chunying Gong. Design of lcl filter for wind power inverter. *IEEE*, 2010.

[14] Yuan Tian Peixuan Tan Xianwen Bao, Fang Zhuo. Simplified feedback linearization control of three-phase photovoltaic inverter with an lcl filter. *IEEE Transactions on power electronics*, June 2013, vol. 28, no. 6, pp: 2739-2752.

[15] Prabha Kundur. Power system stability and control. 1994, McGraw-Hill Education.

[16] A. A. Fouad Paul M. Anderson. Power system control and stability 2nd edition. 2002, Wiley-IEEE Press.

[17] Paolo Chizzolini Noverino Faletti. Trasmissione e distribuzione dell'energia elettrica vol.2. 2005, Patron Editore.